Universiteit Utrecht

Faculty of Geosciences

Morphodynamic equilibrium of width and bed level profile of an estuary in response to adjustable channel widths

Master Thesis

Michal Janssen (5506891)

Earth, Surface and Water

Supervisors:

Dr. Maarten van der Vegt

Prof. dr. Maarten Kleinhans

23 January, 2022

Abstract

In this thesis, the morphodynamic equilibrium of the width and bed level profile of estuaries is studied. This is done by using an one-dimensional hydrodynamic and morphodynamic model that includes variable channel widths. The width is determined by a hydraulic geometry relation that relates the width to the peak in total discharge, which is dependent on both the fluvial and tidal influence. A river discharge is forced on the upstream boundary of the channel and a tide is forced upon the downstream boundary of the channel. The channel starts as a straight channel and then evolves towards a steady state with respect to the channel width and bed level. The equilibrium width and bed level profiles largely depend on the coefficients used in the hydraulic geometry relation. These coefficients were underestimated, but the model produced a realistic cross-sectional area tidal prism relation that did not depend on these coefficients. The results generally show that longer estuaries with a larger ratio between the width at the mouth and the width upstream are developed when the tidal amplitude or initial channel depth are larger, or when the river discharge, the initial slope or the drag coefficient are smaller. The width ratio can actually be directly related to the tide dominance ratio, whereas the estuary length mainly depends on the channel depth at the mouth, the estuary bed slope and the tidal amplitude. More convergent estuaries with a shorter e-folding length scale are developed when the initial slope or drag coefficient are larger or the initial channel depth is smaller. Interestingly, the results show that the convergence is greatly dependent on a balance between the river discharge and tidal amplitude. Generally, the estuary is more convergent with larger tidal amplitudes and smaller river discharges. However, if the river discharge is too low or the tidal amplitude too high, the estuary will develop a concave instead of a convex width profile. The equilibrium bed levels were all concave down with an increasing depth towards the mouth. Overall, the model shows great potential for predicting the equilibrium width and bed level profile of estuaries to changing boundary conditions if the hydraulic geometry relation coefficients are optimized.

Contents

1 Introduction

Estuaries are environments with large significant societal and environmental importance. They provided essential habitats for various flora and fauna with their sheltered brackish waters. Humans depend on estuaries for navigation between the sea and rivers. Estuaries moreover provide very fertile soils that are good for agricultural land uses (Bolla Pittaluga et al., 2015). Humans have a great impact on the estuaries as they try to control their behaviour, for example by placing dikes and dredging. Moreover, most estuaries are subject to a human-induced decrease in sediment supply and a rapid sea-level rise, which are expected to only increase in the coming years (Nienhuis et al., 2020). Estuaries adapt to these changes through their hydro- and morphodynamics. This raises questions about how these estuaries will adapt and what the long term effect will be. Some studies showed that effects of decreasing sediment supply would include erosion and reduction of wetlands and marshes (Syvitski, 2008), bank instability (Hackney et al., 2020), tidal amplification (Eslami et al., 2019) and salinization (Zhang et al., 2013).

The hydrodynamics and morphodynamics of estuaries are complex due to the interaction of river flow and tidal flow, making it hard to predict their behaviour exactly. Most estuaries have a convergent width profile with a larger width at the mouth than upstream. However, still, no fully accepted theory exists that exactly explains why estuaries develop such a convergent shape and what determines the magnitude of convergence (Davies & Woodroffe, 2010). This convergent shape is an essential factor influencing the tidal hydrodynamics in estuaries, as it amplifies the tidal wave. Friction opposes this amplification, so both the convergence and friction together determine the tidal hydrodynamics (Friedrichs & Aubrey, 1994).

To better predict the influence of human interference, it is vital to study the morphodynamic response of the bed level and the channel width of estuaries to changes in their hydrodynamics or morphodynamics. This is often done by studying the morphodynamic equilibrium of estuaries, as estuaries adapt to changes in their hydrodynamics or morphodynamics by evolving towards a new equilibrium (Zhou et al., 2017). There have been several numerical studies that focus on the effect of channel properties and boundary conditions on the equilibrium bed level profile of estuaries and tidal channels (Bolla Pittaluga et al., 2015; Canestrelli et al., 2014; Guo et al., 2015; Hibma et al., 2003; Lanzoni & Seminara, 2002; Todeschini et al., 2008). These studies often prescribe a convergent width profile and assume that the channel banks are stable, so the channel width will not change over time (Todeschini et al., 2005). This assumption of fixed banks could be justified because in many estuaries humans have fixed the banks by embankments. Another used justification is that the time scales on which channels adapt their width are longer than the time scales on which they adapt their bed levels (Bolla Pittaluga et al., 2015; Miori et al., 2006). However, not all estuaries have fixed banks, and it is essential to know how estuaries will evolve in the long term. For example, the Sittaung estuary (Myanmar) (Ahmed et al., 2018) and the Mekong estuary (Vietnam) are experiencing bank erosion (Hackney et al., 2020), while the Yangtze Estuary (China) (Zhao et al., 2018) has experienced an overall deposition trend. These changes in channel width affect the hydrodynamics, which in turn change the bed level of the estuary. This is why it is relevant to study equilibrium width profiles and incorporate adjusting widths to numerical models used in analyzing the equilibrium of estuaries.

Some researchers did include a variable width in their model for estuaries or tidal channels (Lanzoni & D'Alpaos, 2015; Todeschini et al., 2005; Van der Wegen & Roelvink, 2008; Xu et al., 2019). However, most of these models experienced the problem that the width profile did not stabilize but constantly increased, as only erosion processes were considered. Modelling erosion and sedimentation processes is complex, even in rivers where those processes are only influenced by fluvial flow and not by additional tidal flow (Kleinhans et al., 2011). There is moreover still no theory that describes what determines channel width of rivers. However, there have been made significant steps towards such a theory (Dunne & Jerolmack, 2020). There is a solid empirical basis that the channel width of rivers scales with the discharge through a power-law relation (Gleason, 2015). This empirical relation and other empirical relations that link the discharge to channel properties are called hydraulic geometry relations. Miori et al. (2006) and Kleinhans et al. (2011) developed a hydrodynamic and morphodynamic model for rivers that included an adjustable width by using a hydraulic geometry relation that related channel width to the discharge. In these models, the width profile reached a steady state. Hydraulic geometry relations have been less studied in the context of tide influenced estuaries. However, previous studies have shown that the channel width in estuaries and tidal channels scale with the tidal prism (D'Alpaos et al., 2010). This tidal prism is in turn related to the tidal discharge (O'Brien, 1931), so the channel width in estuaries can be related to the discharge (including fluvial and tidal influences) by a hydraulic

geometry relation (O'Brien, 1931; Sassi et al., 2012). This hydraulic geometry relation can then be used to simulate width adjustment in estuaries.

This thesis will study the morphodynamic equilibrium in channel width and bed level of an estuary in response to adjustable channel widths. This is done by using a one-dimensional numerical hydrodynamic and morphodynamic model, where the channel banks are not fixed, so the channel width can adjust to channel properties and boundary conditions. An existing model (Iwantoro et al., 2021) will be adjusted to include width adjustment by using a hydraulic geometry relation for estuaries. This method will be based on the models of Miori et al. (2006), and Kleinhans et al. (2011) in rivers. We will study if the modelled estuaries reach an equilibrium in width and bed level and what channel properties and boundary conditions this equilibrium depends on. Furthermore, will what variables determine the convergence and length of an estuary, as well as the effect of tide dominance on the equilibrium be researched. Lastly, the hydraulic geometry relations the model produces will be studied.

1.1 Structure of thesis

The structure of this thesis will be as follows. In section 2 (theoretical background), the characteristics of an estuary are discussed as well as past research on the morphodynamic equilibrium of estuaries and hydraulic geometry relations. Hereafter a detailed description of the research objective an research questions will be given in section 3 (research objective). In section 4, first, the hydrodynamic and morphodynamic calculations in the numerical model and how the width adjustment was included in the model will be explained. Second, an explanation of the model runs will be given and the method of determining estuary characteristics from the model results. In section 5 (results), the results will then be presented and briefly discussed. First, the results of the runs with an adjustable width but stable bed will be presented, and second, the results of the runs with an adjustable width and bed will be explained. After that, the results will be combined to study the effect of tide dominance on the estuary characteristics and the hydraulic geometry relations the model produces. In section 6 (discussion) the results will be further discussed and compared to past research. Furthermore, this section will contain some suggestions for future research. Last, in section 7 (conclusion), the overall conclusion of this thesis will be presented. The notations used in this thesis are described in the appendices, and a list of the figures and the tables are given therein.

2 Theoretical background

As in this thesis the equilibrium of an estuary is studied, it is helpful to define what an estuary is and explain what characteristics an estuary has. In this section this will be discussed, as well as how studies to the morphodynamic equilibrium of estuaries can give more insight into these characteristics. Furthermore, the previous research on equilibria of estuaries and hydraulic geometry relations will be reviewed.

2.1 Characteristics of estuaries

There has been quite some debate about the correct definition of an estuary (Elliott & McLusky, 2002; Fischer, 1976; Potter et al., 2010). Two widely-used definitions are the definitions of Pritchard (1967) and Dalrymple and Choi (2007):

"An estuary is a semi-enclosed coastal body of water which has a free connection with the open sea and within which sea water is measurably diluted with fresh water derived from land drainage." (Pritchard, 1967, p.3)

"An estuary is a transgressive coastal environment at the mouth of a river, that receives sediment from both fluvial and marine sources, and that contains facies influenced by tide, wave and fluvial processes. The estuary is considered to extend from the landward limit of tidal facies at its head to the seaward limit of coastal facies at its mouth" (Dalrymple & Choi, 2007, p.11)

The definition of Dalrymple only includes transgressive coastal environments, so prograding coastal environments like delta bifurcations are not included. These are included in Pritchard's definition. Another difference is that Pritchard's definition is based on salinity and Dalrymple's definition is based on geology. A schematisation of the difference between these two definitions is shown in figure 1. A slightly different definition will be used as this thesis mainly focuses on the tidal and fluvial influence in transgressive and progressive environments. An estuary will be defined as a coastal environment at the mouth of a river, influenced by tide and fluvial processes. The landward boundary of the estuary is located at the limit of the tidal influence (indicated in figure 1). As will be explained in section 4.2.3, this upstream boundary will be determined as the location where the tidal amplitude has decreased to one-fifteenth of the tidal amplitude at the mouth. A likewise estuary definition was proposed by Fairbridge (1980), who determined the landward boundary by the upper limit of the tidal rise.

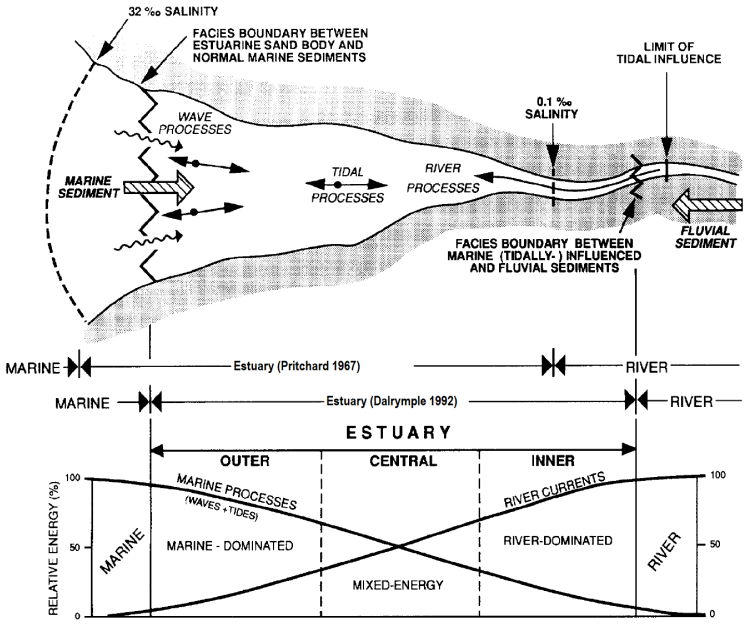

Figure 1: Schematisation of estuary definition of Pritchard (1967) and Dalrymple et al. (1992), including a schematisation of processes and the three estuary facies zones according to Dalrymple et al. (1992) (edited from Dalrymple et al. (1992)).

Estuaries can moreover be classified in different ways (Dalrymple et al., 1992; Dyer, 1973; Hume & Herdendorf, 1988; Pritchard, 1967; Savenije, 2005; Townend, 2012). A classification based on hydrodynamics, where a distinction is made between the relative influences of the tide, wave action and river discharge, is typical for estuaries and deltas (Dalrymple et al., 1992; Galloway, 1975; Nienhuis et al., 2020). Townend (2012) suggested a classification combining such a classification based on the hydrodynamics of Galloway (1975) with the classification of Hume and Herdendorf (1988) based on the landscape setting and the classification of soil properties of Shepard (1954) (figure 2). In this way, Townend (2012) wanted to emphasise that an estuary is a landscape form that adjusts to the influence of the river, tide and waves and depends on the sedimentology. The landscape setting is important as it can limit the accommodation space of an estuary.

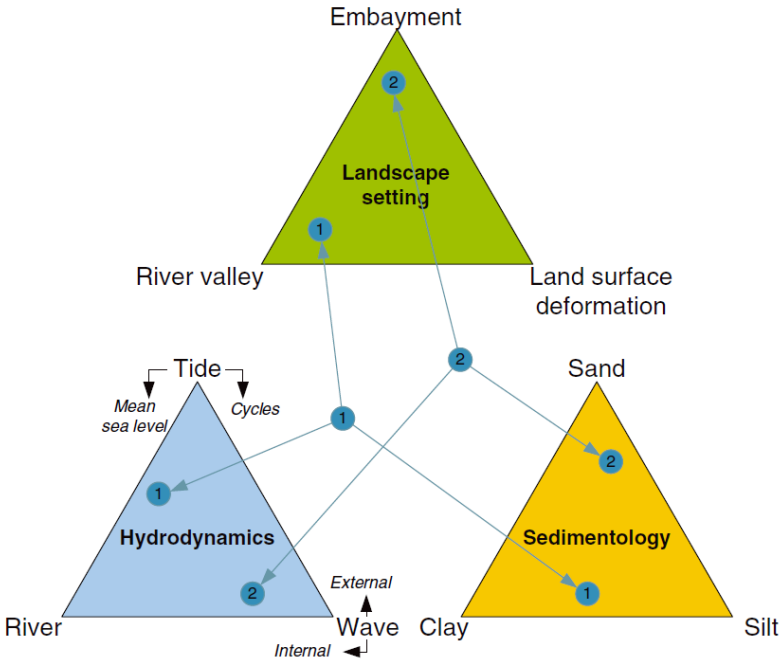

Figure 2: Ternary diagrams of estuary classification from Townend (2012), where 1 illustrates the case of a tidally dominated alluvial river valley and 2 illustrates the case of a sandy wave dominated embayment.

This thesis focuses on tidally dominated alluvial estuaries that are not limited in their length or width by the underlying geology (indicated by the number 1 in figure 2). As Bolla Pittaluga et al. (2015) pointed out: "A tidally dominated estuary can be defined as an alluvial river in which the flow and the morphology are essentially controlled by the tidal propagation which, in turn, is strongly affected both by the tidal range and the estuary geometry" (Bolla Pittaluga et al., 2015, p.76). A more quantitative definition of tide dominance is given by Nienhuis et al. (2018), where, when no wave action is present, tide dominance can be defined by the discharge ratio $I = \frac{Q_{tide}}{Q_{river}}$, where Q_{tide} is the tidal discharge amplitude (m^3/s) and Q_{river} is the mean fluvial discharge (m^3/s). When $I > 1$, the channel is tide-dominated and when $I < 1$, the channel is river-dominated (Nienhuis et al., 2018). Some examples of tide-dominated estuaries are the Charente (France), the Western Scheldt (The Netherlands) and the Hooghly estuary (India) (see figure 3). Moreover, the channels of tide-dominated deltas (for example, the Mahakam delta (Indonesia), figure 3d) often show the same characteristic converging width profiles (Gugliotta & Saito, 2019).

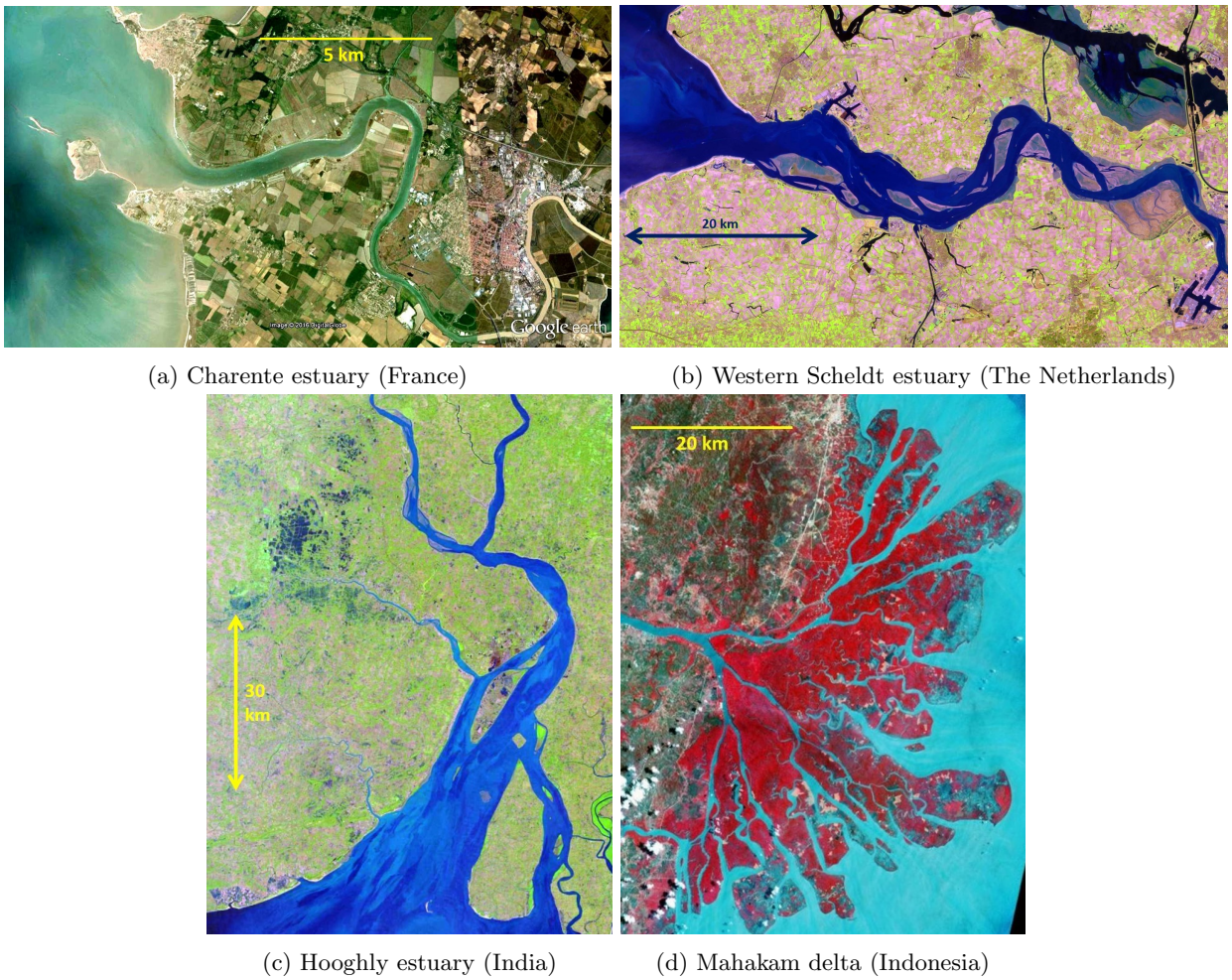

(a) Charente estuary (France)

(b) Western Scheldt estuary (The Netherlands)

(c) Hooghly estuary (India)

(d) Mahakam delta (Indonesia)

Figure 3: Examples of tide-dominated estuaries and deltas from Dronkers (2021).

The planform shape and bathymetry of an estuary are depended on the tidal and fluvial influence. The geometry is a result of the combination of erosion and deposition processes that are affected by these tidal and fluvial influences (Bolla Pittaluga et al., 2015). If these forcing conditions are changed, the erosion and deposition processes will change, and the estuary adapts its geometry Townend (2012). The geometry of tide-dominated alluvial estuaries generally shows an increasing width and cross-sectional area towards the sea with a converging funnel shape (van Rijn, 2011) (see figure 4 for the general morphology of a tide-dominated estuary). This convergent geometry of tide-dominated estuaries can be described by the width of the channel B (m) following an exponential profile:

$$B(x) = B_{mouth} \exp\left(-(L_e - x)/L_b\right), \tag{2.1}$$

or equivalently

$$B(x) = B_{river} \exp\left(x/L_b\right), \tag{2.2}$$

where B_{mouth} is the width at the mouth of the estuary (m), B_{river} is the width of the upstream river (m), L_e is the length of the estuary (m) and L_b is the e-folding length scale (m). x is the spatial axis, where $x = 0$ at the upstream boundary of the estuary, where it connects to the river (Davies & Woodroffe, 2010). Typical e-folding length scales of estuaries are of an order $10 - 50$ km (van Rijn, 2011). The width ratio between the width at the mouth and width of the upstream river B_{mouth}/B_{river} can vary from 2 up to 95, with an average of 13 (Nienhuis et al., 2018). The river itself has a straight channel (Davies & Woodroffe, 2010). Furthermore, various kind of bed profiles can be observed in different estuaries; constant depth profiles and increasing depth profiles with or without a depth decrease at the mouth are present in nature (Leuven et al., 2021; van Rijn, 2011). The estuaries are often flanked by intertidal mud

flats and salt marshes, which are partly inundated at flood or spring tide (Lanzoni & Seminara, 2002). The typical values of characteristics of estuaries that were mentioned and some others are shown in table 1.

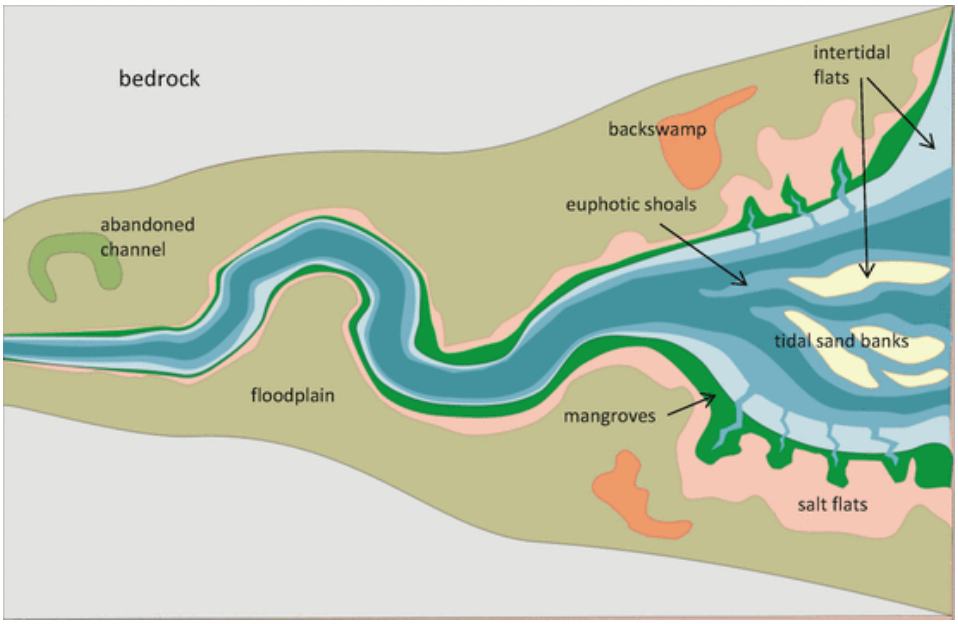

Figure 4: Typical morphology of a tide-dominated estuary by Scanes et al. (2017) who based it on Dalrymple et al. (1992).

Characteristic	Typical range	Average
Width ratio B_{mouth}/B_{river} [1]	2 - 40	13
E-folding length scale L_b [2, 3]	5 - 230 km	30 km
Estuary length L_e [2, 4]	2 - 330 km	70 km
Channel depth upstream river $H_{upstream}$ [1, 4]	3 - 23 m	7 m
Channel depth mouth H_{mouth} [4]	1 - 45 m	11 m
Bed slope S [1]	1.5×10^{-5} - 2×10^{-4}	5.7×10^{-5}
Tidal amplitude a_z [1]	0.5 - 6 m	2.5 m
River discharge Q_{river} [1]	25 - 2×10^5	-

Table 1: Typical values of estuary characteristics from 1. Nienhuis et al. (2018), 2. Todeschini et al. (2008), 3. van Rijn (2011) 4. Leuven, De Haas, et al. (2018).

The convergent shape of the estuary and friction are two essential factors in the tidal hydrodynamics in estuaries (Davies & Woodroffe, 2010; Friedrichs & Aubrey, 1994). The convergent shape amplifies the tidal wave, while friction dampens the tidal wave, so these are two opposite processes that are competing (Davies & Woodroffe, 2010; Friedrichs & Aubrey, 1994). When the tidal wave propagates into the estuary, asymmetries develop in the tidal currents, that are dependent on the bottom friction, channel geometry and tidal amplitude. These asymmetries mainly control the sediment dynamics in an estuary. (Friedrichs & Aubrey, 1988). Friction dominated estuaries have a flood-dominated transport, with high flood velocities with a short duration and a long high-water slack period. This leads to net upstream sediment transport. Estuaries with large extensive intertidal areas have an ebb-dominated transport, with high ebb velocities with a short duration and a long low-water slack period. This leads to a net downstream sediment

transport (Friedrichs & Aubrey, 1988; Lanzoni & Seminara, 2002). Upstream of the estuary, sediment dynamics are controlled by the fluvial processes (Lanzoni & Seminara, 2002).

Why tide-dominated estuaries develop a convergent width profile can still not be entirely explained (Davies & Woodroffe, 2010). It has been argued that the tidal velocities will increase in the downstream direction if the width and depth are constant over the length of the estuary. This leads to erosion at the downstream end of the estuary and, in turn, results in a convergent shape (Davies & Woodroffe, 2010; Savenije, 2005). The convergence could moreover be explained by the upstream decreasing tidal prism (Dronkers, 2017). The tidal prism is the volume of water in an estuary between low and high tide (Luketina, 1998). The tidal prism at the mouth typically has an order of magnitude between the 10^6 and 10^{11} (Leuven, De Haas, et al., 2018; Nienhuis et al., 2018).

When hydrodynamic solutions for estuaries are derived, one often assumes that the estuary is ideal. An ideal estuary is an estuary where the tidal water level amplitude and tidal velocity amplitude are constant throughout the estuary due to the convergence of the channel and the friction precisely balancing each other (Davies & Woodroffe, 2010; Savenije & Veling, 2005). Savenije (2005) derived the e-folding length scale L_b (m), that describes the convergence of such an ideal estuary:

$$L_b = \left(\sqrt{g\,H}\right) / \left(\frac{8\,C_d\,a_u}{3\pi\,H}\right), \tag{2.3}$$

where g is the gravitational acceleration (m/s^2), H is the channel depth (m), C_d is the drag coefficient (-) and a_u is the tidal velocity amplitude (m/s) (Davies & Woodroffe, 2010). (Chappell & Woodroffe, 1994) had another derivation for the e-folding length scale L_b (m) in an ideal estuary:

$$L_b = \frac{T\,\overline{HU}}{4\,a_z}, \tag{2.4}$$

where T is the tidal period (s), $\overline{HU}$ is the time-averaged product of the depth H (m) and the flow velocity U (m/s), and a_z is the tidal water level amplitude (m). Both equations describe a decreasing e-folding length scale with an increasing tidal amplitude and a decreasing channel depth (Davies & Woodroffe, 2010). In an ideal estuary, the depth is constant throughout the estuary, so the depth actually scales with the upstream river discharge, so in both equations, the e-folding length scale depends (indirectly) on the river discharge. This dependence of the e-folding length scale on the tidal amplitude and river discharge was furthermore confirmed by Dronkers (2017). Interestingly, Leuven, van Maanen, et al. (2018) found no clear dependence of the e-folding length scale on the tidal amplitude in his data of 68 estuaries. However, the data did show a relation between the e-folding length scale and upstream channel width. As the upstream channel width often scales with the river discharge, did Leuven, van Maanen, et al. (2018) indirectly confirm the dependence of the e-folding length scale on the river discharge.

The estuary length L_e is next to the e-folding length scale a subject of research. Nienhuis et al. (2018) used a simple estimation of the estuary length in a delta:

$$L_e = \frac{H_{upstream}}{S_{delta}}, \tag{2.5}$$

where $H_{upstream}$ is the depth upstream of the estuary (m) and S_{delta} is the slope of the delta (-). van Rijn (2011) and Prandle (2004) both analytically derived a relation for the estuary length that relates to the depth at the mouth H_{mouth} and the tidal amplitude a_z, where the estuary length increases with an increasing depth or a decreasing tidal amplitude. This means that the relative tidal amplitude a_z/H should be an important factor determining the estuary length.

The channel convergence can additionally be described by the estuary width ratio B_{mouth}/B_{river}. The estuary width ratio and estuary length L_e together determine the e-folding length scale L_b, as equation 2.2 says $B_{mouth} = B_{river}\exp\left(L_e/L_b\right)$. Nienhuis et al. (2018) derived an equation for this width ratio:

$$\frac{B_{mouth}}{B_{river}} = \frac{k_t\,a_z}{S} + 1, \tag{2.6}$$

where k_t is a tidal efficiency coefficient (1/m), a_z is the tidal water level amplitude (m) and S is the slope (-). This tidal efficiency coefficient can be determined by $k_t = \omega\left(\sqrt{\theta_{cr}\,D_{50}\,\frac{g}{C_d}}\,R\,\pi\right)^{-1}$, where ω is the angular velocity of the

tide (1/s), θ_{cr} is the critical Shields number (-), D_{50} is the sediment grain size (m), g is the gravitational acceleration (m/s^2), C_d is the drag coefficient (-), and R is the specific density of sediment (-).

2.2 Equilibrium of estuaries and tidal channels

As explained before, estuaries adapt to changes in the external forcing. To study how these estuaries precisely adapt, often the morphodynamic equilibrium of estuaries is researched through computer models or experimental setups (Zhou et al., 2017). An alluvial estuary or, more general, an alluvial river is said to be in morphodynamic equilibrium when the flow field and bathymetry and planform shape are adjusted to each other in such a way that no accretion or erosion takes place over time (Bolla Pittaluga et al., 2015; Jia et al., 2017). If the external forcing is changed, the estuary will develop towards a new morphodynamic equilibrium. As a tide-dominated estuary does experience fluctuations in discharge and sediment transport in one tidal cycle, a dynamic morphodynamic equilibrium is often used, where there can be fluctuations in a tidal period, but not averaged over a tidal period (Seminara et al., 2012). This dynamic morphodynamic equilibrium is actually a steady-state (Kleinhans et al., 2015). Studying different morphodynamic equilibria can lead to understanding how estuaries develop and on what boundary conditions and other characteristics the geometry of the estuary depend. However, it is essential to note the difference between the "virtual world" and "real world" as Zhou et al. (2017) argues. In the "virtual world", so for example, in hydrodynamic and morphodynamic models, the processes in the "real world" are selected, simplified and completely controlled. The existence of an equilibrium is an almost direct result of the system of equations used in the "virtual world" to describe the "real world". In the "real world", a whole spectrum of processes are operating that all have different time scales and interact differently, so an equilibrium might not even exist. However, it is still beneficial to study these morphodynamic equilibria in the "virtual world", as they provide fundamental steps in the understanding of how natural systems develop under natural conditions (Zhou et al., 2017). The goal in modelling studies to tide-dominated estuaries is that the estuary develops such a dynamic morphodynamic equilibrium that depends on boundary conditions and other parameters, but not on the initial conditions of the bathymetry or planform shape, so that conclusions can be drawn on the dependence of this equilibrium on the boundary conditions and other parameters.

Much research has focused on the equilibrium morphology of estuaries, tidal channels and tidal embayments, which primarily studies the bed level and depth profiles. This research has been done in different ways, for example by numerical modelling (Bolla Pittaluga et al., 2015; Canestrelli et al., 2014; Guo et al., 2015; Hibma et al., 2003; Lanzoni & Seminara, 2002; Schuttelaars & De Swart, 2000; Todeschini et al., 2008) and experimental set-ups (Tambroni et al., 2005). The effect of a converging width was often studied in these numerical modelling studies, but this width was kept fixed in time. Bolla Pittaluga et al. (2015) is one of whom that investigated the equilibrium of tidally dominated alluvial estuaries focussing on bed level profiles. They did this by seeking the equilibrium bed profile for a given planform through a 1-dimensional numerical model. It was found that an equilibrium bed profile of estuaries exists with a constant fluvial and tidal forcing. The bed profiles evolved towards a concave down profile. The model produced steeper slopes at the mouth for larger tidal amplitudes, smaller fluvial discharges, larger grain sizes and larger fluvial sediment concentrations. These steeper slopes were combined with more bed degradation in the upstream river-dominated part of the estuary. Lanzoni and Seminara (2002) also used a 1-dimensional model to investigate the equilibrium of funnel-shaped estuaries. They mainly looked at ideal friction dominated estuaries with non-cohesive sediments and no inter-tidal storage of water on tidal flats. The equilibrium bed profile of these estuaries showed a concave up shape where the concavity increased with increasing estuary convergence. The depth profile showed a shallower area upstream at the landward end of the estuary. These equilibrium bed profiles were reached on a time scale of hundreds of years. Interestingly, the one-dimensional model of Leuven et al. (2021) developed depth profiles with a scour, where the depth first increased towards the sea, but at the mouth, a sudden decrease in depth was present. They found that this scour like bed profile developed when the tidal amplitude was large or the river discharge was small, and the e-folding length scale of the estuary was short, so the estuary was very convergent. In other cases, a bed profile developed with a constantly increasing depth, like in the study of Bolla Pittaluga et al. (2015); Lanzoni and Seminara (2002). Overall, studies show that the bed profile depends on the relative strength of the tide and the river discharge, and the convergence of the channel (Bolla Pittaluga et al., 2015; Canestrelli et al., 2014; Guo et al., 2015; Lanzoni & Seminara, 2002; Leuven et al., 2021; Seminara et al., 2010; Todeschini et al., 2008).

Less research has been done on the equilibrium width profiles of estuaries. Existing numerical studies do often not incorporate a variable width in their models, but have a fixed width in time, as the studies discussed above. This

means that the channel banks can not erode or accrete. Since less research is done on the channel width of estuaries, the research done to the channel width in rivers will be furthermore discussed. This can give a more general view on what determines channel width. First, the bank erosion processes in rivers and estuaries will be briefly discussed. After that, the research, that includes a variable channel width in their numerical model in rivers and estuaries, will be considered.

There is still no complete theory that explains what precisely determines river width (Dunne & Jerolmack, 2020). Dunne and Jerolmack (2020) hypothesised that the river geometry will adjust to the threshold fluid entrainment stress of the most resistant material lining the channel. They found that river width could be predicted by the bankfull discharge, the slope of the channel, the friction factor and the entrainment stress of the most resistant material. Parker et al. (2011) reviewed the existing literature and methods for modelling bank erosion processes in river meander bends. Parker et al. (2011) developed a new model where the migration of the eroding bank and the depositing bank are modelled separately. This can be used in cross-sectional models, but including bank erosion and accretion processes in a model for a whole channel is complex, as pointed out by Kleinhans et al. (2011), due to the dependence on many empirical parameters. Vegetation has a significant impact on the bank strength, but this influence is again dependent on the type of vegetation (Kleinhans et al., 2011). In estuaries salt marshes often flank the channel. These salt marshes lead to flow resistance and are essential for sedimentation in the estuary. Brückner et al. (2019) studied the effect of these kinds of vegetation and found that they affect the large-scale pattern of channels and the overall planform of the estuary. Furthermore, the type of sediment that the banks are made of is crucial (Kleinhans et al., 2011). The bed generally consists of sand in estuaries, but the banks can be made of mud. Mud is more cohesive and affects the estuary width. Braat et al. (2017) showed with a 2DH numerical model that estuaries with a larger mud concentration developed smaller channel widths and can confine the estuary. Furthermore, a larger mud concentration led to shorter estuaries and a stronger convergence when the mud was fluvial. When the estuary consisted of only sand and no mud, the estuary continuously expanded. Braat et al. (2017) hypothesised that the tidal prism in an estuary can continue to increase with increasing width and that this process is only limited by the cohesion of sediments, so a specific concentration of mud or vegetation is needed to reach an equilibrium.

The 2DH model of Braat et al. (2017) did include bank erosion by dry cell erosion. This means that erosion occurs in a dry cell when an adjacent wet cell experiences erosion. So, implicitly sediment is transported from a dry cell to a wet cell, so the bed level of the wet cell does not change. In the study of Braat et al. (2017) the estuaries increased in size with increasing tidal amplitude. Furthermore, they found that smaller river discharges led to a more convergent estuary. This model was moreover used by Van der Wegen and Roelvink (2008), who studied the long-term evolution of estuary morphodynamics in which they made a particular emphasis on the pattern formation. In their model, bank erosion was too included by applying dry cell erosion. They compared the obtained cross-sectional areas and tidal prisms to the empirical relation of Jarrett (1976) (see section 2.3) and found that the basins evolved towards a similar relation, but the model produced somewhat bigger cross-sectional areas. This was probably due to the model developing deeper channels than expected. Furthermore, did the width not stabilise, as only erosion of the banks was taken into account and no deposition processes. The bed level showed a concave up profile throughout the estuary, where the depth decreases throughout the estuary. The width profile showed a convex funnel shape. They also compared their results to a more simple 1-dimensional model and found that the results of both models compared well in the case of bed level profiles.

Both Lanzoni and D'Alpaos (2015) and Xu et al. (2019) used a coupled numerical model to study tidal channels. Two one-dimensional models were combined; one consisted of nodes in the longitudinal direction and the other of nodes in the cross-sectional direction. Channel widening could be modelled by erosion of one of the nodes placed on the bank or tidal flat. The model of Xu et al. (2019) additionally included sedimentary processes. Tidal channels have a closed landward boundary, so no river discharge is forced upon the channel, only a tide. Xu et al. (2019) found that short tidal channels eventually reached a dynamic equilibrium. The channel width in their model showed a good relation to the channel depth and a friction coefficient, where the width was larger with larger channel depths and a smaller friction coefficient. Lanzoni and D'Alpaos (2015) especially focused on the funnel shape of tidal channels, but their results showed that a linear fit instead of an exponential fit of the width profile was good as well. Moreover, their results showed a good relation between the cross-sectional area and the tidal prism. Furthermore, the channels with a strong convergence showed concave up bed profiles, and channels with a lower convergence showed a more linear bed profile. The width of the channels increased with increasing tidal amplitude and decreasing critical shear stress.

Besides two dimensional numerical models that include width adjustment, some one-dimensional numerical models that include width adjustment are developed. These 1D models take a lot less computation time. Todeschini et al. (2005) developed such a 1D model for estuaries and used a physically-based erosion law. They used the assumption of Darby and Thorne (1996), that channel widening occurs when the bed shear stress τ_b exceeds a threshold value $\tau_{b,cr}$. An equation for the width evolution was obtained:

$$\frac{\partial B}{\partial t} = k_e \left(\frac{\tau_b}{\tau_{b,cr}} - 1 \right) \text{ for } \tau_b > \tau_{b,cr}, \tag{2.7}$$

where B is the channel width (m), t is time (s), and k_e is the lateral erosion rate (m/s). Their model used a $\tau_{b,cr}$ of 0.1 N/m^2 and a k_e of 10^{-10} m/s. This is an erosion law, meaning that when this kind of equation is used, the width of the channel can only become larger (i.e. erode) and not become smaller (i.e. accrete). The results showed that indeed no equilibrium could be reached as the width continued to widen while the bed became stable. The width profiles developed into a concave shape when no river discharge was incorporated and the bed was movable. Moreover, the bed profiles showed quite steep slopes in those cases. On the other hand, a convex funnel shape was developed with no river discharge when the bed level was fixed. Interestingly, the width profiles also showed a more convex funnel shape when a river discharge was forced on the channel, and the bed could adjust. Furthermore, smaller slopes developed compared to the runs where no river discharge was forced. Overall the channels developed a larger width with higher tidal amplitudes.

As explained, there are many uncertainties in modelling bank erosion and the models which do include bank erosion do not include bank accretion. This is why Miori et al. (2006) and Kleinhans et al. (2011) based width adjustment in their model for rivers on an equilibrium width. They assumed that the width evolves towards an equilibrium width, based on an empirical hydraulic geometry relation:

$$\frac{\partial B}{\partial t} = \frac{B_e - B}{T_w}, \tag{2.8}$$

where B_e is an equilibrium width where the channel width evolves towards, and T_w is a timescale on which this width evolution happens (i.e. time scale for width adjustment). Both studies used an empirical hydraulic geometry relation between the equilibrium width and river discharge that holds for rivers (more on these empirical relations in section 2.3). Kleinhans et al. (2011) showed that the eventual reached modelled equilibrium morphology did not depend on the time scale for width adjustment. Only how fast this equilibrium was reached did depended on the time scale. In the study of Kleinhans et al. (2011) was the width change moreover included in the Exner equation for sediment conservation.

Overall, several studies have included width adjustment in their numerical model for rivers and estuaries. Such a model is needed to study the width profile of estuaries and to understand what boundary conditions and other channel characteristics this width profile depends on. The studies together showed that the channel width in estuaries is larger when the tidal amplitude or the channel depth is larger, or when the friction or critical shear stress is smaller. Furthermore, more convergent estuaries often developed when the tidal amplitude was larger or the river discharge was smaller. This corresponds to the theory discussed in section 2.1.Nevertheless, most of the two-dimensional models experienced a continuous widening of the channel (except for the model of Xu et al. (2019)). Moreover, two-dimensional models take much computational time (up to a month) (Braat et al., 2017). The one dimensional model of Todeschini et al. (2005) for estuaries likewise showed no stabilisation of the width profile due to only using an erosion model. The model of Miori et al. (2006) and Kleinhans et al. (2011) did reach a stable width profile but is developed for rivers and not estuaries. However, it is possible to develop the same kind of model for estuaries; the question then remains what empirical hydraulic geometry relations can be applied to estuaries.

2.3 Empirical hydraulic geometry relations

As no pure physical analytical relations between the width and the hydrodynamics have been developed in rivers and estuaries, empirical relations play an essential role (Savenije, 2005). These empirical relations are a great predictive tool for long-term morphology in tide influenced channels (D'Alpaos et al., 2010). They are applied in different ways, from monitoring the discharge and investigating flow conditions in the past (Gleason, 2015) to predicting the geometry of tidal channels for tidal wetland restoration projects (Williams et al., 2002).

Leopold and Maddock (1953) developed hydraulic geometry relations for rivers. Hydraulic geometry relations describe the empirical relation between river discharge and the width B (m), depth H (m) and flow velocity U (m/s) in a channel by:

$$B = aQ^b, \tag{2.9}$$

$$H = cQ^f, \tag{2.10}$$

$$U = kQ^m. \tag{2.11}$$

As the discharge relates to the width, depth and flow velocity like

$$Q = BHU, \tag{2.12}$$

the multiplication of the coefficients must be equal to 1:

$$ack = 1, \tag{2.13}$$

and the sum of the exponents must also be equal to 1:

$$b + f + m = 1. \tag{2.14}$$

It was determined that the average river in the mid-western United States had values of $b = 0.5$, $f = 0.4$ and $m = 0.1$ (Leopold & Maddock, 1953).

The hydraulic geometry relations are still a topic of discussion. They have been applied to observations in different studies to verify them. This resulted in different values for the exponents. Xu et al. (2021) combined the b-f-m ternary diagrams of Park (1977), Rhodes (1977) and Rhodes (1987), who in turn combined data of various researches (see figure 5). The figure makes a distinction between the at-a-station hydraulic geometry relationships (AHG) and downstream hydraulic geometry relationships (DHG). This thesis is interested in the DHG, as the DHG focuses on spatial variability and AHG on temporal variability. Note that there is no clear trend between the exponents. However, most of the data is in the range 0.4-0.7 for b, 0.2-0.5 for f and 0-0.3 for m. The interest in the coefficients a, c and k have been much less (Xu et al., 2021). Xu's (Xu et al., 2021) collected hydraulic geometry relations show that a varies between 2 and 21, c varies between 0.07 and 1.12 and k varies between 0.11 and 2. Gleason (2015) has also written a review about the hydraulic geometry relations for rivers. Herein it is discussed that researchers have expanded the hydraulic geometry relations by incorporating other variables, such as sediment properties or bank vegetation and strength parameters, to explain these relations better.

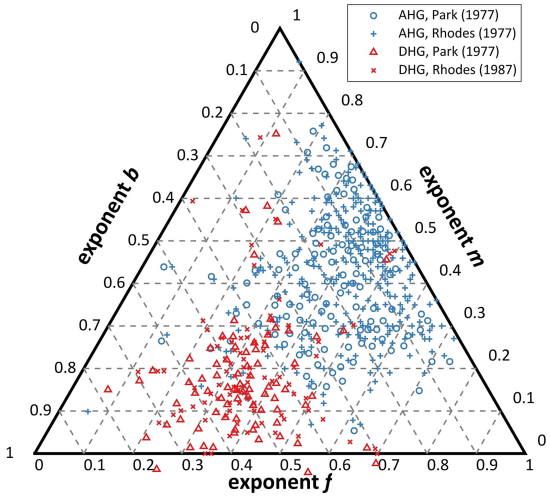

Figure 5: b-f-m ternary diagram of at-a-station hydraulic geometry and downstream hydraulic geometry exponents (Xu et al., 2021).

The research on hydraulic geometry especially focuses on the hydraulic geometry of upstream rivers and less on estuaries (Gisen & Savenije, 2015). For estuaries, if equation 2.9 is used with the discharge Q being the mean discharge, the geometry relation will not explain the increasing downstream width since generally the mean discharge is the same along the estuary, so another kind of discharge needs to be used that incorporates the tidal effect. Myrick and Leopold (1963) and Langbein (1963) were the first to apply hydraulic geometry relations to tidal estuaries. Myrick and Leopold (1963) theoretically arrived at the exponents $b = 0.71$, $f = 0.24$ and $m = 0.05$. While Langbein (1963) derived almost the same exponent of $b = 0.72$, $f = 0.23$ and $m = 0.05$. This derivation is based on the assumption that the morphology of estuaries develops such that there is equal energy dissipation and a minimum of total work. The first one would imply that $B \propto Q^1$, whereas the second one implies that $B \propto Q^{0.45}$. Langbein (1963) took the average of these two (Davies & Woodroffe, 2010). To note is that the discharge Q that was used to check this relation was a discharge corresponding to the mean stage. This discharge increases downstream, so it can potentially explain the downstream width increase, but did not explicitly include the tidal effect.

Next to these hydraulic geometry relations, another important empirical relation is used in tide-dominated estuaries or tidal channels; the tidal prism cross-sectional area relation:

$$A = \alpha_{AP} P^{\beta_{AP}}, \tag{2.15}$$

where A is the cross-sectional area (m^2), and P is the tidal prims (m^3) (D'Alpaos et al., 2010). This relation has been confirmed to hold for estuaries and tidal channels by different observations and numerical analyses (D'Alpaos et al., 2010), so it has a strong empirical basis. O'Brien (1931) was one of the first who developed this relation, where β_{AP} was 0.85 and α_{AP} was 9×10^{-4} in case of dual jetties and β_{AP} was 1 and α_{AP} was 6.6×10^{-5} in case of unprotected or single jetty (van der Wegen et al., 2010). Jarrett (1976) later arrived at a general β_{AP} of 0.95 and a α_{AP} of 1.6×10^{-4}. When the tidal prism cross-sectional area relation was first introduced, it related the cross-sectional area of the mouth to the tidal prism at the mouth. Later it was shown that the relation holds along the whole tidal channel and everywhere the local cross-sectional area could be related to the local tidal prism in the same way (D'Alpaos et al., 2010). The tidal prism cross-sectional area relation was furthermore studied by D'Alpaos et al. (2010). It was noted that β_{AP} typically varies between a value of 0.85 and 1.1 between different systems in the world. D'Alpaos et al. (2010) found that the theoretically derived value by Marchi (1990) of $6/7 \approx 0.86$ for β_{AP} and 1.2×10^{-3} for α_{AP} could be best validated by results of several models, and observations in the Venice lagoon.

O'Brien (1931) showed that the tidal prism was in turn related to the peak in total discharge over one tidal cycle Q_{peak}.

$$P \propto Q_{peak}^{0.85}, \tag{2.16}$$

This total peak discharge consists of the river discharge Q_{river} (m^3/s) and the peak in tidal discharge Q_{tide} (m^3/s) (i.e. $Q_{peak} = Q_{river} + Q_{tide}$). As the cross-sectional area is related to the tidal prism and the tidal prism is related to the total peak discharge, the cross-sectional area is moreover related to the total peak discharge with a power-law relation (Savenije, 2005).

Another hydraulic geometry relation was developed by Sassi et al. (2012). This relation included river and tidal discharge:

$$A = \alpha_A (Q_{river} + Q_{t,max})^{\beta_A}, \tag{2.17}$$

where A is the cross-sectional area (m^2), Q_r is the river discharge (m^3/s) and $Q_{t,max}$ is the maximum tidal discharge amplitude (m^3/s). The discharge $Q(t)$ can be composed at each section into a combination of the river discharge $Q_{river}(t)$ and the tidal discharge $Q_t(t)$.

$$Q(t) = Q_{river}(t) + Q_t(t) \tag{2.18}$$

The tidal discharge $Q_t(t)$ can, in turn, be composed of the contribution of the different tidal constituents $Q_l(t)$

$$Q_t(t) = \sum_{l=1,2,4} Q_l(t), \tag{2.19}$$

$$Q_l(t) = a_{Q,l}(t)\, \cos(i\, \omega_l\, t + \phi_l), l = 1, 2, 4, \tag{2.20}$$

where $1, 2$ and 4 denote the different tidal constituents (with a diurnal, semi-diurnal and quarter-diurnal period), a_Q is the amplitude of the discharge (m^3/s), ω is the angular velocity ($1/s$) and ϕ is the phase (-). The maximum tidal discharge amplitude $Q_{t,max}$ is then defined as

$$Q_{t,max} = \sum_{l=1,2,4} a_{Q,l}. \tag{2.21}$$

The study of Sassi et al. (2012) focussed on the Mahakam Delta (Indonesia). For the Mahakam Delta α_A is 2.32 ± 0.43 and β_A is 0.77 ± 0.06 were found to be a good fit against observations.

Overall it is clear that in estuaries, the cross-sectional area is related to a total peak discharge Q_{peak} that consists of the sum of the river discharge Q_{river} and a representative maximum tidal discharge Q_{tide} or $Q_{t,max}$. As the cross-sectional area is a product of the channel depth and channel width, the channel width can be related to this total peak discharge. If the channel depth is constant along the channel or the channel depth increases with increasing total peak discharge, the channel width increases with increasing total peak discharge. This means that $B \sim Q_{peak}^{\beta}$. This could explain the converging estuary shape, as the total peak discharge increases in an estuary from the landward boundary to the mouth. Furthermore, this equation is comparable to equation 2.9 for rivers. Savenije (2005) indeed argued that the similarity between the hydraulic geometry equations of rivers and estuaries suggests that the morphology of these both do not differ considerably. The difference is that in estuaries, the peak tidal discharge needs to be included next to the river discharge.

3 Research objective

The discussed literature (section 2) indicates that there is no clear theory on why an estuary forms a convergent channel shape and what determines the estuary length. The research on the morphodynamic equilibrium of estuaries mainly studies the equilibrium bed level of an estuary with fixed channel banks with a fixed prescribed convergence and estuary length. Research that does include adjustable channel banks often only includes erosion processes, and the width profile does not stabilise. This thesis will study the convergent channel shape (width ratio and e-folding length) and estuary length by using a one-dimensional hydrodynamic and morphodynamic model that includes an adjustable channel width. A one-dimensional model is chosen as the computational time is much shorter than in a two-dimensional model. In this one-dimensional model, the channel convergence and the estuary length will be self-formed and will be an effect of the boundary conditions and channel characteristics. Furthermore, with this model it can be studied how the bed level and channel width respond to each other if both are adjustable.

The one-dimensional model of Iwantoro et al. (2021) that can model channels in estuaries was extended to include a time variable width. The width adjustment in the model is based on the variable width in the river model of Miori et al. (2006) and Kleinhans et al. (2011), as this model reaches an equilibrium in bed level and width profile when modelling rivers, so there is a greater chance that the model will reach an equilibrium when modelling an estuary than a model that only includes an erosion law. For the empirical hydraulic geometry relation that the model uses, a relation that relates the channel width to the total discharge peak is chosen based on Sassi et al. (2012) and O'Brien (1931).

The main question that will be answered with the results of the model is:

What is the effect of a dynamic width on the morphodynamic equilibrium of estuaries?

As discussed, Braat et al. (2017) hypothesised that the tidal prism, which is related to the total peak discharge, could continue to increase with increasing width, so it is not directly expected that the model will reach an equilibrium. Furthermore, the discussed studies (section 2.1 and 2.2) overall showed that the relative strength of the tidal and fluvial influence would probably be essential factors determining channel convergence. The e-folding length scale and width ratio are often dependent on the tidal amplitude and (indirectly) on the river discharge. The estuary length could also depend on the tidal amplitude and indirectly on the river discharge through the depth upstream. Moreover, the reviewed studies show that the relative strength of the tide versus the river is important for the bed level profile. The model results of this study will confirm or contradict these hypotheses by showing if the modelled estuary reaches an equilibrium in width profile and bed level profile and on to what extent this equilibrium is depended on the boundary conditions (tidal amplitude, river discharge) and channel properties (bed slope, depth, friction). It is moreover important that the effect of the used empirical hydraulic geometry relation, initial channel shape and other chosen model parameters on the results will be studied. This all led to the following sub-questions:

- Does the width and bed level profile reach an equilibrium?
- In what way do the width profile (width ratio, e-folding length scale), the bed level profile (depth, slope) and the estuary length depend on changes in boundary conditions, like tidal amplitude and river discharge?
- In what way are the width profile (width ratio, e-folding length scale), the bed level profile (depth, slope), and estuary length dependent on changes in channel properties, like initial channel depth, initial bed slope and drag coefficient?
- How do the width ratio, e-folding length scale, depth and estuary length depend on the tide dominance ratio?
- In what way do the width profile (width ratio, e-folding length scale), bed level profile (depth, slope) and estuary length depend on the prescribed hydraulic geometry relation?
- What hydraulic geometry relations (next to the prescribed one) do the modelled estuaries follow?
- Is the equilibrium in width and bed level profile dependent on the initial channel shape, chosen time scale for width adjustment or chosen Exner equation? If yes, to what extent?

To answer these questions, first, a set of model runs will be done where the width can adjust, but the bed level is fixed, so the channel depth and slope can not adapt. This will be done to isolate the effect of the boundary conditions

and channel properties on the estuary width profile. Second, a set of model runs will be performed where both the width and bed level can adjust to the boundary conditions and channel properties. These runs will show the effect of an adjustable width on the bed level. Furthermore, in comparing the two sets of runs, the effect of the combination of an adjustable width and bed level on the width profile, the bed level profile and the estuary length will be made clear. All results together will show if tide dominance is a controlling factor in determining the width ratio, estuary length or e-folding length scale and what hydraulic geometry relations the model produces.

4 Method

In this section the model of this study will be explained. The hydrodynamic calculations and morphodynamic calculations for the sediment transport and the bed level update will first be discussed. These are based on an existing model. Thereafter the adjustment to the existing model to include channel width adjustment will be explained. Furthermore, this section contains a description of all the model runs that were performed and a short explanation of the result analysis.

4.1 Model

The model that is used in this thesis is based on the model from Iwantoro et al. (2021), a 1-dimensional numerical model that simulates the hydro- and morphodynamics of a bifurcating channel in a delta. The focus in this thesis lies on the effect of width adjustment to an estuary's hydro- and morphodynamics, so a more simple model that simulates one channel was derived from Iwantoro's model. This model first calculates the hydrodynamics, then determines the sediment transport and then updates the bed level accordingly. The channel width in this model can not adapt, so the model was extended to accommodate an adjustable channel width. Some of the used notations are explained in figure 6.

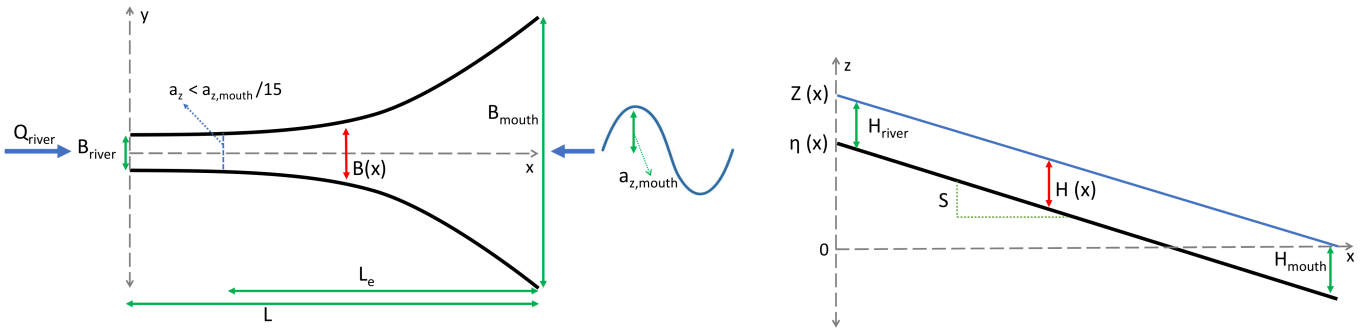

(a) Planform view

(b) Side view

Figure 6: Sketch of used notations. Note that the sea level is taken as the reference level for the z-axis.

4.1.1 Hydrodynamics and morphodynamics

The hydrodynamics are computed by solving the Saint-Venant equations, that represent the mass and momentum balance:

$$B\,\frac{\partial Z}{\partial t} + \frac{\partial Q}{\partial x} = 0 \tag{4.1}$$

$$\frac{\partial Q}{\partial t} + \frac{\partial}{\partial x}\left(\frac{Q^2}{A}\right) + g\,A\,\frac{\partial Z}{\partial x} + C_d\,\frac{|Q|\,Q\,W_p}{A^2} = 0 \tag{4.2}$$

where B is the channel width (m), Z is the water level (m), Q is the discharge (m^2/s), A is the cross-sectional area (m^2), g is the gravitational acceleration (m/s^2), C_d is the drag coefficient (-) and W_p is the wetted perimeter (m). x and t are the spatial (m) and temporal (s) axes. The drag coefficient can be related to the Chézy coefficient C ($m^{1/2}/s$) by $C_d = g/C^2$. The Saint-Venant equations are solved with an implicit Preissmann scheme. For more details see Cunge (1980) and Iwantoro et al. (2021). It will be assumed that the channel width evolves on a long time scale

and the width is therefore not changing within a tidal cycle.

An open boundary is present at the channel's upstream and downstream ends. At the upstream boundary, a river discharge Q_{river} can be imposed. The water level can be forced with a tide at the downstream boundary. This tide can consist of different constituents with different periods T (s), tidal water level amplitudes a_z (m) and phases ϕ (rad). When just one tidal constituent is used, the equation will look as follows:

$$Z_{mouth} = a_z \sin\left(\frac{2\pi}{T}\, t - \phi\right), \tag{4.3}$$

where $\omega = 2\pi/T$ is the angular velocity of the tide (1/s).

The sediment transport in the channels is computed by the method developed by Engelund and Hansen (1967) or Van Rijn (1984) and Rijn (1984). The advantage of using the van Rijn method is that the bedload and suspended load can be computed separately. However, the bed level showed more instabilities when using this method, so the Engelund and Hansen method was eventually preferred and used. In the method of Engelund and Hansen (1967) the total sediment transport Q_s (m^3/s) is calculated as

$$Q_s = q_b^\star \sqrt{R\, g\, D_{50}^3}\, B \tag{4.4}$$

with $q_b^\star$ the dimensionless total sediment load per unit width (-), D_{50} the median grain size (m), and R the specific gravity of sediment (-). $R = (\rho_s/\rho) - 1$, with ρ_s the density of sediment (kg/m^3) and ρ the density of water (kg/m^3). The total sediment load per unit width is determined by

$$q_b^\star = \frac{0.05\,\theta^{2.5}}{C_f}, \tag{4.5}$$

with θ the Shields number (-) and C_f the friction coefficient (-). The Shields number is calculated with

$$\theta = \frac{\tau_b}{\rho\, R\, g\, D_{50}}, \tag{4.6}$$

with the bed shear stress τ_b (N/m^2):

$$\tau_b = C_f\, \rho\, U^2, \tag{4.7}$$

where U is the flow velocity (m/s). The friction coefficient C_f is based on the White-Colebrook formulation (Kleinhans, 2005):

$$C_f = \left(5.75\, \log_{10}\left(\frac{12.2\, H}{k_s}\right)\right)^{-2}, \tag{4.8}$$

with k_s the roughness height (m) and H the depth (m). The value of 5.75 is related to the Von Karman constant v_k ($= 0.4$): $5.75 = \frac{1}{\log_{10}(e^1) v_k}$.

The bed level change is computed by solving the Exner equation for sediment conservation:

$$\frac{\partial \eta}{\partial t} = \frac{1}{(1 - p_s)\, B} \frac{\partial Q_s}{\partial x}, \tag{4.9}$$

where η is the bed level (m), p_s is the bed sediment porosity (-), and Q_s is the total sediment transport (m^3/s). The Exner equation is solved with a modified FTCS scheme (Forward in Time, Central in Space), for details see Iwantoro et al. (2021). A morphological acceleration factor $Morfac$ is used to accelerate the computational duration. This is done by multiplying the total sediment transport Q_s with this factor before computing the bed level change. However, this acceleration factor affects the stability. Iwantoro et al. (2021) found that the condition for numerical stability is:

$$Morfac \frac{Q_s}{A} \frac{\Delta t}{\Delta x} \leq 1 \tag{4.10}$$

The model has two different methods to calculate the morphodynamic change. The first method is as described

above. The morphodynamic change is calculated every time step with the morphological acceleration factor, and the bed is updated accordingly. This method will be called the standard morfac method. For the second method the morphodynamic change is not calculated every time step but every tidal cycle. The total sediment transport is saved every time step for one entire tidal cycle. The average total sediment transport over the tidal cycle is then calculated at every spatial step. This average transport is then multiplied by the $Morfac$, and the morphodynamic change is computed. (In this case, $\Delta t = T$, instead of the chosen model time step.) This method will be called the tidally averaged morfac method.

4.1.2 Width adjustment

To accommodate width adjustment in the model, Kleinhans et al. (2011) developed a method to include width evolution in a 1D river bifurcation model. This method was partly based on Miori et al. (2006), who developed a method for width adjustment for a 1D model of bifurcations in a gravel-bed river. This method was chosen, as the model of Kleinhans et al. (2011) evolved toward a stable width in rivers, so an equilibrium was reached. Other studies (mentioned in section 2.2) showed a constant increase in width. This method of Kleinhans et al. (2011) has already been briefly discussed in section 2.2.

A new equation for the width evolution over time is needed to include a variable width in the model. The assumption is made that the width evolves towards an equilibrium width, so the actual width is a relaxation to this equilibrium:

$$\frac{\partial B}{\partial t} = \frac{B_e - B}{T_w}, \tag{4.11}$$

where B_e is the equilibrium width (m) and T_w is a time scale for width adaptation (s). A relation needs to be applied to calculate the equilibrium width. Kleinhans et al. (2011) used an empirical hydraulic geometry relation of the form

$$B_e = a\, Q_{river}^{b}, \tag{4.12}$$

where the width depends on the river discharge. As in this thesis, tidally influenced estuaries will be simulated, the tidal influence must be incorporated. As explained in section 2.3, Sassi et al. (2012) developed a downstream hydraulic geometry relation for a tidally influenced delta:

$$A = \alpha_A \left(Q_{river} + Q_{t,max}\right)^{\beta_A}, \tag{4.13}$$

with Q_{river} the river discharge and $Q_{t,max}$ the maximum discharge amplitude. As a relation for the width instead of the cross-sectional area is needed, the assumption is made that the width also follows a like wise power-law relation:

$$B_e = \alpha_t \left(Q_{river} + Q_{t,max}\right)^{\beta_t}. \tag{4.14}$$

If this relation is used for the width adjustment, the river discharge Q_{river} and the maximum tidal discharge amplitude $Q_{t,max}$ needs to be computed. The river discharge Q_{river} is equal to the tidally averaged discharge $\overline{Q}$ and can be calculated by taking the mean of the discharge of the previous tidal cycle. The maximum tidal discharge amplitude $Q_{t,max}$ can be determined by performing a harmonic analysis on the discharge of at least the last tidal cycle. Performing a harmonic analysis costs much computational time. As the choice for a 1-dimensional model is based on the computational time, another power-law relation is eventually used. Instead of the maximum tidal discharge amplitude, the tidal discharge peak Q_{tide} was used. The tidal discharge peak Q_{tide} can be determined as follows

$$Q_{tide} = \max(\,|Q(t) - Q_{river}|\,). \tag{4.15}$$

The eventual used equation for the equilibrium width than becomes

$$B_e = \alpha \left(Q_{river} + Q_{tide}\right)^{\beta}. \tag{4.16}$$

That O'Brien (1931) showed that the cross-sectional area also related to the peak discharge $Q_{peak} = Q_{river} + Q_{tide}$, as mentioned in section 2.3, further justified this choice.

Furthermore, a choice for the time scale for width adjustment T_w needs to be made. Kleinhans et al. (2011) showed that the equilibrium configuration of the river bifurcation did not depend on this time scale. Only the time it took to reach this equilibrium depends on this time scale. Still, a derivation for the time scale was shown and led to the equation:

$$T_w = \frac{B\,H}{\gamma_b\,q_s}, \tag{4.17}$$

where q_s is the sediment transport rate per unit width (m^2/s) ($q_s = \frac{Q_s}{B}$). In the derivation for this time scale, it is assumed that $B\,H$ is the unit volume of sediment involved in changing the local cross-sectional area and $q_{s,bank}$ is the local sediment transport rate causing the change. It is then furthermore assumed that the sediment transport rate that contributes to erosion or accretion of the bank is a fraction γ_b of the total sediment transport rate per unit width ($q_{s,bank} = \gamma_b\,q_s$). Kleinhans et al. (2011) chose a γ_b of H/B as a first approximation. This fraction will be no good approximation in estuaries, as channel widths can increase much from the upstream boundary of the estuary to the mouth, and H/B can have large variations along the estuary. As an example, if a γ_b equal to H/B would be used in an estuary where the channel width increases with a factor 10 from upstream to the mouth and the depth is constant, the time scale T_w will be 100 times larger at the mouth in comparison to the upstream boundary of the estuary. As there is quite some uncertainty in determining a relation for the time scale of width adjustment, a constant fixed time scale is chosen. A set of model runs will be done where this timescale is changed to check the effect of this timescale on the results of the model (further explained in section 4.2.2).

Next to adding the equation for width evolution to the model, Kleinhans et al. (2011) included the width change in the Exner equation, so the sediment is conserved. If the width increases, sediment is eroded from the banks and is deposited on the bed. If the width decreases, sedimentation occurs on the banks and this is sediment is taken from the bed. The Exner equation will then become:

$$\frac{\partial \eta}{\partial t} = \frac{1}{(1-p_s)\,B}\frac{\partial Q_s}{\partial x} + \gamma\,\frac{\partial B}{\partial t}\,\frac{H}{B} = 0, \tag{4.18}$$

where η is the bed level (m), p_s is the sediment porosity (m), B is the channel width (m), Q_s is the total sediment transport (m^3/s), and H is the channel depth (m). $\gamma = 1$ if the width adjustment is incorporated in the sediment balance and $\gamma = 0$ if the width adjustment is not incorporated in the sediment balance. If $\gamma = 0$ the equation reduces to equation 4.9.

4.2 Model runs

Runs were first performed that included an adjustable width but did not include morphodynamic changes to the bed, so the bed was stable in time. This was done to single out the influence of the channel properties and boundary conditions on the width profile. This is precisely opposite to modelling research, where the bed level is variable, but the channel width is fixed, to study the bed level. As these first runs do not include a changing bed, the sediment transport is not calculated. The model only calculates the hydrodynamics, then calculates the width change after every tidal cycle and updates the width (see figure 7a). Second, a set of runs was done, including an adjustable bed and width. For these runs, it was first chosen not to incorporate the width change in the Exner equation, so equation 4.18 with a γ of 0 was used (see figure 7b). A few runs were done that did use this new Exner equation (equation 4.18 to check the effect of including the width change in the sediment balance, see figure 7c). As mentioned in section 4.1.2, determining an equation for the time scale is complex. Furthermore, Kleinhans et al. (2011) showed that the eventual equilibrium of rivers did not even depend on the time scale for width change. This is why a short constant time scale for width change T_w was chosen at first in both the set of runs with and without an adjustable bed, so the computation time can be as short as possible. A few runs with an adjustable bed were later done where this time scale was changed to check the effect of the time scale for width change.

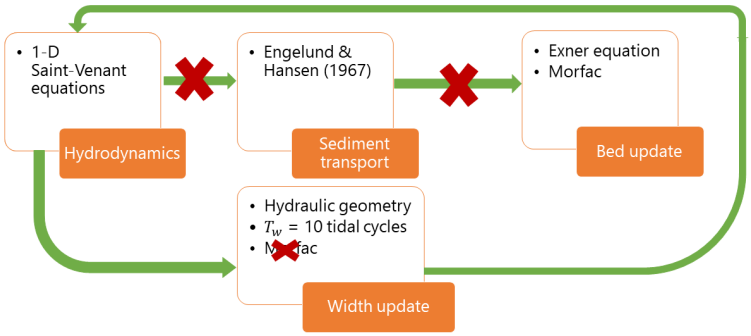

(a) For runs with a stable bed

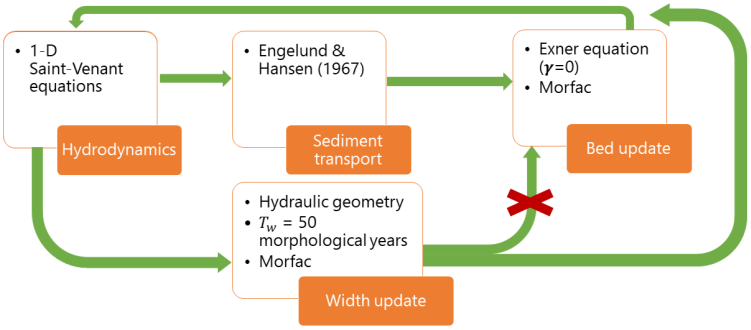

(b) For runs with an adjustable bed and $\gamma = 0$

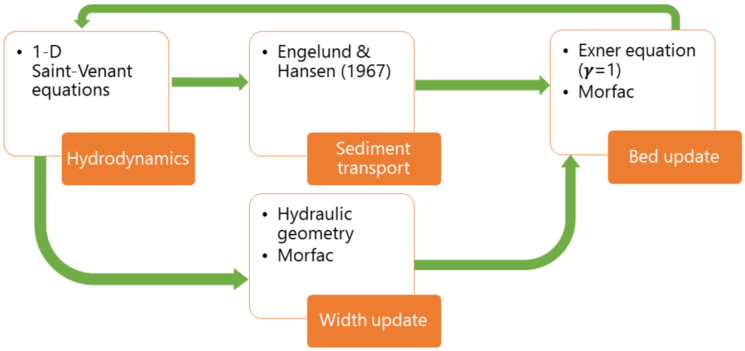

(c) For runs with an adjustable bed and $\gamma = 1$

Figure 7: Schematisation of the modelling processes each tidal cycle in a) runs with a stable bed, b) runs with an adjustable bed, where $\gamma = 0$, so the width adjustment is not included in the Exner equation and c) runs with an adjustable bed, where $\gamma = 1$, so the width adjustment is included in the Exner equation.

The detailed settings of all runs done will be explained further on, but first, the default settings of all the runs will be presented. All channels start as a straight channel with a long length $L = 400$ km, as the tide needs to be died out at the upstream boundary. The spatial step Δx for the numerical scheme is chosen as 500 m, so the channel consists of 801 nodes. The water level at the downstream boundary was forced with a semidiurnal tide with a period of 12 hours and a default tidal amplitude $a_{z,0}$ of 1.5 m. For the default settings of the model parameters α and β, a first estimate was made based on the hydraulic geometry of rivers. A β of 0.5 was chosen as most rivers correspond to this β (see 2.3). The data of Xu et al. (2021) shows that quite some hydraulic geometry relations have an α around 4. Furthermore, Leuven, Verhoeve, et al. (2018) who made an empirical assessment tool for bathymetry, flow velocity and salinity in estuaries used for the hydraulic geometry relation of the upstream river the relation developed by Hey and Thorne (1986), where $B = 3.67Q^{0.45}$. This led us to eventually choose an α of 4 as a first approximation. In table 2, the values of the other parameters and boundary conditions are shown for the default settings. A small default bed slope S_0 of 3×10^{-5} and default drag coefficient $C_{d,0}$ of 2.725×10^{-3} were prescribed. As upstream the width needs to be constant over time, the river discharge needs to follow the used empirical hydraulic geometry relation:

$$Q_{river} = \left(\frac{B}{\alpha}\right)^{1/\beta}. \tag{4.19}$$

this leads to a default river discharge $Q_{river,0}$ of 306.25 m^3/s with the chosen default initial width B_0 of 70 m. If the

Chézy equation:

$$U = \sqrt{\frac{g\,S\,H}{C_d}}, \tag{4.20}$$

is combined with the fact that:

$$Q = U\,B\,H, \tag{4.21}$$

it follows that the default depth H_0 needs to be around 6 m.

Parameter	Value
Spatial step Δx	500 m
Time step Δt	300 s
Channel length L	400 km
Initial channel width B_0	70 m
Bed slope S_0	3e−5
Drag coefficient $C_{d,0}$	2.725×10^{-3}
River discharge $Q_{river,0}$	306.25 m^3/s
Depth H_0	6 m
Tidal amplitude $a_{z,0}$	1.5 m
Period of tide T	12 h
Model parameter α_0	4
Model parameter β_0	0.5
Median grain size D_{50}	0.25×10^{-3} m
Roughness height k_s	0.035 m
Sediment porosity p	0.35
Gravitational acceleration g	9.81 m/s^2
Sediment density ρ_s	2650 kg/m^3
Water density ρ	1000 kg/m^3

Table 2: Values of the default settings.

4.2.1 Runs with only width update and a stable bed

All runs with an adjustable width but stable bed were run for 5 years with a time step Δt of 300 seconds. The timescale for width change T_w was set to ten tidal cycles, so 5 days. In figure 7a a schematisation is given for the runs with a stable bed. In the first set of runs, the upstream boundary only needs to follow the empirical hydraulic geometry relation (equation 4.19), so the system did not always have an equilibrium depth. The set of runs that was done (for which the parameter value ranges can be found in table 3) is:

1. Name: Tidal amplitude: The tidal amplitude is changed relative to the default settings, and everything else is kept the same.
2. Name: Discharge+B: The upstream river discharge is changed relative to the default settings. As the upstream boundary needs to meet the empirical relation between discharge and width, the initial width of the channel is changed accordingly. Everything else is kept the same.
3. Name: Slope: The slope of the channel is changed relative to the default settings, and everything else is kept the same.
4. Name: Depth: The depth of the channel is changed relative to the default settings, and everything else is kept the same.

5. Name: Drag coefficient: The drag coefficient is changed relative to the default settings, and everything else is kept the same.

6. Name: Alpha+Q: The model parameter α is changed relative to the default settings. As the upstream boundary needs to meet the empirical relation between discharge and width and the width is kept the same, the river discharge is changed accordingly. Everything else is kept the same.

7. Name: Beta+alpha: The model parameter β is changed relative to the default settings. As the upstream boundary needs to meet the empirical relation between discharge and width and the discharge and width are kept the same, the coefficient α is also changed accordingly.

Changing parameter	Values
Tidal amplitude a	0.25 m, 0.5 m, 0.75 m, 1 m, 1.5 m, 2 m, 2.5 m, 3m
River discharge Q_r	50 m^3/s, 100 m^3/s, 150 m^3/s, 200 m^3/s, 250 m^3/s, 300 m^3/s, 350 m^3/s
Slope S	1e-5 2.5e-5, 5e-5, 7.5e-5, 1e-4, 2.5e-4
Depth H	3 m, 4 m, 5 m, 6 m, 7 m, 8 m, 9 m, 10 m, 11 m, 12 m
Drag coefficient C_d	2e-3, 2.25e-3, 2.5e-3, 2.75e-3, 3e-3, 3.25e-3, 3.5e-3, 3.75e-3, 4e-3
α	2, 4, 6, 8, 10
β	0.25, 0.5, 0.65, 0.75, 0.85, 0.95

Table 3: Values of the changing parameters with only width update, no bed update and where the upstream boundary only follows the empirical hydraulic geometry relation.

A second set of runs was done where it was additionally assumed that the upstream river followed the Chézy equation (equation 4.20), so the system has an equilibrium depth. The prescribed channel depth is then determined according to

$$H = \sqrt{\frac{Q^2\, C_d}{g\, S\, B}}. \tag{4.22}$$

A larger channel depth is prescribed if the river discharge or drag coefficient increases or the slope decreases. When the model parameter α is increased, the prescribed river discharge is additionally decreased, so the hydraulic geometry relation is met (equation 4.19), so the prescribed channel depth is also decreased. When the model parameter β is increased, this time the prescribed river discharge is also additionally decreased, so the hydraulic geometry relation is met, so the prescribed channel depth also decreases. The second different set of runs that was done (for which the parameter value ranges can be found in table 4) is:

1. Name: Discharge+B+H: The upstream river discharge is changed relative to the default settings. As the upstream boundary needs to meet the empirical relation between discharge and width, the initial width of the channel is changed accordingly. As the upstream boundary moreover needs to meet the Chézy equation, the channel depth is changed accordingly. Everything else is kept the same.

2. Name: Slope+H: The bed slope is changed relative to the default settings. As the upstream boundary moreover needs to meet the Chézy equation, the channel depth is changed accordingly. Everything else is kept the same.

3. Name: Drag coefficient+H: The drag coefficient is changed relative to the default settings. As the upstream boundary moreover needs to meet the Chézy equation, the channel depth is changed accordingly. Everything else is kept the same.

4. Name: Alpha+Q+H: The model parameter α is changed relative to the default settings. As the upstream boundary needs to meet the empirical relation between discharge and width, the river discharge is changed accordingly. As the upstream boundary moreover needs to meet the Chézy equation, the channel depth is changed accordingly. Everything else is kept the same.

5. Name: Beta+Q+H: The model parameter β is changed relative to the default settings. As the upstream boundary needs to meet the empirical relation between discharge and width, the river discharge is changed accordingly. As the upstream boundary moreover needs to meet the Chézy equation, the channel depth is changed accordingly. Everything else is kept the same.

Changing parameter	Values
River discharge Q_r	50 m^3/s, 100 m^3/s, 200 m^3/s, 400 m^3/s, 600 m^3/s, 800 m^3/s, 1000 m^3/s
Slope S	1e-5 2.5e-5, 5e-5, 7.5e-5, 1e-4, 2.5e-4
Drag coefficient C_d	2e-3, 2.5e-3, 3e-3, 3.5e-3, 4e-3, 5e-3, 6e-3
α	2, 4, 6, 8, 10
β	0.25, 0.5, 0.65, 0.75

Table 4: Values of the changing parameters with only width update, no bed update and where the upstream boundary follows the empirical hydraulic geometry relation and the Chézy equation.

4.2.2 Runs with width and bed update

Runs were performed that included and adjusting bed level next to an adjusting channel width to study how the bed responses to the width adjustment. Using the tidally averaged morfac method for the bed update would be logical as the width changes every tidal cycle. However, instabilities quickly occurred in the bed level when this method was used. These instabilities were an effect of the sediment transport being tidally averaged and the time step of morphodynamic change being equal to a tidal period, which is quite large relative to the model time step of 300 seconds. This led to non-continuous sediment transport. This is why the standard morfac method was used for the bed update. The width update was then also done using this standard morfac method. This meant that every time step, the mean discharge Q_0 and the tidal discharge peak Q_{tide} of the last 12 hours was computed and used for the width update of that time step.

The runs with width and bed change all consisted of three sequential runs, where the output of the previous run was used as input for the next run. These three sequential runs have different morphological factors and are run for different run times. Where the morphological factor is increased with respect to previous run. This was done because the morphological change is at first quite extensive, and no large $Morfac$ factor can be used, as equation 4.10 will not be met. When the morphological change is more minor, a larger $Morfac$ can be used to speed up the computation. The first sequential run had a $Morfac$ of 30 and a run time of 10 years, so 300 morphological years were simulated. The second sequential run had a $Morfac$ of 300 and a run time of 7 years, so 2100 morphological years were simulated. The third and last sequential run had a $Morfac$ of 4000 and a run time of 12 years, so 48000 morphological years were simulated. In total, the three runs together simulate 50400 morphological years. The time scale of width change T_w was still set to 10 run time tidal cycles in the first two runs of 10 years with a $Morfac$ of 30 and of 7 years with a $Morfac$ of 300. In the last runs of 12 years with a $Morfac$ of 4000, the time scale of width change was set to a value of 50 morphological years. For all these runs with width and bed change, the width change was not incorporated into the Exner equation, so equation 4.18 with a γ of 0 was used. In figure 7b a schematisation of the processes in these runs is shown.

The first set of runs with width and bed change were equivalent to the first set of runs with width but without bed change, only with a smaller parameter value range (see table 5), so the upstream river only needed to follow the empirical hydraulic geometry relation 4.19. These runs will be called: “Tidal amplitude+bed”, “Discharge+B+bed”, “Slope+bed”, “Depth+bed”, “Drag coefficient+bed”, “Alpha+Q+bed”, “Beta+alpha+bed”. The second set of runs where the upstream river also needed to follow the Chézy equation (equation 4.20) was not done as the depth upstream can adapt to the hydrodynamics in the runs with width and bed change.

Changing parameter	Values
Tidal amplitude a	0.5 m, 1 m, 1.5 m, 2 m, 3m
River discharge Q_r	50 m^3/s ,150 m^3/s, 250 m^3/s, 350 m^3/s, 450 m^3/s
Slope S	1e-5, 7.5e-5, 1e-4
Depth H	4 m, 8 m, 10 m, 12 m
Drag coefficient C_d	2.25e-3, 3.5e-3, 4e-3
α	2, 4, 6, 8, 10
β	0.25, 0.5, 0.65, 0.75, 0.85

Table 5: Values of the changing parameters with width and bed update.

Four other different sets of runs were done to check the effect of the time scale of width adjustment, the initial channel shape and the different Exner equation on the equilibrium. In all these sets of runs the time scale of width adjustment was changed relative to the other runs with an adjustable bed. The time scales were chosen such that they would be close to the time scale for bed change or even bigger. This meant that first a run needed to be done where only the bed level could change and the channel width was fixed to determine the time scale for bed change (run called: "Only bed+default"). It was chosen to do this run with the default settings. This runs showed that the time scale for bed change lies around 20000 morphological years in this case. It is expected that using a time scale for width adjustment around 20000 morphological years will lead to the runs not reaching an equilibrium in the 48000 morphological years all other runs with a movable bed are simulated. That is why every run in these four different sets of runs where the time scale for width change is large, will consist of four sequential runs instead of three. A fourth run will be added with a $Morfac$ of 4000 that will be run for 12 years, so the total run time of all four sequential runs combined is 98400 morphological years. In all four sequential runs the time scale for width change will be the same.

In the set of runs called "Tw+bed", only the time scale of width adjustment was changed relative to the default settings. The chosen time scales are: 2500, 10000, 20000 and 35000 morphological years. In the set of runs called "Tw+exner+bed", all runs use the new Exner equation (equation 4.18 with $\gamma = 1$), where the width change is incorporated in the sediment balance. Furthermore, is the time scale for width adjustment changed, where the chosen time scales are: 5000, 10000, 20000 and 35000 morphological years. As in these runs the width update is taken into account in the Exner equation, these runs follow the process cycle as schematised by figure 7c. Lastly, two different sets of runs were done where the initial channel was not straight, but converging, with an e-folding length scale of 30 km for the last 100 km of the channel. The first 300 km of the channel is straight. In the set of runs called "Tw+Lb+bed", in all runs the initial shape of the channel is convergent and the time scale for width adjustment was furthermore changed in every run. In the set of runs called "Tw+Lb+Exner+bed", in all runs the initial shape of the channel is convergent and the new Exner equation (equation 4.18 with $\gamma = 1$) is used, and the time scale for width adjustment is changed every run. In both these set of runs the chosen time scales are: 5000, 10000, 20000 and 35000 morphological years.

4.2.3 Characteristics derived from the model output

Various characteristics were derived from the model output. The width ratio $\frac{B_{mouth}}{B_{river}}$, the e-folding length scale L_b and the estuary length L_e are determined. The width ratio is the ratio between the width at the mouth and the width upstream and represents the spatial change in width. The e-folding length scale is determined by fitting an exponential function to the width profile. This fit is done from the location where the width has increased by more than 1 m with respect to the upstream boundary to the mouth. In figure 8 the fit to the width profile of the runs called "Tidal amplitude", where the bed was fixed, and the tidal amplitude was changed, is shown. For the estuary length, it is assumed that the estuary ends where the tidal water level amplitude a_z becomes less than one-fifteenth of the tidal amplitude at the mouth. This means that the estuary length is not directly dependent on the width or bed level profile, but on the water level profile (figure 12 in section 5.1 shows the upstream end of the estuary of the default run with a stable bed).

To analyse the bed profile for the runs where the bed could adjust next to the channel width, the depth at the mouth, the depth upstream, the slope of the estuary and the slope of the upstream river are determined. The slopes

are derived by a linear fit of the bed level. For the estuary slope, the bed level of the last two-thirds of the estuary is fitted, and for the upstream slope, the bed level from the upstream channel boundary to the upstream estuary boundary is fitted.

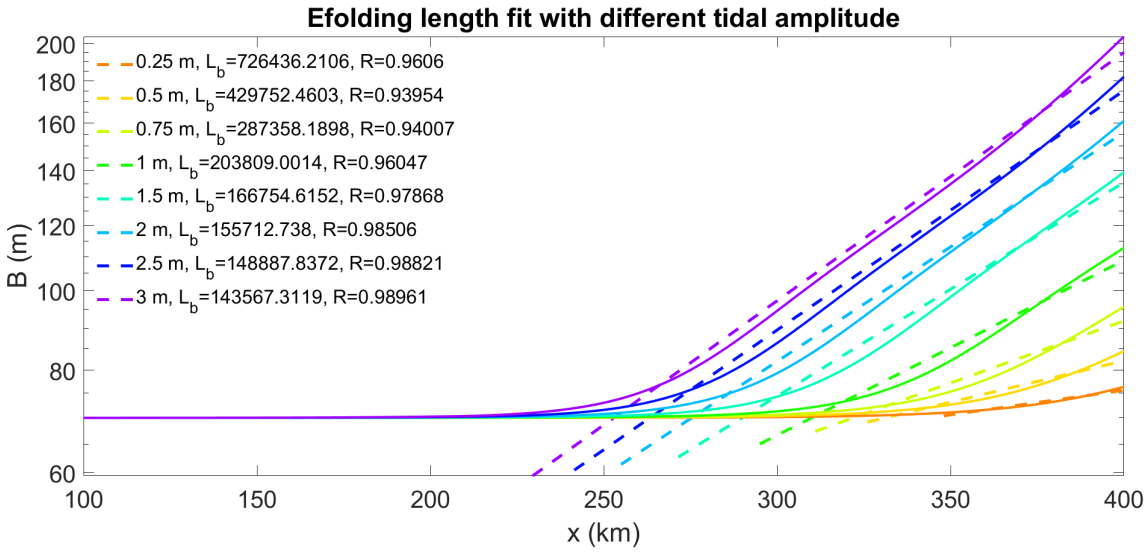

Figure 8: An example of how the e-folding length is fitted from the width profile for the runs called: Tidal amplitude

5 Results

The results of all the model runs that were performed (see section 4.2 for details) will be discussed in this section. First, the width profiles and estuary characteristics of the runs with an adjustable width but stable bed level will be analysed, and second, the width profiles, bed level profiles and estuary characteristics of the runs with an adjustable width and bed are discussed. After that the results of the runs with a different time scale for width adjustment, different initial channel shape and different Exner equation will be considered. Lastly, the results of these runs together are used to determine if estuary characteristics can be linked to tide dominance and to study the hydraulic geometry relations the model produces.

5.1 Results of runs with adjustable width and stable bed level

5.1.1 Is an equilibrium reached?

In the default run with an adjustable width but a stable bed level, the width profile first evolves fast and then stabilises, as shown in figure 9. This behaviour can besides be observed in the absolute rate of change of the width dB/dt at the mouth (see figure 10), which is 6.94 m/day at the beginning of the run and then rapidly decreases towards a value of 5.54×10^{-12} after 222 days. Hereafter, dB/dt fluctuates around 5.35×10^{-12} till the end of the run. Furthermore, it can be determined that the width at the mouth stabilises in 100 days for all the runs called "Tidal amplitude" (see figure 11). This all together shows that the width profile approaches a steady state. The same behaviour is observed for all other runs with an adjustable width but stable bed, so all these runs reach an equilibrium in their width profile.

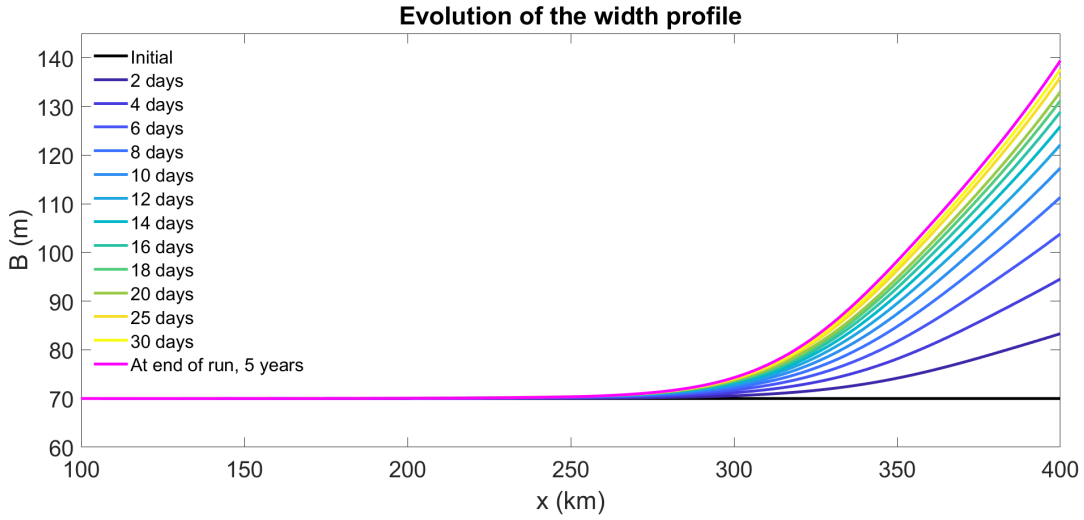

Figure 9: The evolution of the width profile for the default run with a stable bed for the first 30 days and the width profile at the end of the run.

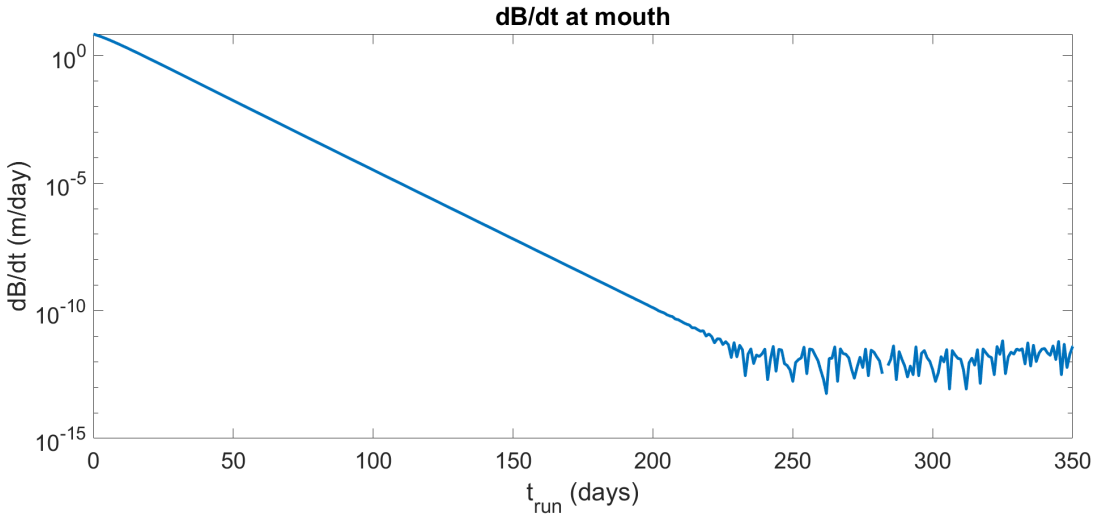

Figure 10: The absolute rate of change of the width $\mathrm{d}B/\mathrm{d}t$ at the mouth over time for the default run with a stable bed.

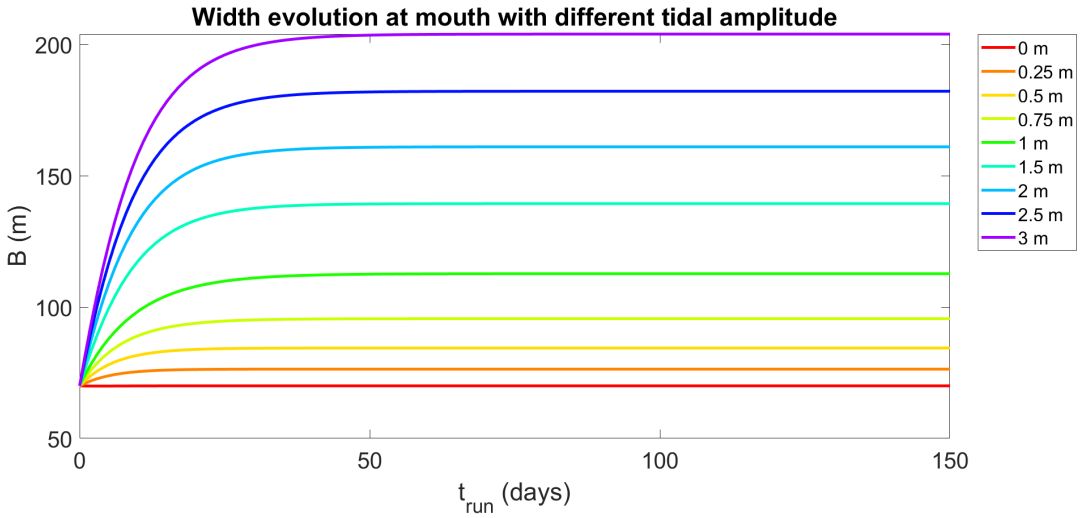

Figure 11: The width evolution at the mouth over time for the runs: Tidal amplitude.

It is clear that the width profile evolves towards an equilibrium, but does the model produce an ideal estuary in terms of amplitude (see section 2.1 for definition)? The water level amplitude a_z of the last tidal cycle of the default run decreases throughout the estuary, as well as the flow velocity amplitude (see figure 12). This means that no ideal estuary has developed. In the other runs with an adjustable width but stable bed, no ideal estuary is developed as well. The width profile needs to be more convergent to develop an ideal estuary, as the bed is stable in these runs. However, apparently, this convergence is limited in the model, probably due to the empirical hydraulic geometry relation used.

The water level amplitude a_z furthermore determines where the upstream boundary of the estuary is located. In section 4.2.3 it was explained that the upstream boundary of the estuary is located where the tidal amplitude is only one-fifteenth of the tidal amplitude at the mouth. In the case of the default run, the upstream boundary of the estuary is located at 295.5 km, so the estuary has a length of 104.5 km (see figure 12). Moreover, the mean flow velocity U_0 is shown in figure 12 and is not spatially constant, the fluctuations are due to the residual currents, an effect of the tidal asymmetry

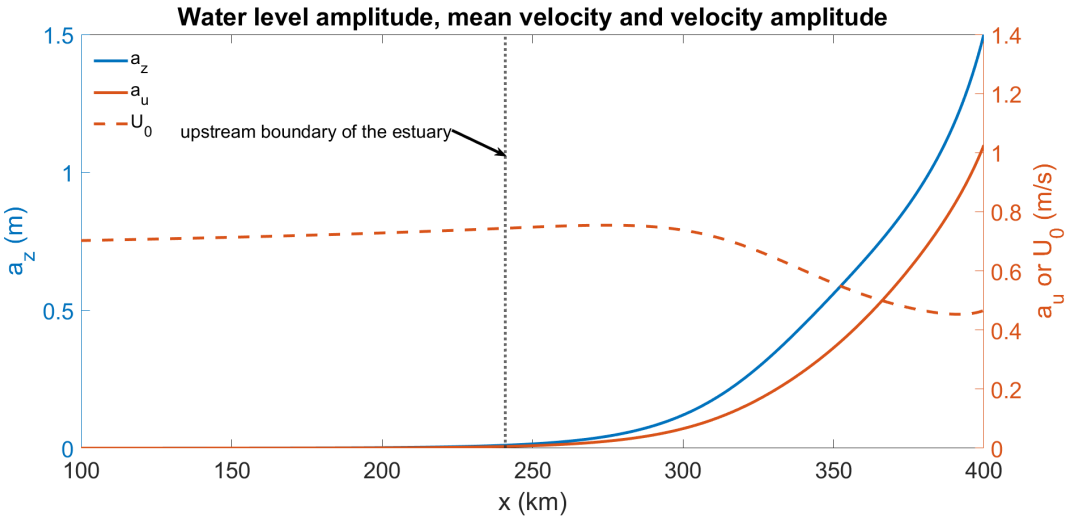

Figure 12: The water level amplitude a_z, flow velocity amplitude a_u and mean flow velocity U_0 of the last tidal cycle throughout the channel of the default run with a stable bed. The determined upstream boundary of the estuary is indicated.

5.1.2 Effect of changing channel properties or boundary conditions

The different runs with an adjustable bed but stable bed resulted in different equilibrium width profiles (see figure 13). From these profiles the width ratio B_{mouth}/B_{river}, length of the estuary L_e and e-folding length scale of the estuary L_b were determined, as explained in section 4.2.3 (see figure 14, 15 and 16). What stands out is that the model does not produce very large width ratios when the model parameters β and α are unchanged and equal to their default setting ($\beta = 0.5$, $\alpha = 4$). The width ratio in those cases varies between 1 and 3.8. When the parameter α is increased the width ratio rises up to 9.2 when $\alpha = 10$. Even bigger width ratios are produced when the parameter β is increased. Moreover, the lengths of the estuaries are quite long, especially when the depth of the channel is increased. The model produces lengths from 32 km to almost 360 km. Furthermore, the model results show relatively large e-folding lengths, when again the model parameters β and α are unchanged. These vary between 90 km and 725 km in those cases.

The trends in the width ratio and length of the estuary are reasonably as expected (see figure 13, 14, 15). The model develops longer estuaries with larger width ratios when the tidal amplitude, the channel depth, or the model parameters α or β are increased. Increasing the tidal amplitude leads to a larger tidal discharge peak throughout the estuary, so the channel width increases. As the upstream discharge is prescribed the same, the upstream width does not change. This results in larger width ratios. The width ratio increases almost linearly with increasing tidal amplitude. As the amplitude is larger, the tidal wave can propagate further up the channel until it dies out due to friction, resulting in a longer estuary. When the channel depth is increased less bed friction dampens the tidal wave, so a longer estuary can develop. This relation between the depth and estuary length is linear. Moreover, increasing the depth leads to a larger tidal discharge peak, so the width increases more. Again the relation between the width ratio and depth is almost linear. If the model parameter α is changed, the model uses a different coefficient in the empirical relation to calculate the channel width (see equation 4.16). If α is increased, the determined channel width is larger for the same discharge. In the runs "Alpha+Q", the upstream width is kept the same, so if α increases, the river discharge also decreases. This results in the tidal wave propagating further up the channel since the wave is damped less by the river discharge, so a longer estuary develops. Furthermore, the downstream width increases more, since less discharge is needed to develop the same channel width. This results in larger width ratios. The relation between the width ratio and the model parameter α is approximately exponential. Likewise, if the model parameter β is changed, the exponent of the empirical hydraulic geometry relation changes (see equation 4.16). Again a larger β leads to larger channel widths with the same discharge. As explained in section 4.2, in the runs "Beta+alpha", when β is increased, α is decreased, so the same river discharge results in the same width upstream. However, downstream

where also the tidal discharge comes into play, the width becomes larger with the same total peak discharge. This leads to a larger width ratio and a somewhat longer estuary.

Shorter estuaries with lower width ratios develop when the river discharge, the slope, or the drag coefficient is increased (see figures 13, 14 and 15). Increasing the river discharge, the slope, or the drag coefficient leads to the tidal wave propagating less far into the channel. In case of an increased river discharge or drag coefficient, the tidal wave is damped more by this larger discharge or larger friction, so shorter estuaries develop. When the slope of the channel is increased, the tidal wave has to propagate onto a steeper slope, so the wave dies out further downstream as well. Furthermore, increasing the river discharge leads to a larger total discharge downstream ($Q_{river} + Q_{tide}$) and upstream (Q_{river}), but the ratio between the total discharge peak downstream and upstream becomes smaller ($(Q_{river} + Q_{tide})/Q_{river}$). This results in a smaller width ratio. When the slope or the drag coefficient is larger, the total upstream discharge is prescribed the same, but the total downstream discharge decreases, leading to smaller width ratios as well.

Figure 14 shows that changing the model parameter α or β has the most effect on the width ratio. The tidal amplitude and the channel depth also have quite some influence. The influence of these two is almost the same. On the other hand, the bed slope has the least effect on the width ratio. The influence of the bed slope on the length of the estuary is of greater importance. However, the drag coefficient has even a bit more effect on the estuary length. The most important parameter influencing the length of the estuary is the channel depth. Interestingly, the model parameter β and α have minimal effect on the estuary length.

In addition to the width ratio and estuary length, the e-folding length scale was studied (see figure 16). Shorter e-folding length scales, so more convergent estuaries develop when the tidal amplitude, slope, drag coefficient, α or β increases or the river discharge decreases. The relation between the e-folding length scale and the depth of the channel is a little less straightforward. If the channel depth increases but is relatively small (< 5 m), the e-folding length scale decreases. However, when the channel depth is increased even more (> 5 m), the e-folding length scale increases again. Again the model parameter α and β have the most influence on the e-folding length scale. The tidal amplitude is moreover important for the e-folding length scale.

The e-folding length scale is determined from the estuary length and the estuary width ratio. If an estuary is more convergent, this can be due to a larger width ratio with the same estuary length or a shorter estuary length with the same width ratio. Of course, a change in width ratio and estuary length is possible as well, and the trend with the steepest slope then determines what the trend in the e-folding length scale will be like. The estuary length is determined by how far the tidal wave can propagate into the channel, whereas the total discharge peak determines the width ratio. When the tidal amplitude or depth increases, the width ratio and the length of the estuary both increase. In the case of the tidal amplitude, the width ratio increases relatively more, so the e-folding length scale decreases. In the case of the depth, the width ratio first increases relatively more, so the e-folding length scale first decreases. However, the width ratio increases relatively less when the depth increases even more (> 5 m), so the e-folding length scale increases.

Increasing the bed slope, the drag coefficient or the river discharge leads to a decreasing width ratio and estuary length. The estuary length decreases relatively more than the width ratio for both the bed slope and drag coefficient. The bed slope has even almost no effect on the width ratio (see figure 14a). The e-folding length scale is related to both the slope and drag coefficient by a power law. When the river discharge and accompanying upstream channel width increases, the width ratio decreases relatively more than the estuary length, resulting in less convergent estuaries. This means that the river discharge and accompanying upstream channel width has more influence on the total discharge peak than on how far the tidal wave can propagate into the estuary.

For the model parameters α and β, the model develops a more convergent estuary if one of these is increased. This is because in both cases, the width ratio increases faster than the estuary length. Especially when the parameter β is increased, as this parameter has almost no effect on the length of the estuary. When α is very small ($\alpha = 2$), the e-folding length scale is suddenly quite large. Such a small value for α leads to the width increasing very little with an increasing total discharge peak, so the channel is almost straight and has a large e-folding length scale.

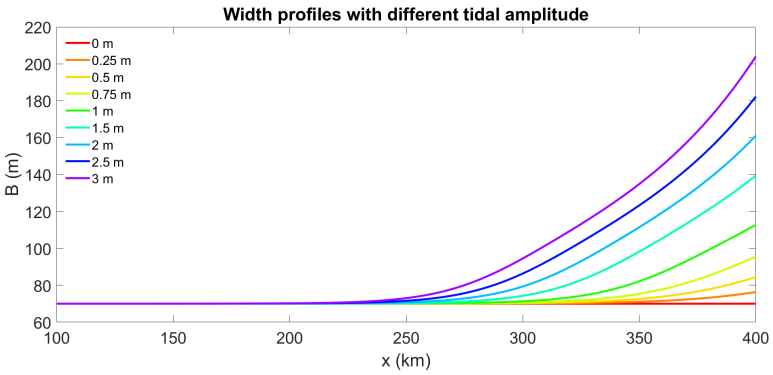

(a) Run: Tidal amplitude

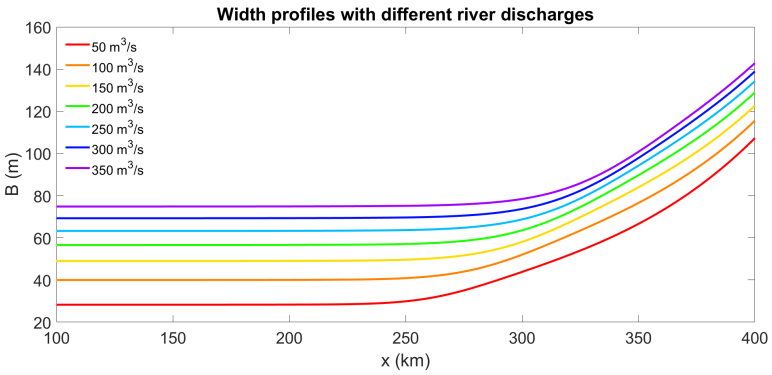

(b) Run: Discharge+B

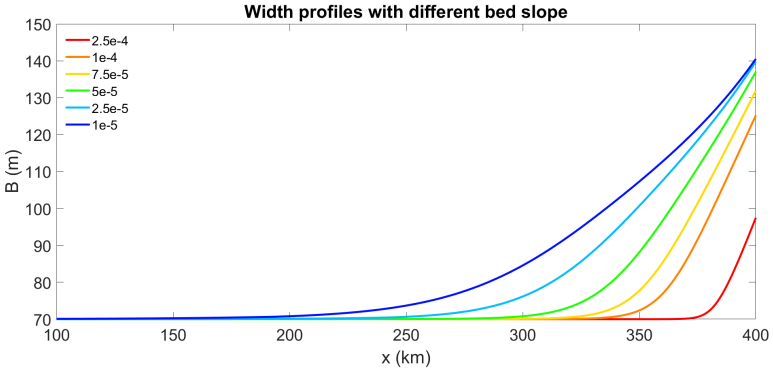

(c) Run: Slope

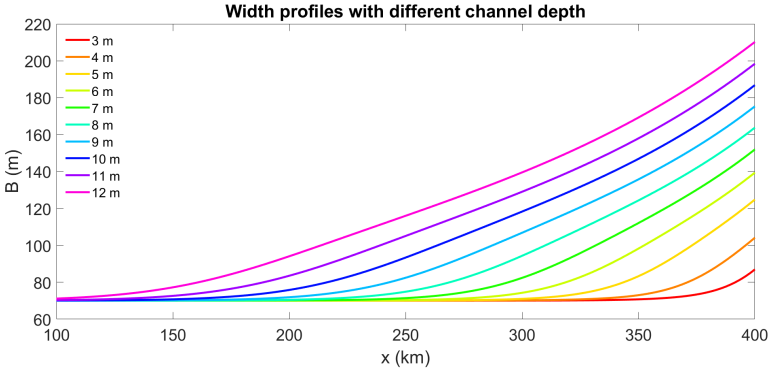

(d) Run: Depth

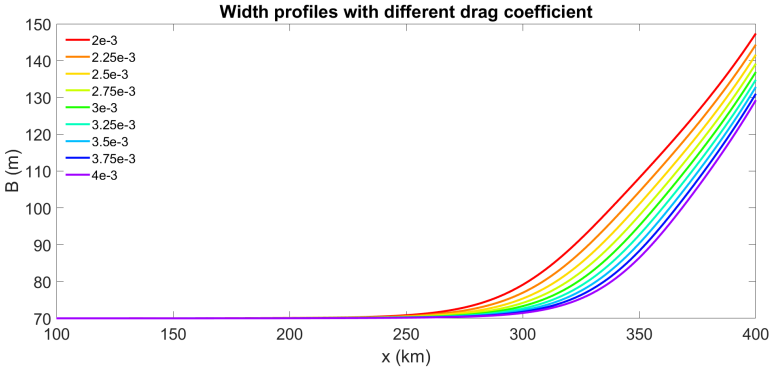

(e) Run: Drag coefficient

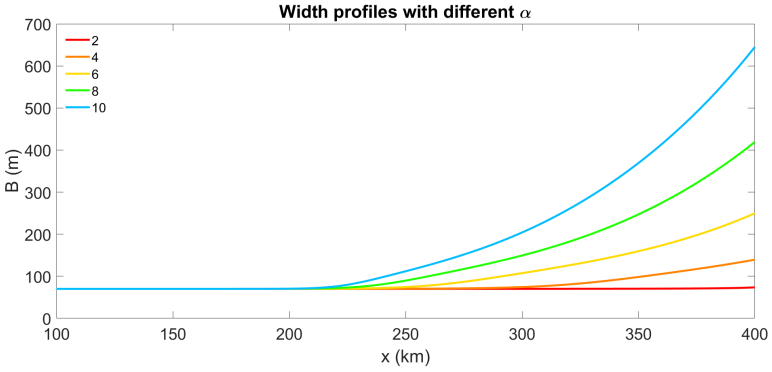

(f) Run: Alpha+Q

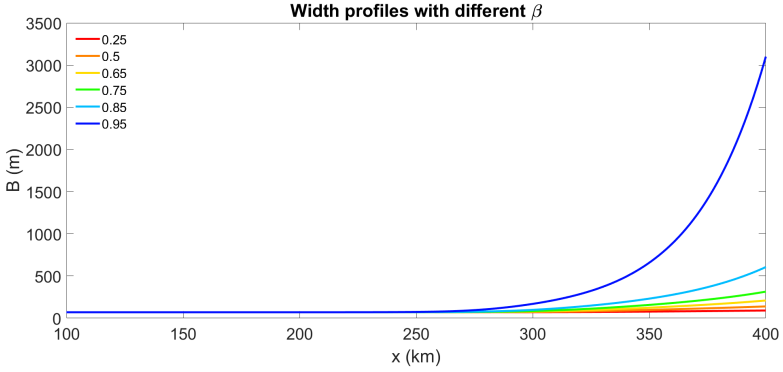

(g) Run: Beta+alpha

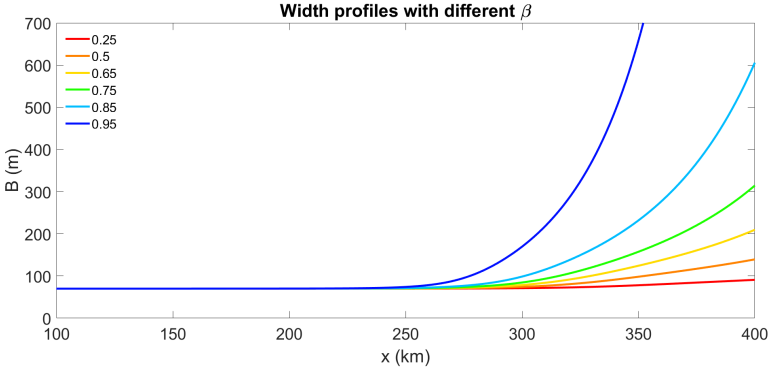

(h) Zoomed in figure of run: Beta+alpha

Figure 13: Equilibrium width profiles of the runs with an adjustable width and a stable bed.

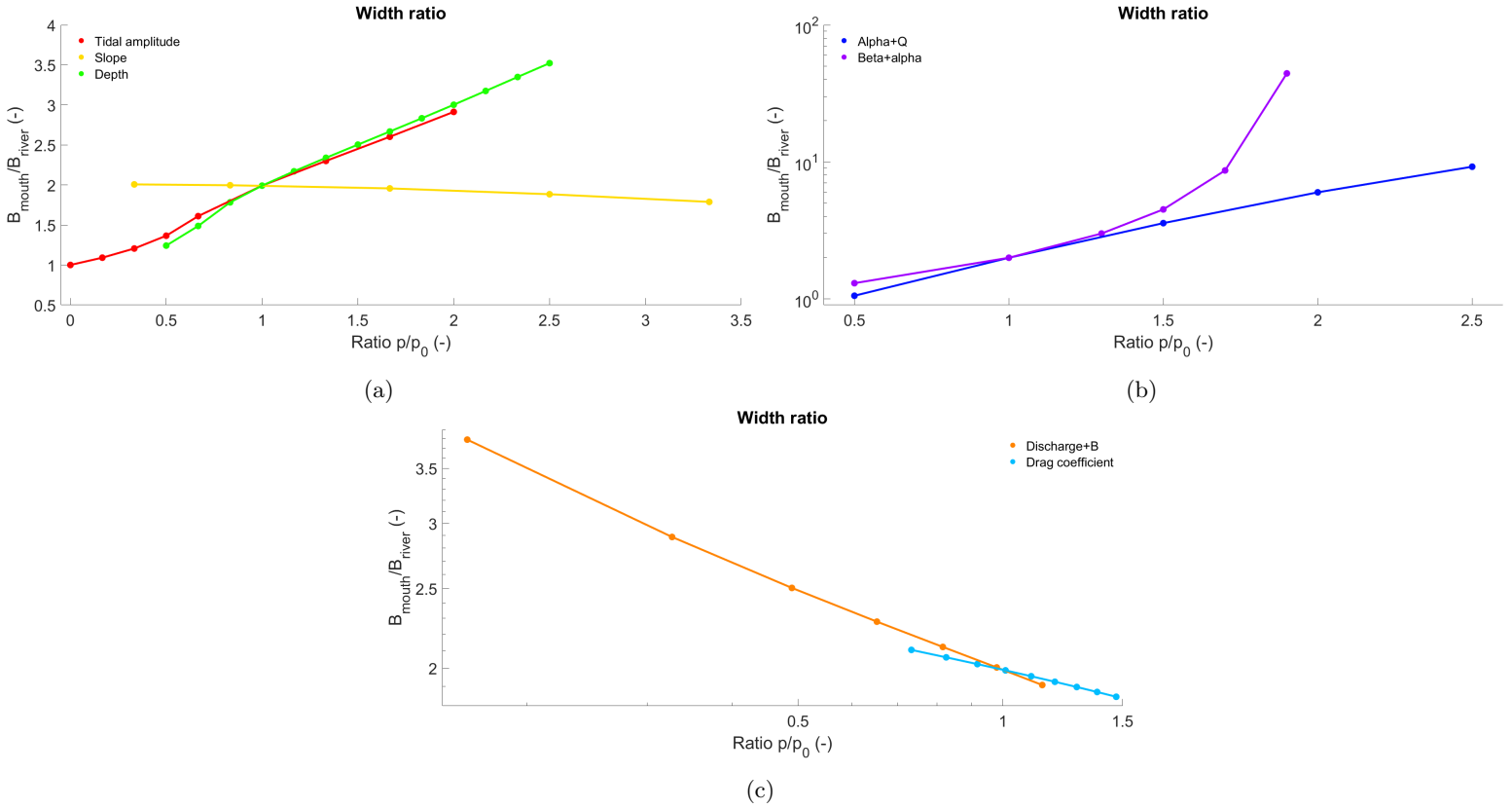

Figure 14: The width ratio B_{mouth}/B_{river} as a function of the ratio of the changing parameter p against the value of the parameter is the default run p_0. For run Tidal amplitude: $p/p_0 = a_z/a_{z,0}$, for run Discharge+B: $p/p_0 = Q_r/Q_{r,0}$, for run Slope: $p/p_0 = S/S_0$, for run Depth: $p/p_0 = H/H_0$, for run Drag coefficient: $p/p_0 = C_d/C_{d,0}$, for run Alpha+Q: $p/p_0 = \alpha/\alpha_0$ and for run Beta+alpha:$p/p_0 = \beta/\beta_0$, where the value of the default parameters are given in table 2. Note: sub-figures have different axis scales.

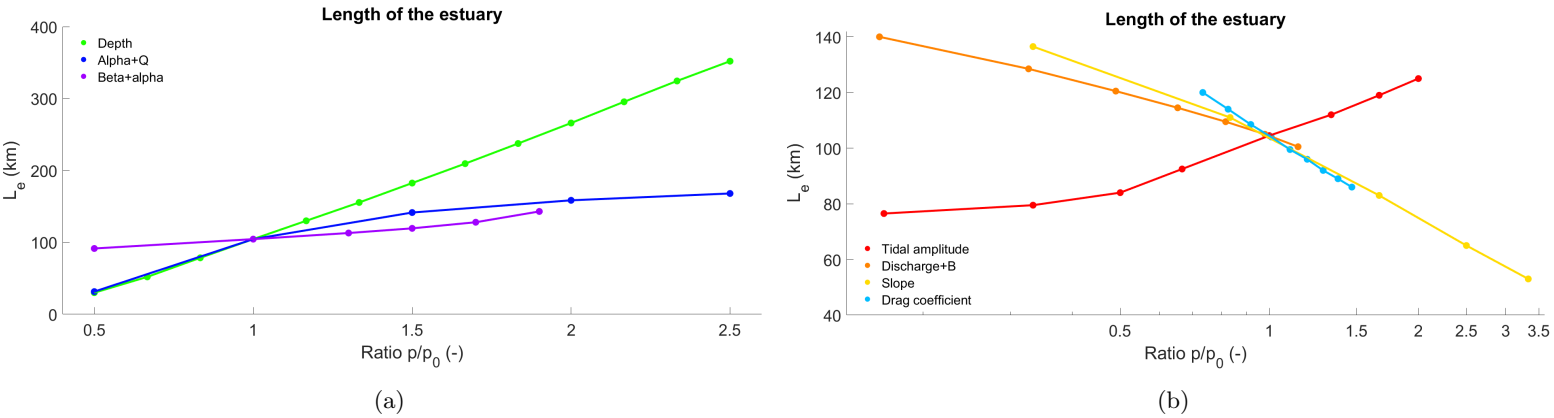

Figure 15: The estuary length L_e as a function of the ratio of the changing parameter p against the value of the parameter is the default run p_0. For run Tidal amplitude: $p/p_0 = a_z/a_{z,0}$, for run Discharge+B: $p/p_0 = Q_r/Q_{r,0}$, for run Slope: $p/p_0 = S/S_0$, for run Depth: $p/p_0 = H/H_0$, for run Drag coefficient: $p/p_0 = C_d/C_{d,0}$, for run Alpha+Q: $p/p_0 = \alpha/\alpha_0$ and for run Beta+alpha:$p/p_0 = \beta/\beta_0$, where the value of the default parameters are given in table 2. Note: sub-figures have different axis scales.

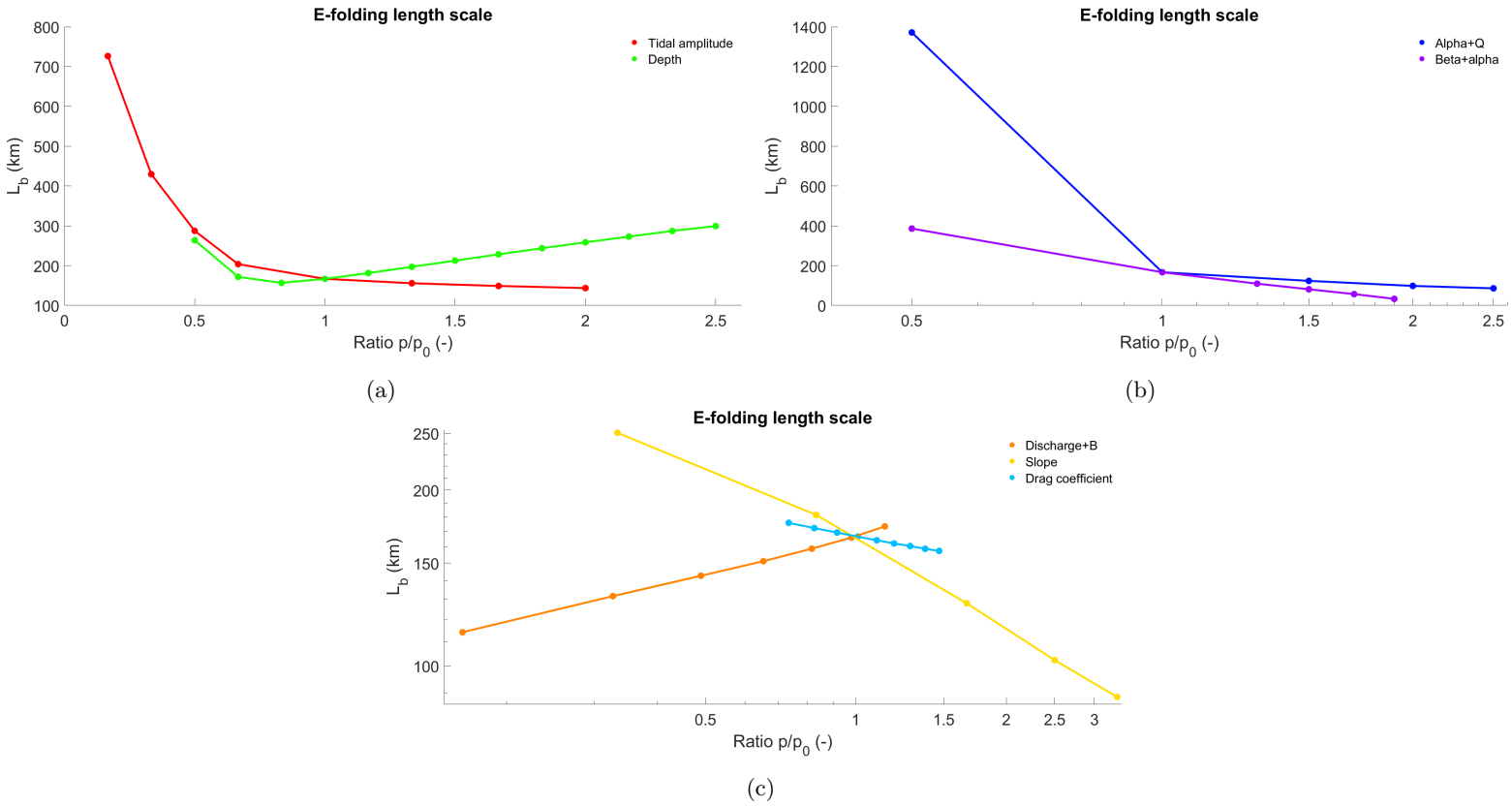

Figure 16: The e-folding length scale L_b as a function of the ratio of the changing parameter p against the value of the parameter is the default run p_0. For run Tidal amplitude: $p/p_0 = a_z/a_{z,0}$, for run Discharge+B: $p/p_0 = Q_r/Q_{r,0}$, for run Slope: $p/p_0 = S/S_0$, for run Depth: $p/p_0 = H/H_0$, for run Drag coefficient: $p/p_0 = C_d/C_{d,0}$, for run Alpha+Q: $p/p_0 = \alpha/\alpha_0$ and for run Beta+alpha:$p/p_0 = \beta/\beta_0$, where the value of the default parameters are given in table 2. Note: sub-figures have different axis scales.

A second set of runs with an adjusting width but stable bed was done, where the boundary and initial conditions needed to meet the Chézy equation (eq 4.20) next to the empirical hydraulic geometry relation (eq 4.19). This was done by additionally changing the depth of the channel, as explained in section 4.2.1. These are the runs called: Discharge+B+H, Slope+H, Drag coefficient+H, Alpha+Q+H, Beta+Q+H. From the developed equilibrium width profiles of these runs (see figure 17) again the width ratio B_{mouth}/B_{river}, estuary length L_e and e-folding length scale L_b were determined (see figure 18). The trends in the width ratio when changing the river discharge, slope, drag coefficient or model parameter α, and additionally the channel depth, is quite the same as the trends when one of these parameters is changed, but the channel depth stays the same (compare figure 18a and figure 14). The slopes of the trends are somewhat smaller.

In these runs, where additionally the channel depth is changed, the channel depth increases with increasing river discharge, slope or drag coefficient and decreases with increasing α. This leads to competing trends. As was clear from the previous runs, when only the channel depth is increased, this leads to larger width ratios (see figure 14a). When only the river discharge, slope or drag coefficient is increased, this leads to smaller width ratios and increasing only the model parameter α leads to larger width ratios. These competing trends lead to the smaller slopes in the eventual trends of the runs where the river discharge, slope, drag coefficient or the model parameter α and additionally the channel depth is changed. Moreover, the estuary length shows the result of the competing effects of changing the channel depth versus the river discharge, slope, drag coefficient or α. This again leads to smaller slopes in the estuary length trends of the runs "Slope+H" and "Drag coefficient+H" in comparison to the runs "Slope" and "Drag coefficient" (compare figure 18b and 15). Interestingly, the estuary length trends of the runs "Discharge+B+H" and

"Alpha+Q+H" show an opposite trend than the runs "Discharge+B" and "Alpha+Q" (compare figure 18b and 15). The effect of changing the channel depth is that these runs overpower the effect of changing the river discharge or model parameter α, so the trend is changed. In the results of the e-folding length scale, the competing effects are apparent in the run "Slope+H", when the slope and channel depth are small and are increased, it leads to smaller e-folding length scales, but if the slope and channel depth are increased even more the e-folding length scale again increases, as it does in the runs where only the channel depth is increased (see figure 16a).

The run "Beta+Q+H" can not be directly compared to the run "Beta+alpha", since the model parameter α is set to de default setting and kept the same in the run "Beta+Q+H". The run"Beta+Q+H" can show the effect of changing the model parameter β independently from changing the the model parameter α. Interestingly, the runs "Alpha+Q+H" and "Beta+Q+H" follow the same trend in e-folding length scale if the model parameter β varies between 0.25 and 0.5 and the model parameter α between 2 and 4 (see figure 18c, where the blue line is not entirely visible as it is covered by the purple line.). Furthermore, it is clear that increasing β has a large effect on the width ratio and e-folding length scale where the width ratio increases and the e-folding length scale decreases with increasing β. The effect on the estuary length is smaller, but still quite large.

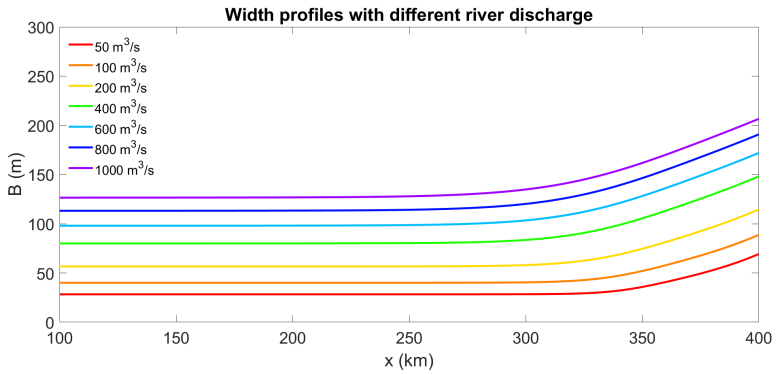

(a) Run: Discharge+B+H

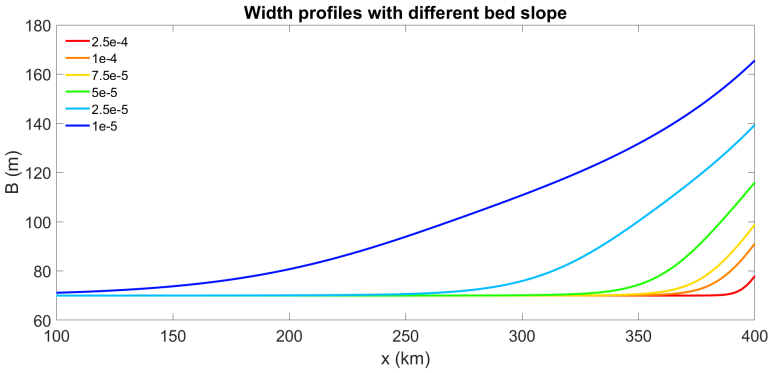

(b) Run: Slope+H

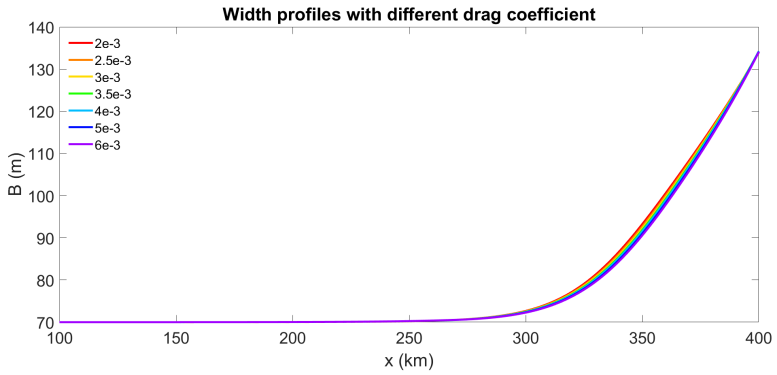

(c) Run: Drag coefficient+H

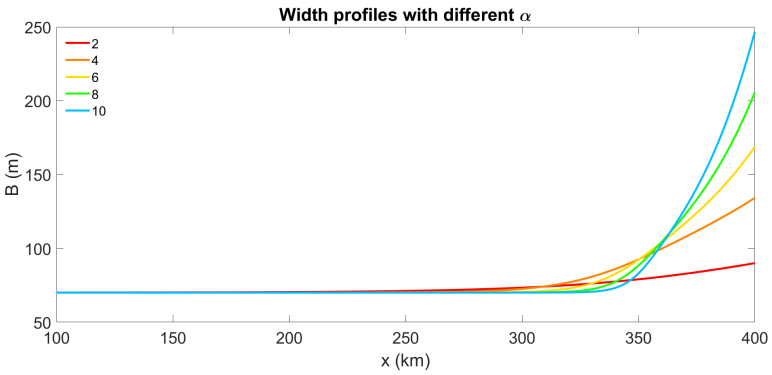

(d) Run: Alpha+Q+H

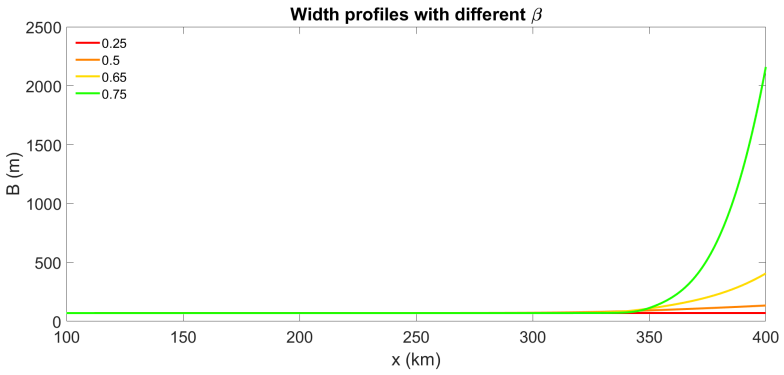

(e) Run: Beta+Q+H

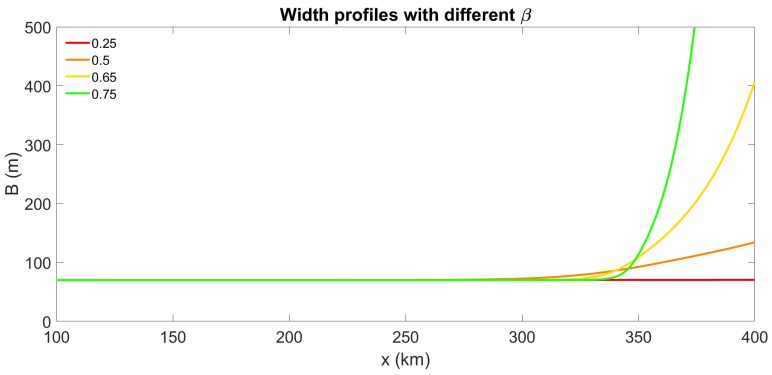

(f) Zoomed in figure of run: Beta+Q+H

Figure 17: Equilibrium width profiles of the runs with an adjustable width and a stable bed, where the depth is additionally changed and follows the Chézy equation (equation 4.20).

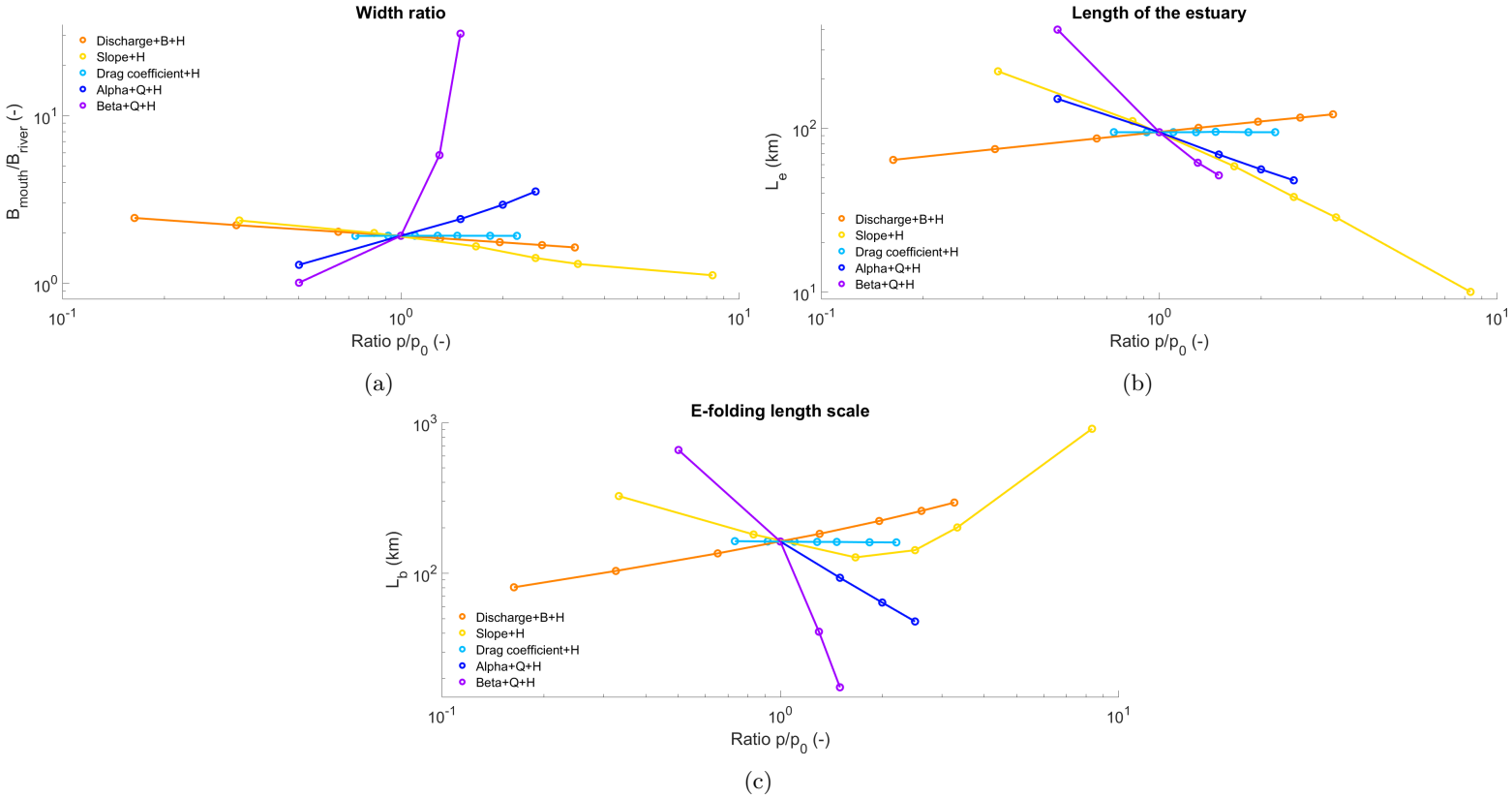

Figure 18: The width ratio B_{mouth}/B_{river}, estuary length L_e and e-folding length scale L_b as a function of the ratio of the changing parameter p against the value of the parameter is the default run p_0. For run Discharge+B+H: $p/p_0 = Q_r/Q_{r,0}$, for run Slope+H: $p/p_0 = S/S_0$, for run Drag coefficient+H: $p/p_0 = C_d/C_{d,0}$, for run Alpha+Q+H: $p/p_0 = \alpha/\alpha_0$ and for run Beta+Q+H:$p/p_0 = \beta/\beta_0$, where the value of the default parameters are given in table 2.

5.2 Results of runs with adjustable width and adjustable bed

5.2.1 Is an equilibrium reached?

In figure 19 the evolution of the width and bed level at the mouth is shown over time for the runs where the tidal amplitude is changed (run: "Tidal amplitude+bed"). It can be seen that the width and bed level have stabilised in 50000 morphological years and that a larger tidal amplitude leads to a longer time to reach this equilibrium. Furthermore, the width stabilises faster than the bed level. When looking at this width and bed level evolution for the other runs, it was clear that not all runs have reached an equilibrium in the run time. The runs that have not yet reached an equilibrium were the runs of "Alpha+Q+bed", where $\alpha = 8$ and 10. The results of these runs will not be included or discussed. All the other runs reached equilibrium in the width and bed level profile.

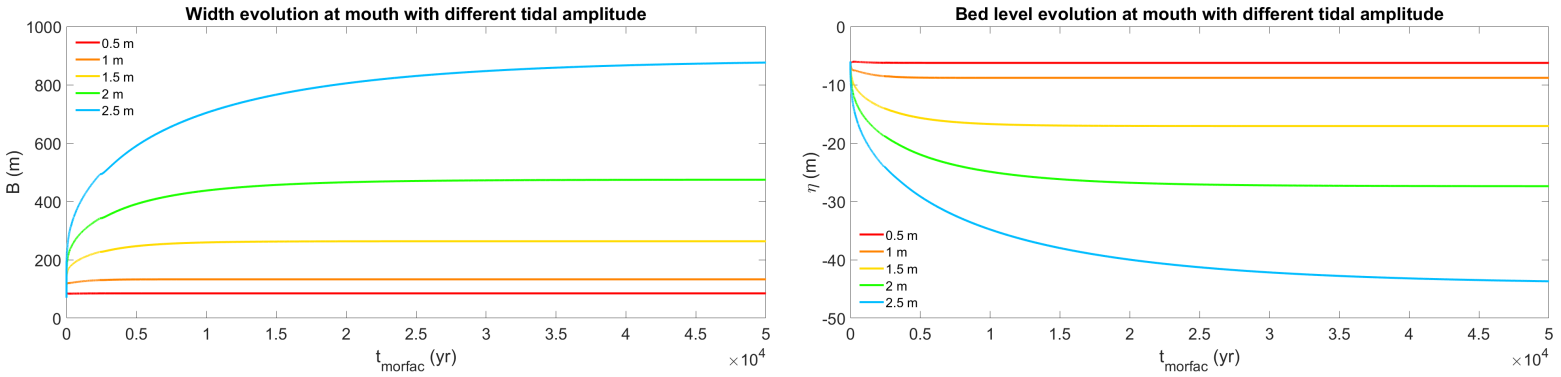

(a) (b)

Figure 19: Width B and bed level η evolution at the mouth for the run: Tidal amplitude+bed.

In figure 20 the water level amplitudes and flow velocity amplitudes of the last tidal cycle of the run are shown for the runs with different tidal amplitudes (run: "Tidal amplitude+bed"). When the tidal amplitude increases from 0.5 m to 1 m, a change in the trend in the water level and flow velocity amplitude can be seen. With a tidal amplitude of 0.5 m, the water level and flow velocity amplitude rapidly decrease throughout the estuary. However, with a tidal amplitude of 1 m, the water level and flow velocity amplitude decrease more slowly. When the tidal amplitude becomes 2 m, even an increase in amplitudes upstream from the mouth can be observed. The amplitudes show that no ideal estuary is developed in one of these runs. The other runs with a movable bed did also not develop an ideal estuary.

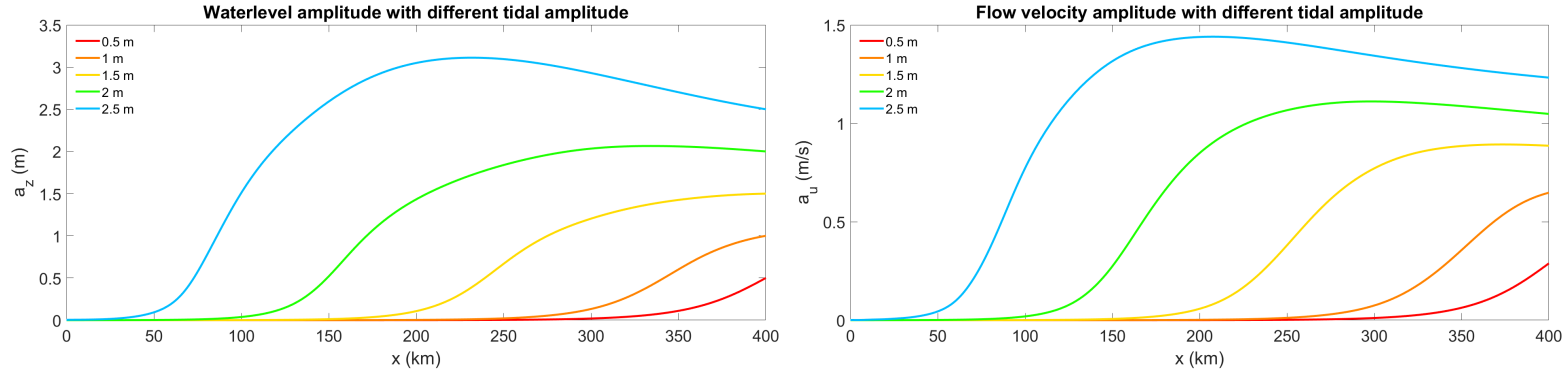

(a) (b)

Figure 20: Water level amplitude a_z and flow velocity amplitude a_u for the last tidal cycle of the runs called Tidal amplitude+bed.

5.2.2 Effect of changing channel properties or boundary conditions

For the runs with a movable bed alongside an adjustable width, the width ratio B_{mouth}/B_{river} (see figure 22), the length of the estuary L_e (see figure 23), the e-folding length scale of the estuary L_b (see figure 24), the depth at the mouth H_{mouth} (see figure 26), the slope of the estuary S_e (see figure 27), the depth of the river upstream H_{river} (see figure 28) and the slope of the river upstream S_r (see figure 29) were determined from the equilibrium width profiles (see figure 21) and bed level profiles (see figure 25), as explained in section 4.2.3.

The model produces larger width ratios and longer estuary lengths in the runs where the bed can adjust in comparison to the runs with a stable bed with the same parameter settings and boundary conditions (see results in section 5.1 and this section). In the runs with an adjustable bed where the model parameters α and β are unchanged, the width ratio ranges from approximately 1 to 14. When α or β are increased, even larger width ratios are developed.

In all the runs with a movable bed together, the estuary length varies between approximately 50 km to 350 km. The e-folding length scale ranges from 600 km to 100 km, in the runs where β stays the same. If β is increased, the e-folding length scale is shorter, up to around 45 km. The e-folding length scales of the runs with an adjustable width but stable bed lie in the same range, keeping in mind that the parameter ranges in these runs were larger.

The data of the runs with an adjustable width and bed do mainly show the same kind of trends between the width ratio, the estuary length and the e-folding length scale and the parameters and boundary conditions as the runs with an adjustable width but stable bed (compare figures 14-16 to figures 22-24). Larger width ratios and longer estuaries are developed when the tidal amplitude, the channel depth, or the model parameter α are increased or the river discharge, the drag coefficient, or the bed slope are decreased. Moreover, shorter e-folding length scales are developed when the bed slope, the drag coefficient, or the model parameter β increases or the channel depth decreases. Again the model parameters β and α have the most effect on the width ratio and the e-folding length scale. However, the effect of the tidal amplitude and the discharge on the width ratio is too quite significant. Furthermore, the initial depth and initial slope are still important for the length of the estuary, but the tidal amplitude has increased its effect.

The trends do have different slopes than the trends in the runs with a stable bed. Generally, the slopes of the trends of the width ratio and estuary length are steeper in the runs with a movable bed. This is probably due to the effects being amplified by the adjustable bed level. A different relation in the runs with an adjustable bed than in the runs with a stable bed can be seen between the e-folding length scale and the tidal amplitude, the river discharge, and the model parameter α. These relations show first a decrease in the e-folding length scale with the increasing parameter and then an increasing e-folding length scale when the parameter is increased even more.

Noteworthy is the behaviour of the runs with a different river discharge and accompanying upstream channel width (see figure 21b, called "Discharge+B+bed") in comparison to this set of runs without bed change (see figure 13b, called "Discharge+B"). The runs with a smaller river discharge and upstream channel width develop larger channel widths at the mouth than runs with larger river discharges and upstream channel widths. This is a different behaviour than the equivalent runs (called "Discharge+B") show. This difference in behaviour is a result of the bed level adapting, and the channel depth increasing when the river discharge is decreased, in the runs with a movable bed (see figure 25b). This results in larger channel widths at the mouth. When the river discharge is larger than 150 m^3/s and is increased, the e-folding length scale increases, leading to a less convergent estuary. This means that the width ratio decreases faster than the length of the estuary with increasing river discharge. The opposite trend can be observed when the river discharge is between the 50 and 150 m^3/s . Increasing the river discharge leads to a shorter e-folding length scale, so a more convergent estuary. In this case, the length of the estuary decreases faster than the width ratio with increasing river discharge. The e-folding length scale will be further discussed in section 6.2.

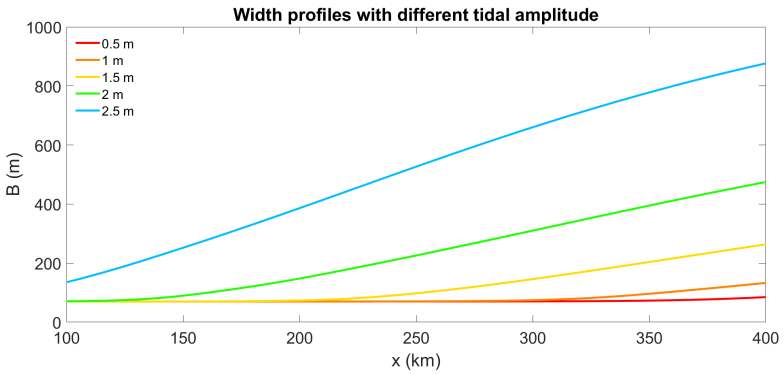

(a) Run: Tidal amplitude+bed

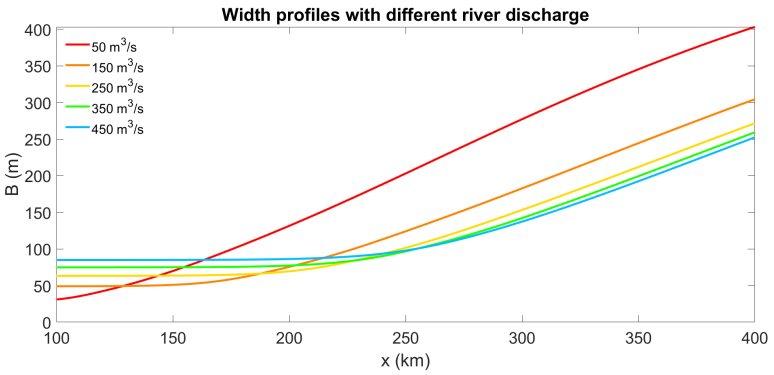

(b) Run: Discharge+B+bed

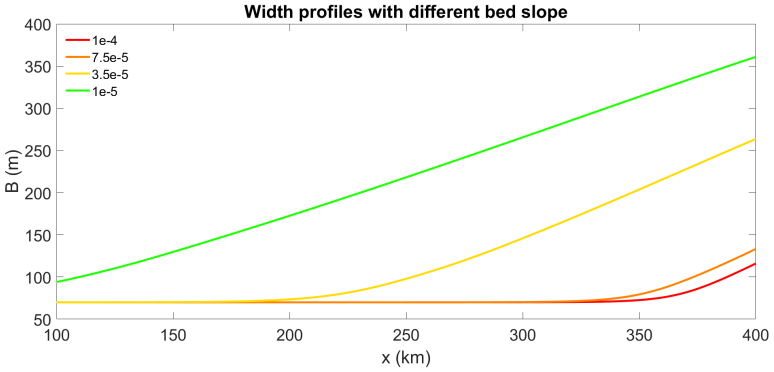

(c) Run: Slope+bed

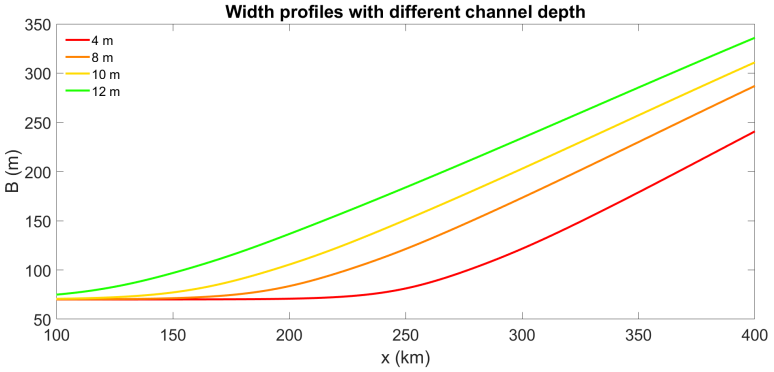

(d) Run: Depth+bed

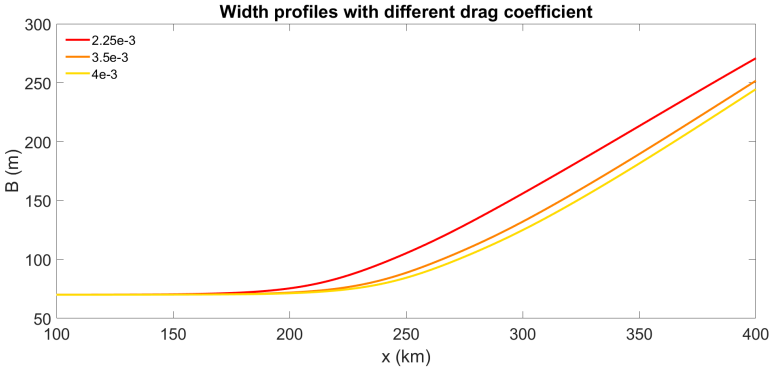

(e) Run: Drag coefficient+bed

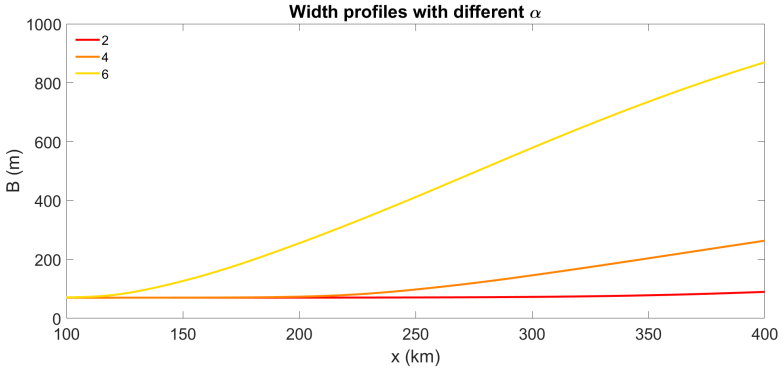

(f) Run: Alpha+Q+bed

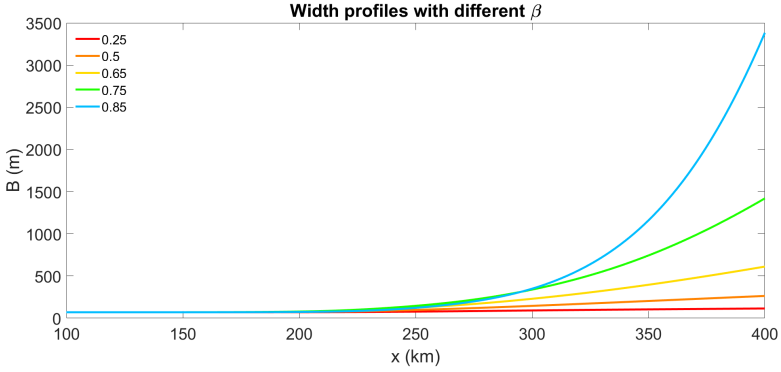

(g) Run: Beta+alpha+bed

Figure 21: Equilibrium width profiles of the runs with an adjustable width and bed.

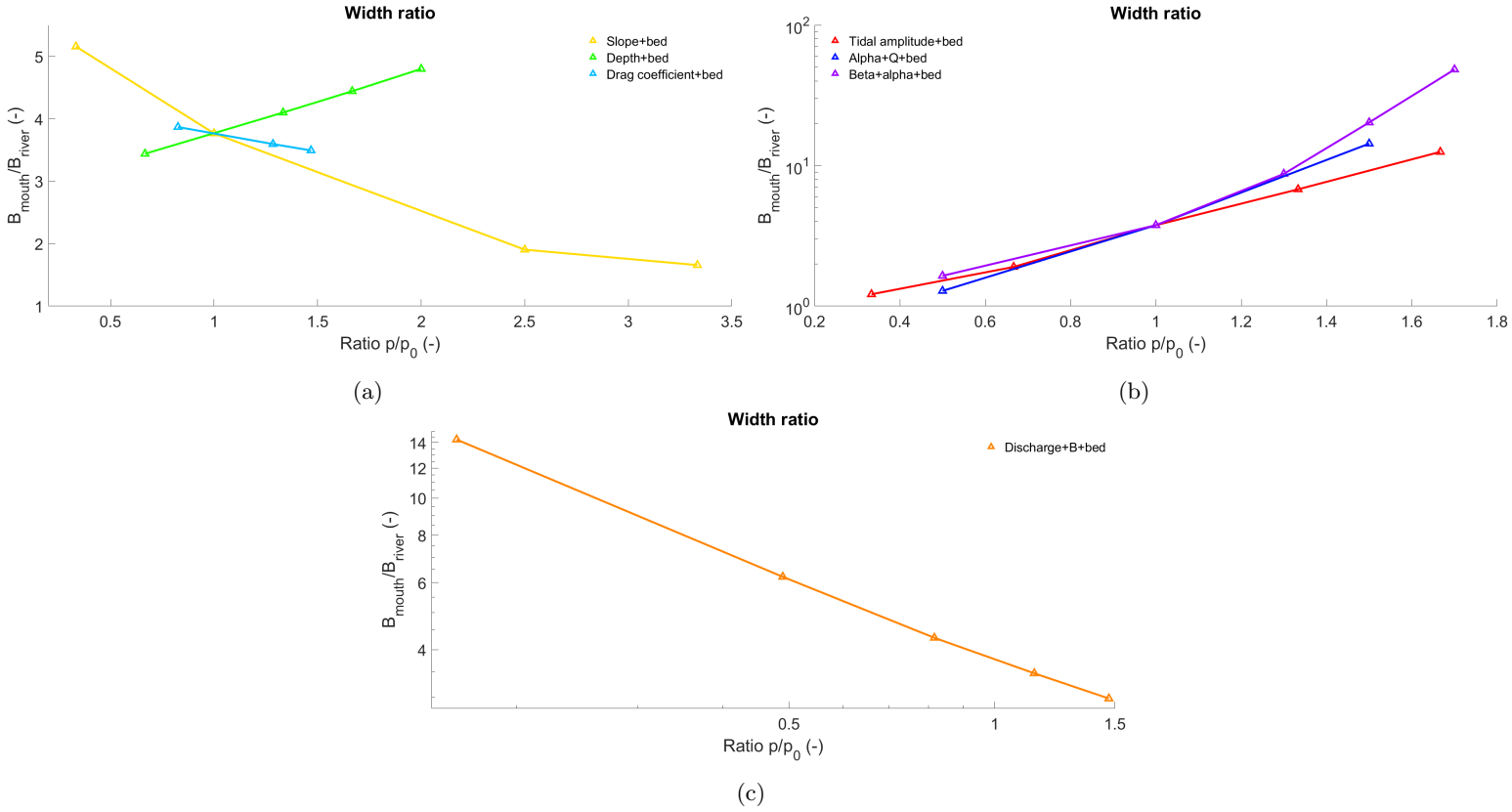

Figure 22: The width ratio B_{mouth}/B_{river} as a function of the ratio of the changing parameter p against the value of the parameter is the default run p_0. For run Tidal amplitude+bed: $p/p_0 = a_z/a_{z,0}$, for run Discharge+B+bed: $p/p_0 = Q_r/Q_{r,0}$, for run Slope+bed: $p/p_0 = S/S_0$, for run Depth+bed: $p/p_0 = H/H_0$, for run Drag coefficient+bed: $p/p_0 = C_d/C_{d,0}$, for run Alpha+Q+bed: $p/p_0 = \alpha/\alpha_0$ and for run Beta+alpha+bed:$p/p_0 = \beta/\beta_0$, where the value of the default parameters are given in table 2. Note: subfigures have different axis scales.

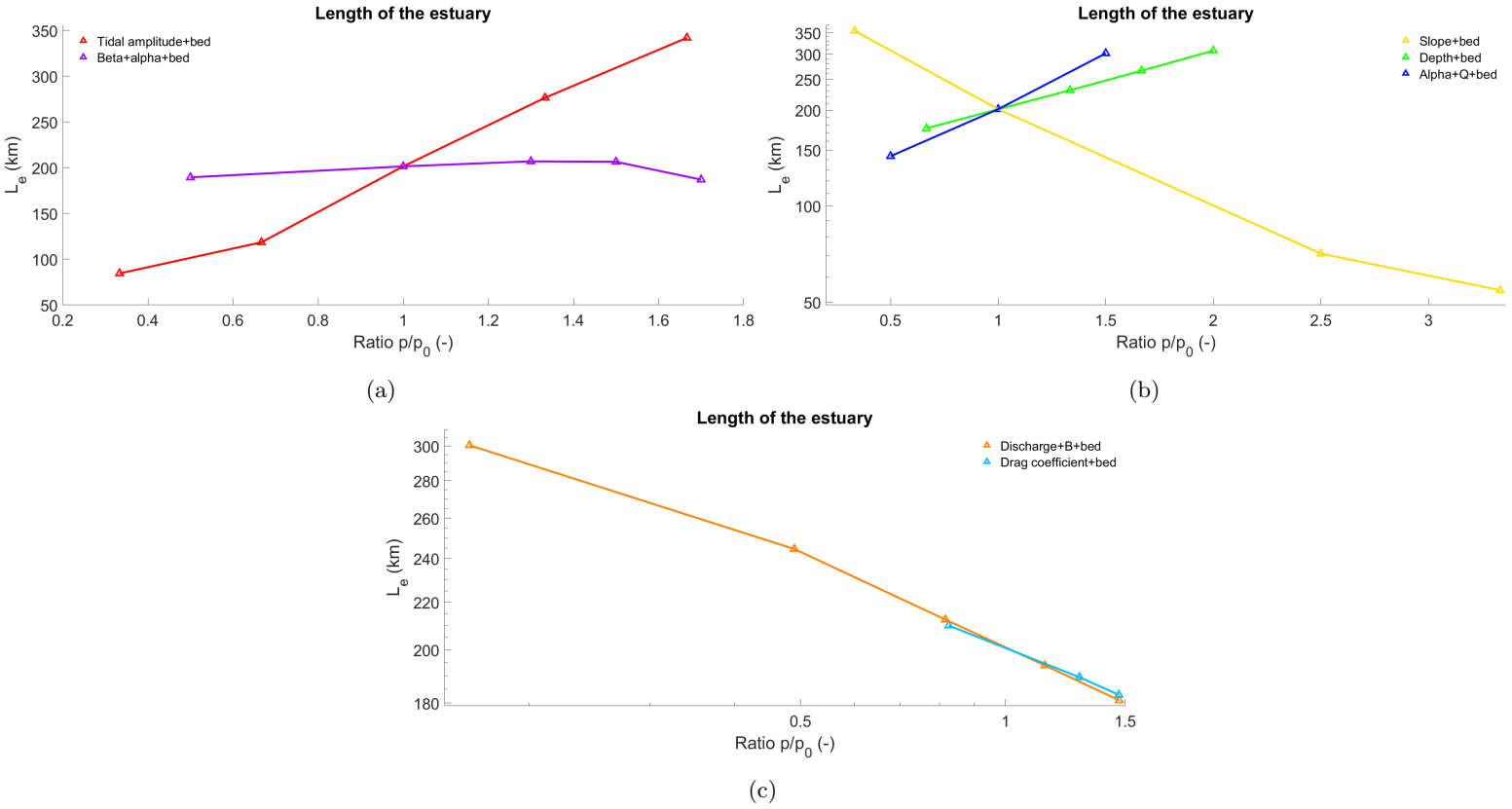

Figure 23: The estuary length L_e as a function of the ratio of the changing parameter p against the value of the parameter is the default run p_0. For run Tidal amplitude+bed: $p/p_0 = a_z/a_{z,0}$, for run Discharge+B+bed: $p/p_0 = Q_r/Q_{r,0}$, for run Slope+bed: $p/p_0 = S/S_0$, for run Depth+bed: $p/p_0 = H/H_0$, for run Drag coefficient+bed: $p/p_0 = C_d/C_{d,0}$, for run Alpha+Q+bed: $p/p_0 = \alpha/\alpha_0$ and for run Beta+alpha+bed:$p/p_0 = \beta/\beta_0$, where the value of the default parameters are given in table 2. Note: sub-figures have different axis scales.

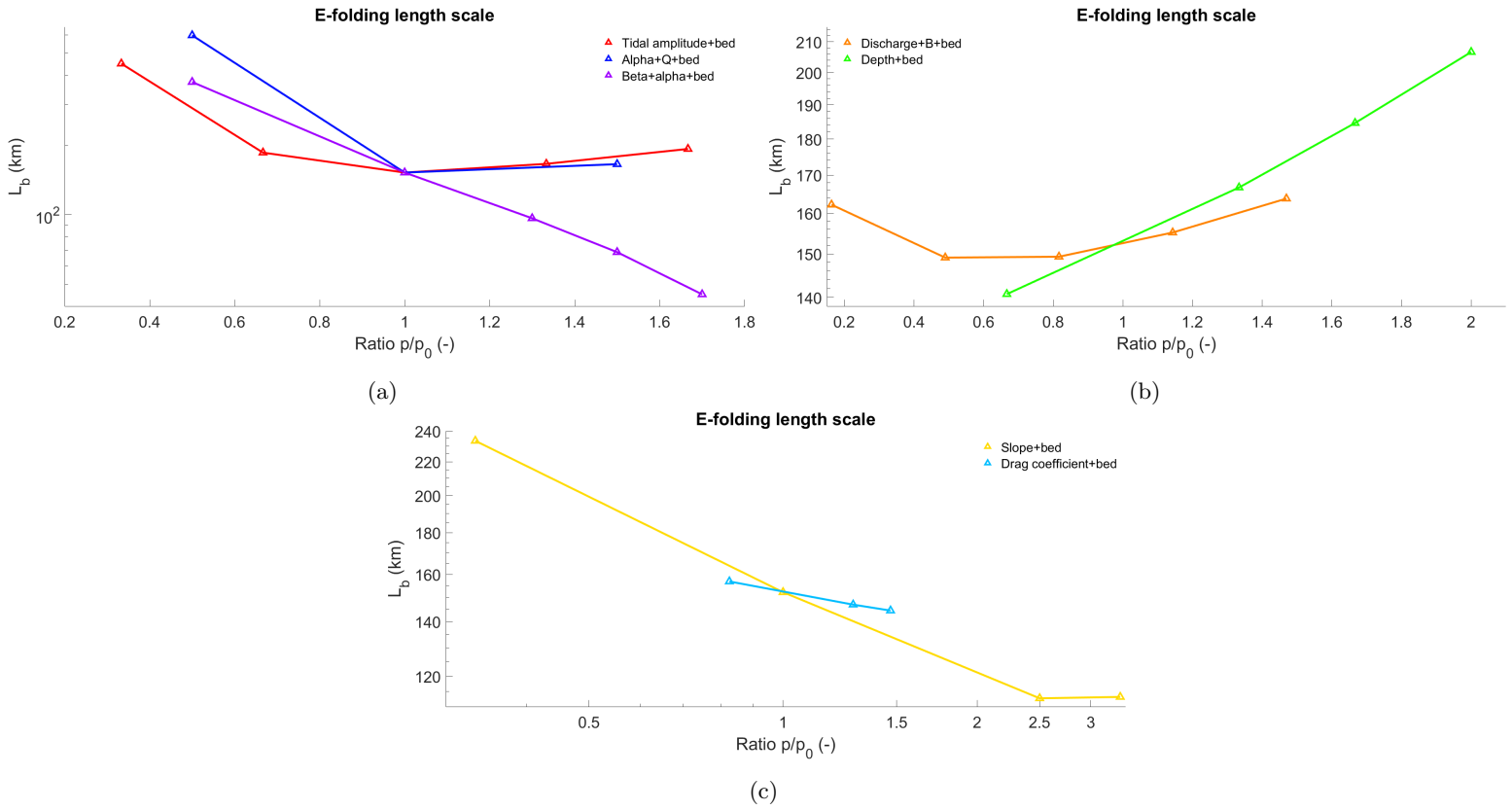

Figure 24: The e-folding length scale L_e as a function of the ratio of the changing parameter p against the value of the parameter is the default run p_0. For run Tidal amplitude+bed: $p/p_0 = a_z/a_{z,0}$, for run Discharge+B+bed: $p/p_0 = Q_r/Q_{r,0}$, for run Slope+bed: $p/p_0 = S/S_0$, for run Depth+bed: $p/p_0 = H/H_0$, for run Drag coefficient+bed: $p/p_0 = C_d/C_{d,0}$, for run Alpha+Q+bed: $p/p_0 = \alpha/\alpha_0$ and for run Beta+alpha+bed:$p/p_0 = \beta/\beta_0$, where the value of the default parameters are given in table 2. Note: sub-figures have different axis scales.

In addition to the influence of parameters on the width profile, the influence of parameters and boundary conditions on the bed level profile can be studied for the runs with a movable bed (see figure 25 and figures 26-29). The model develops channel depths between 5 m and 46 m at the mouth and depths between 2 m and 14 m upstream. The majority of these runs develop a channel depth upstream that is smaller than the initial depth of 6 m. Especially the tidal amplitude and the initial bed slope have a considerable influence on the depth at the mouth, whereas the model parameter α has the most significant effect on the depth upstream. Interestingly, the model parameter β has almost no effect on the upstream channel depth. Furthermore, the estuary slopes range from 3×10^{-5} and $16 \times 10{-}5$, where the tidal amplitude has the most considerable influence together with the model parameters α and β. Again, the upstream river's slope is mainly dependent on the initial bed slope and tidal amplitude. The river develops slopes between the 2.5×10^{-5} and 11×10^{-5} of which the majority is above the value of the initial bed slope.

Larger channel depths at the mouth are developed when the tidal amplitude, the initial depth, the drag coefficient, or the model parameter α is increased or when the river discharge, the initial bed slope or model parameter β is decreased (see figure 26). Interestingly, the trends in the channel depth upstream are different (see 28). Larger channel depths upstream are produced if the river discharge, the initial depth, or the drag coefficient is increased or if the tidal amplitude, the initial slope or the model parameter α is decreased. While, decreasing the river discharge or the initial channel depth, or increasing the tidal amplitude or the drag coefficient, results in a steeper estuary and upstream river slope. The initial slope of the channel has a different effect on the estuary slope, where the estuary slope first increases with increasing initial slope and than slowly decreases again when the initial slope is further increased. While, the slope upstream shows an almost linear relation with initial slope, where a steeper

initial slope leads to a steeper slope upstream. Furthermore, to note is that steeper estuary slopes are developed when the parameter β is decreased or the parameter α is increased. The upstream slope generally increases with increasing β.

Important to note, starting with another channel depth results in just a slight difference in the channel depth upstream, but a large difference in the channel depth in the estuary (see figures 25d, 26a, 28a). In addition to different bed slopes upstream and in the estuary (see figures 27a, 29a). This means that the initial condition of the channel bed level, has an influence on the eventually reached equilibrium. This was not expected since the initial conditions should not matter, and the equilibrium should only depend on model parameters and boundary conditions.

When the model parameter β of the empirical hydraulic geometry relation is increased (runs called: "Beta+alpha+bed"), a different kind of bed level is developed by the model (see figure 25g). In most of the other runs, the depth only increases throughout the channel, but the data of the runs with a different β show a depth profile where the depth first decreases at the beginning of the estuary upstream, if $\beta > 0.5$. The depth and bed slope upstream do barely differ when β is changed, while the estuary's depth and slope decrease with increasing β.

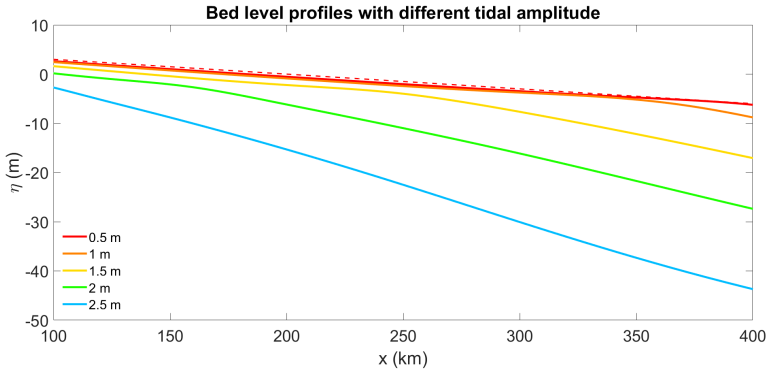

(a) Run: Tidal amplitude+bed

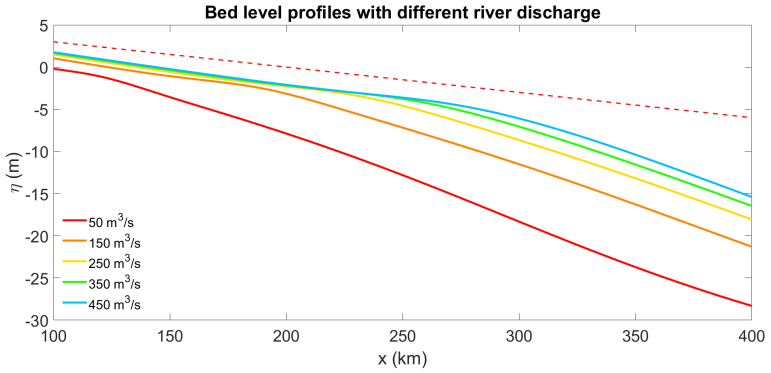

(b) Run: Discharge+B+bed

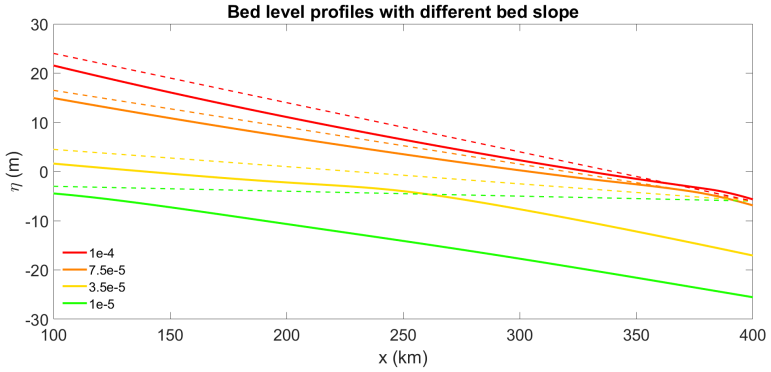

(c) Run: Slope+bed

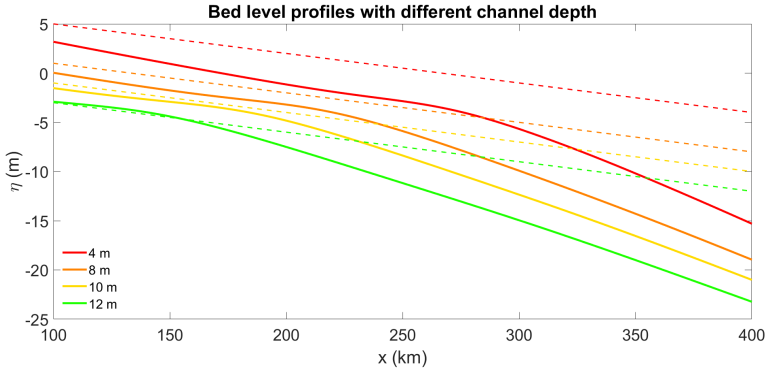

(d) Run: Depth+bed

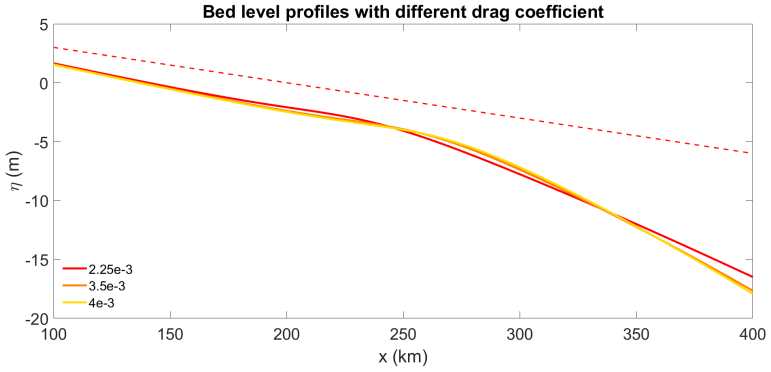

(e) Run: Drag coefficient+bed

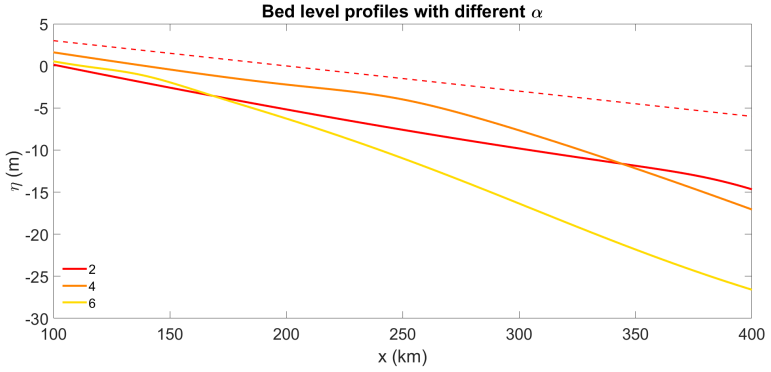

(f) Run: Alpha+Q+bed

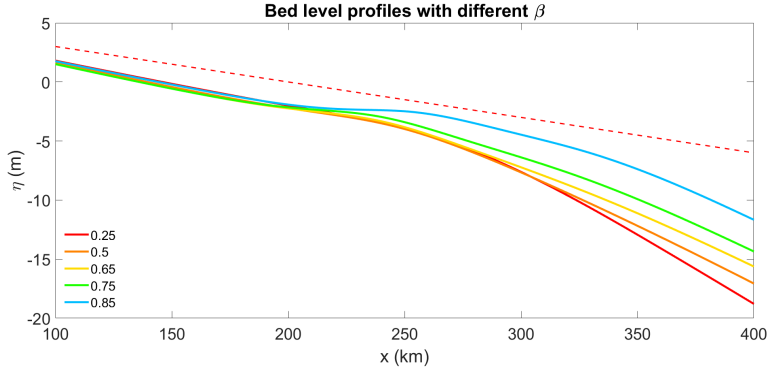

(g) Run: Beta+alpha+bed

Figure 25: Equilibrium bed level profiles of the runs with an adjustable width and bed.

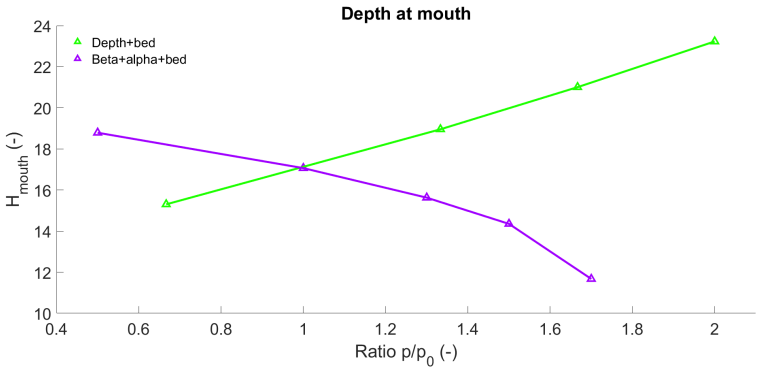

(a)

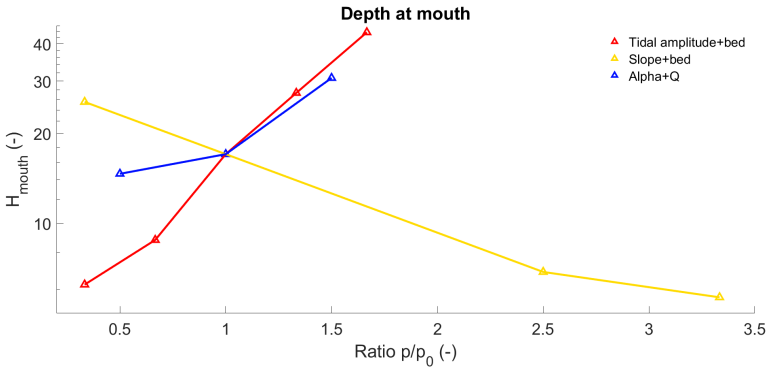

(b)

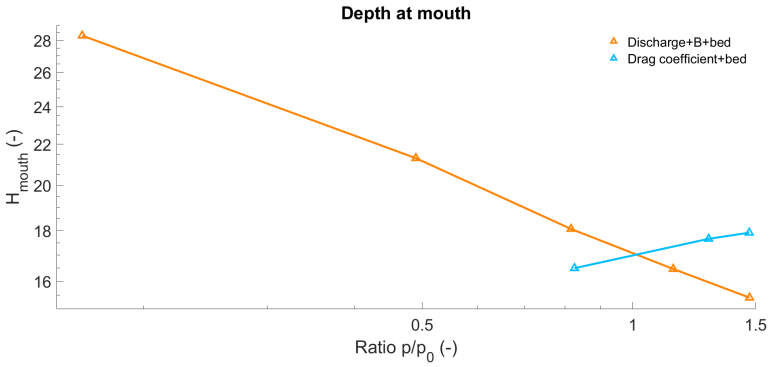

(c)

Figure 26: The depth at the mouth H_{mouth} as a function of the ratio of the changing parameter p against the value of the parameter is the default run p_0. For run Tidal amplitude+bed: $p/p_0 = a_z/a_{z,0}$, for run Discharge+B+bed: $p/p_0 = Q_r/Q_{r,0}$, for run Slope+bed: $p/p_0 = S/S_0$, for run Depth+bed: $p/p_0 = H/H_0$, for run Drag coefficient+bed: $p/p_0 = C_d/C_{d,0}$, for run Alpha+Q+bed: $p/p_0 = \alpha/\alpha_0$ and for run Beta+alpha+bed:$p/p_0 = \beta/\beta_0$, where the value of the default parameters are given in table 2. Note: sub-figures have different axis scales.

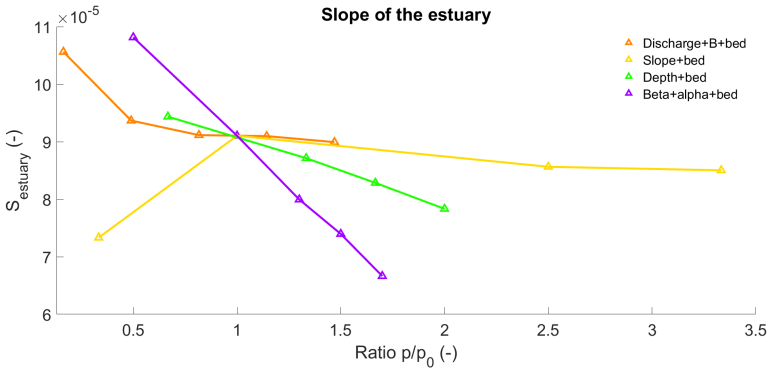

(a)

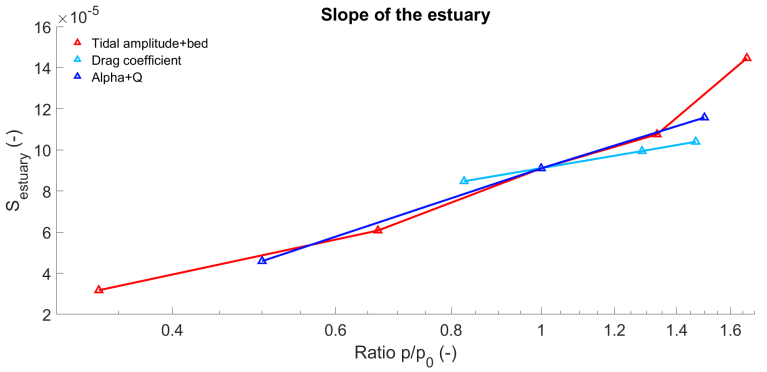

(b)

Figure 27: The slope of the estuary $S_{estuary}$ as a function of the ratio of the changing parameter p against the value of the parameter is the default run p_0. For run Tidal amplitude+bed: $p/p_0 = a_z/a_{z,0}$, for run Discharge+B+bed: $p/p_0 = Q_r/Q_{r,0}$, for run Slope+bed: $p/p_0 = S/S_0$, for run Depth+bed: $p/p_0 = H/H_0$, for run Drag coefficient+bed: $p/p_0 = C_d/C_{d,0}$, for run Alpha+Q+bed: $p/p_0 = \alpha/\alpha_0$ and for run Beta+alpha+bed:$p/p_0 = \beta/\beta_0$, where the value of the default parameters are given in table 2. Note: sub-figures have different axis scales.

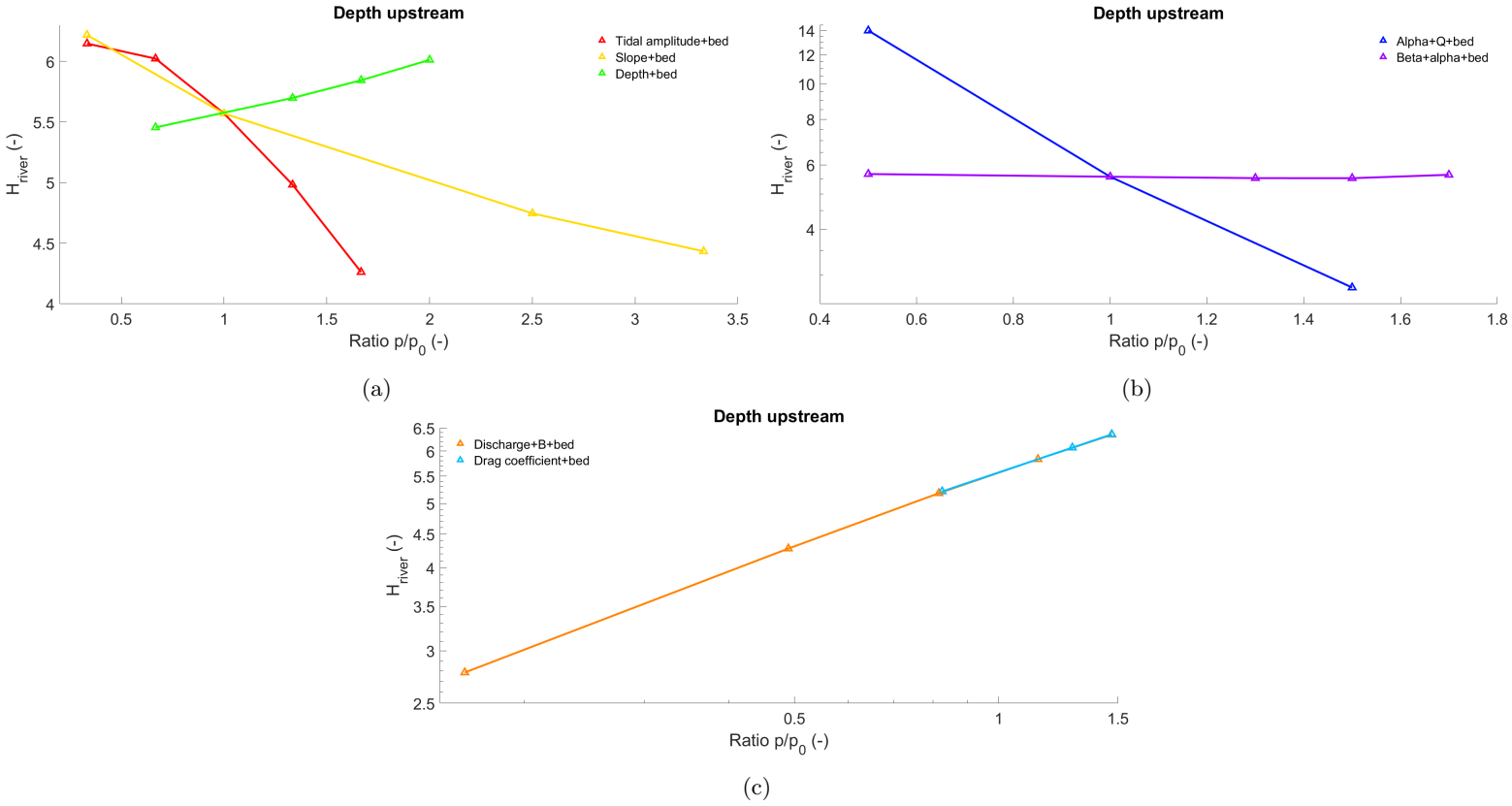

Figure 28: The depth upstream H_{river} as a function of the ratio of the changing parameter p against the value of the parameter is the default run p_0. For run Tidal amplitude+bed: $p/p_0 = a_z/a_{z,0}$, for run Discharge+B+bed: $p/p_0 = Q_r/Q_{r,0}$, for run Slope+bed: $p/p_0 = S/S_0$, for run Depth+bed: $p/p_0 = H/H_0$, for run Drag coefficient+bed: $p/p_0 = C_d/C_{d,0}$, for run Alpha+Q+bed: $p/p_0 = \alpha/\alpha_0$ and for run Beta+alpha+bed:$p/p_0 = \beta/\beta_0$, where the value of the default parameters are given in table 2. Note: sub-figures have different axis scales.

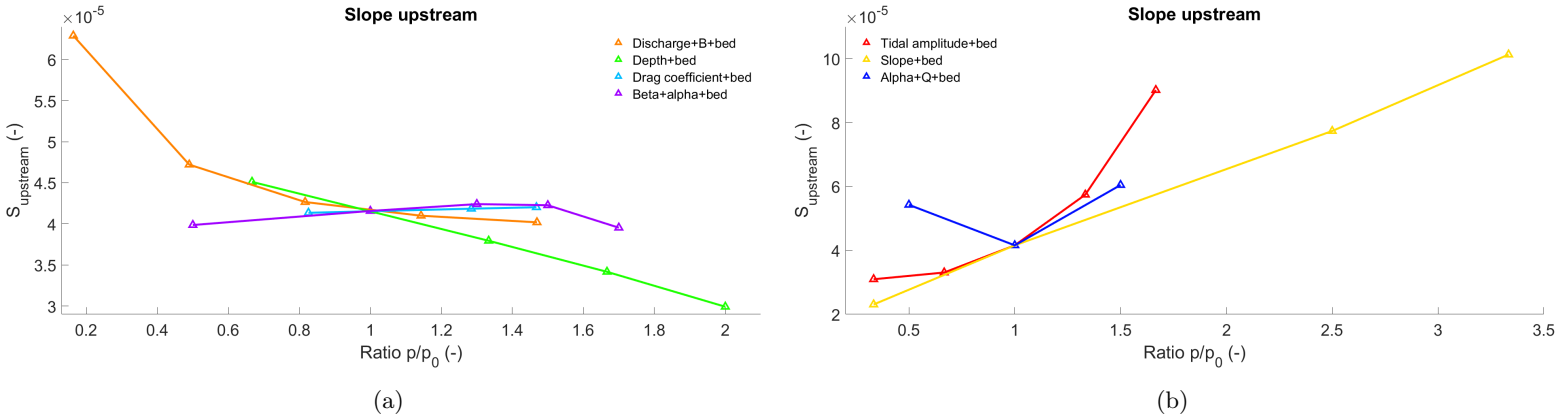

Figure 29: The slope upstream S_{river} as a function of the ratio of the changing parameter p against the value of the parameter is the default run p_0. For run Tidal amplitude+bed: $p/p_0 = a_z/a_{z,0}$, for run Discharge+B+bed: $p/p_0 = Q_r/Q_{r,0}$, for run Slope+bed: $p/p_0 = S/S_0$, for run Depth+bed: $p/p_0 = H/H_0$, for run Drag coefficient+bed: $p/p_0 = C_d/C_{d,0}$, for run Alpha+Q+bed: $p/p_0 = \alpha/\alpha_0$ and for run Beta+alpha+bed:$p/p_0 = \beta/\beta_0$, where the value of the default parameters are given in table 2. Note: sub-figures have different axis scales.

5.2.3 Effect of the time scale of width adjustment, the initial channel shape and the choice for the Exner equation

The effect of the width adjustment's time scale, the initial channel shape, and the different Exner equations were studied. For this, four separate set of runs were carried out as explained in section 4.2.2.

In all the model runs with a movable bed for which the results were discussed in the previous sections, the time scale for the width adjustment used in equation 4.11 was taken as 50 morphological years. This means that the width adapts way faster to the hydrodynamics than the bed level does. In the run ""Only bed+default", where only the bed level can adapt, the bed level adjust within 20000 morphological years. It could be expected that if the time scale for width adjustment in the model is around the same order of magnitude as the time scale for bed level adjustment, the model develops a different bed level and width profile. However, this is not the case. The bed level profiles at the end of the runs with a longer time scale for width adjustment are, in fact, almost the same (see figure 30b, runs called: "Tw+bed"). The width profiles are not exactly the same (see figure 30a). The reason for this is that not all the runs are in equilibrium. From figure 30a it is presumed that if the model had run longer, the eventual equilibrium width profiles and bed level profiles would be the same in all the runs. This means that the chosen timescale for width adjustment does not affect the eventual equilibrium reached in the model. Notwithstanding, the timescale for width adjustment influences how fast this equilibrium is reached in the model. The effect of the timescale is greater on the time it takes to reach an equilibrium for the width profile than for the bed level profile.

As explained in section 4.2.2, the choice was made to first use the Exner equation 4.18 with a γ of 0 (called old Exner equation in this section). In this old Exner equation the width change is not included in the sediment balance. Using instead equation 4.18 with a γ of 1 (called new Exner equation in this section), where the width change is included in the sediment balance, could lead to a different equilibrium. In this new Exner equation, the sediment eroded from the channel banks is deposited on the bed if the width increases and the sediment deposited on the channel banks are eroded from the bed if the width decreases. The results of the runs "Tw+Exner+bed", show that the the eventually reached equilibrium will be the same in the runs where the new Exner equation is used as the runs where the old Exner equation is used (see figure 30c and 30d). However, it will take longer to reach this equilibrium.

The time scale for width adjustment and the type of Exner equation does not affect the eventually reached equilibrium. However, the initial channel of these runs and the other previous runs was straight. The effect of this initial condition needs to be tested. Starting with a convergent instead of a straight channel means that the initial hydrodynamics are different, but the boundary conditions and other parameters are not. If the time scales for width and bed level adjustment are around the same order of magnitude, it could be expected that the eventually reached equilibrium is different. Figures 30e-30h show that the eventually reached equilibrium will not depend on the initial channel shape. All the runs in both the set of runs called "Tw+Lb+bed" and "Tw+Lb+Exner+bed" will eventually reach the same equilibrium and this equilibrium will be the same as when the channel starts as a straight channel and the same boundary conditions and other parameters are used. Not all these runs have already reached this equilibrium, but still this conclusion can be made. This means that the initial shape of the channel does not affect the eventual reached equilibrium width profile and bed level profile.

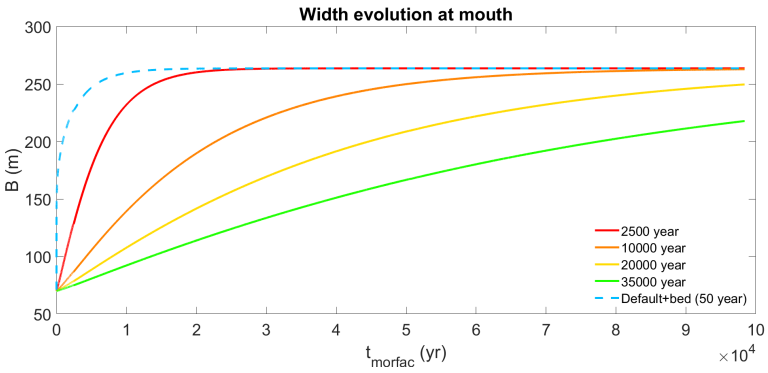

(a) Run called: "Tw+bed"

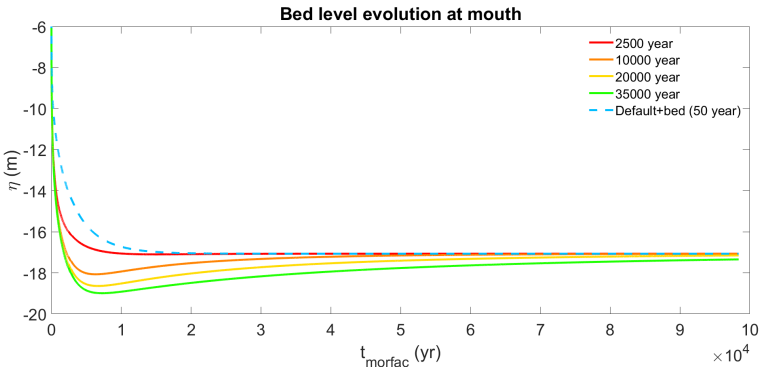

(b) Run called: "Tw+bed"

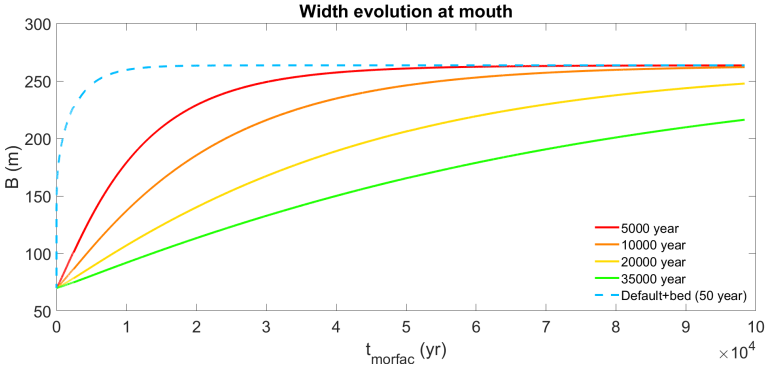

(c) Run called: "Tw+Exner+bed"

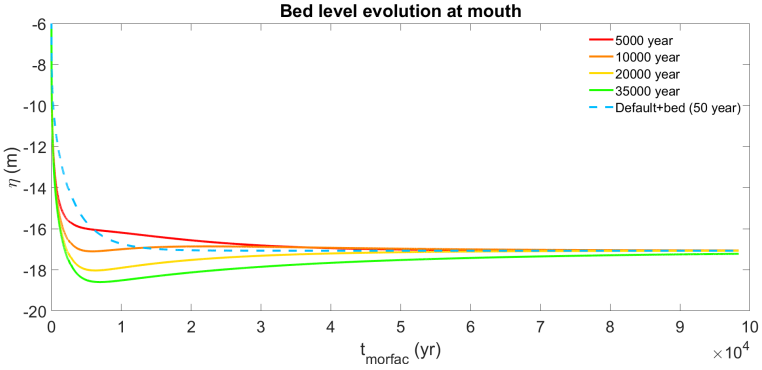

(d) Run called: "Tw+Exner+bed"

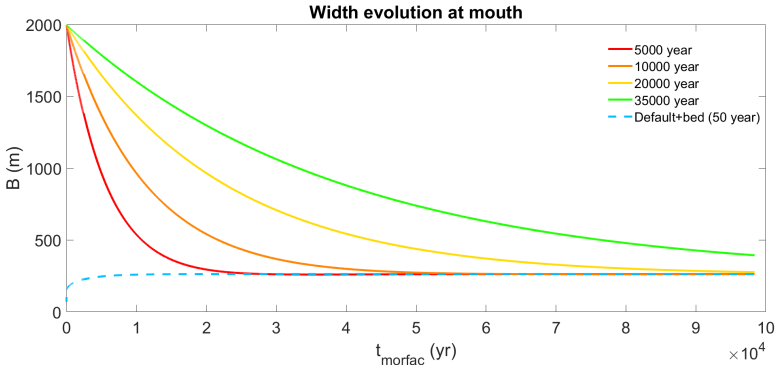

(e) Run called: "Tw+Lb+bed"

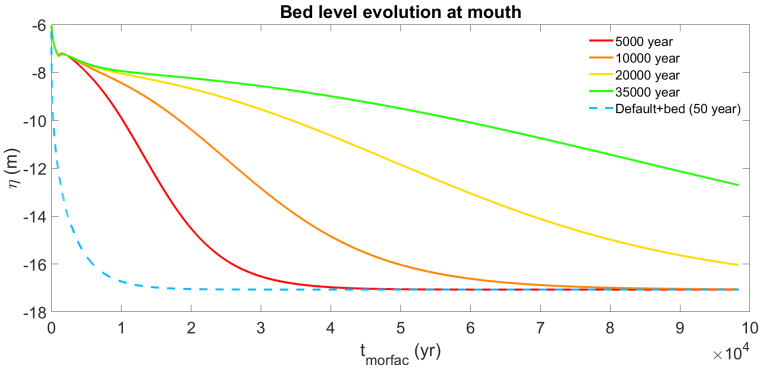

(f) Run called: "Tw+Lb+bed"

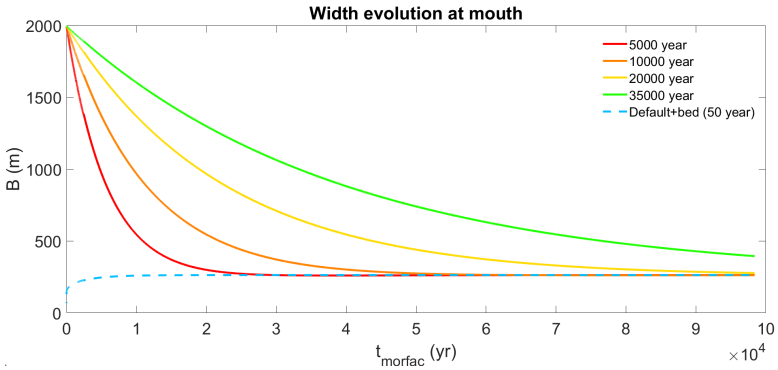

(g) Run called: "Tw+Lb+Exner+bed"

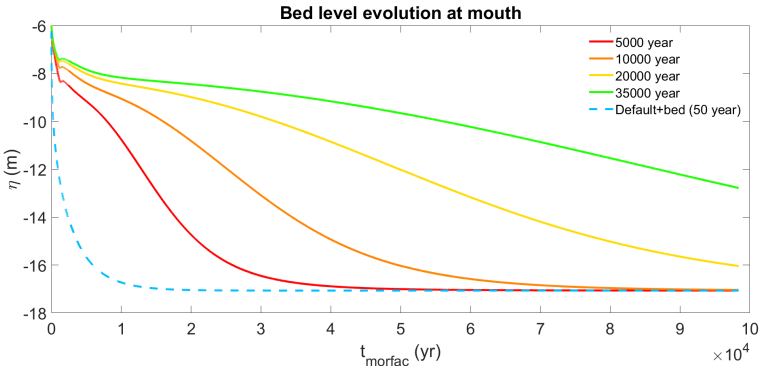

(h) Run called: "Tw+Lb+Exner+bed"

Figure 30: Width B and bed level η evolution at the mouth for runs where the time scale for width adjustment is changed or/and the Exner equation or/and the initial shape. The blue line indicates the width and bed level evolution for the run where the default settings are used and the channel starts as a straigth channel and the bed can change.

5.3 Relation to tide dominance

The previous section studied the effect of changing the model parameters and the boundary conditions on the estuary characteristics. These parameters and boundary conditions determine the tide dominance of the estuary. Changing parameters or boundary conditions can lead to a larger or smaller discharge ratio between the discharge due to the tide and the mean river discharge Q_{tide}/Q_{river}. This, in turn, determines if the estuary is tide-dominated. As explained in section 2.1, if Q_{tide}/Q_{river} is larger the estuary is more tide-dominated. In figure 32a it is clear that changing parameters or boundary conditions that lead to a more tide-dominated estuary, lead to an estuary with a larger width ratio B_{mouth}/B_{river}. Actually, a power-law trend $B_{mouth}/B_{river} = 1.18(Q_{tide}/Q_{river})^{0.47}$ can be observed in all the runs (without or with an adjustable bed) where the model parameter β is unchanged ($\beta = 0.5$). This could, of course, be expected as the empirical hydraulic geometry relation used to determine the width is a power-law relation with the peak discharge $Q_{tide} + Q_{river}$. When the discharge ratio Q_{tide}/Q_{river} becomes smaller or even less than 1 (so if the estuary is river-dominated instead of tide-dominated), the data deviates from this power-law relation, as B_{mouth}/B_{river} does not become smaller than 1. This is because the discharge can not become less than the river discharge upstream in the model, so the width can not become smaller than the width upstream. The trend between the width ratio and the discharge ratio changes if the model parameter β is adjusted (see figure 32b). How the power-law relation exactly adjusts, differs in the runs with a stable bed and a movable bed. In the runs with a movable bed, increasing β leads to even larger width ratios and discharge ratios than in the runs with a stable bed.

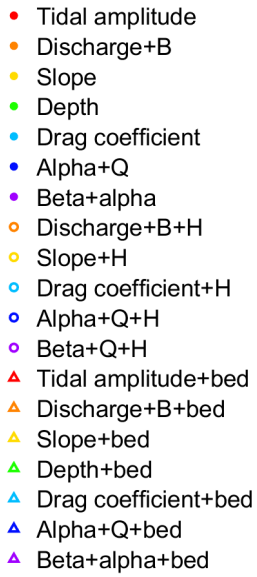

Figure 31: The complete legend for figures 32a, 35a, 35b and 36a.

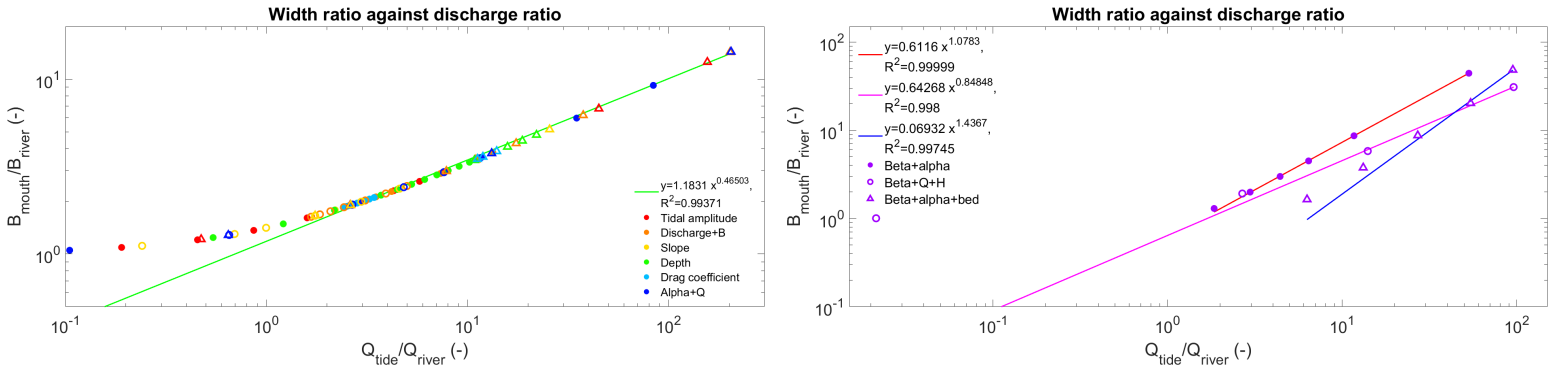

Figure 32: Width ratio B_{mouth}/B_{river} plotted against the discharge ratio Q_{tide}/Q_{river} at the mouth. a) shows the relation in all runs with the same model parameter β and b) shows how this relation is altered in the runs where β is changed. The closed circles indicate the runs with an adjustable width and stable bed, as indicated in the legend. The open circles indicate the runs with an adjustable width and stable bed, where additionally the channel depth is changed. The triangles indicate the equivalent runs, but with an adjustable width and an adjustable bed. For the complete legend see figure 31.

The depth ratio H_{mouth}/H_{river} does too follow a distinct trend with the tide dominance Q_{tide}/Q_{river} (see figure 33a). This relation is only studied in the runs where the bed level could additionally adjust next to the channel width (Runs: "Name of changing parameter(s)"+bed), as in these runs, the depth of the channel was not prescribed and could adjust to the parameters and boundary conditions. The trend is a power-law relation: $H_{mouth}/H_{river} = 0.96(Q_{tide}/Q_{river})^{0.46}$. This is not a relation that is expected straight away since observations of estuaries in nature show a variety of depth profiles, where besides profiles where the depth increases towards the mouth, also profiles, where the depth stays almost constant throughout the estuary or even decreases towards the mouth, are observed, as explained in section 2. The model does not develop these kinds of profiles. Again changing the model parameter β leads to a different relation between the depth ratio and discharge ratio, where smaller depth ratios occur with larger discharge ratios (see figure 33b). As both the width ratio B_{mouth}/B_{river} and the depth ratio H_{mouth}/H_{river} can be related to the discharge ratio Q_{tide}/Q_{river}, these two ratios can moreover be related to each other by a linear relation (see figure 34a). Interestingly, the aspect ratio B/H does not show a clear relation with the tide dominance, while the width ratio and depth ratio do (see figure 34b).

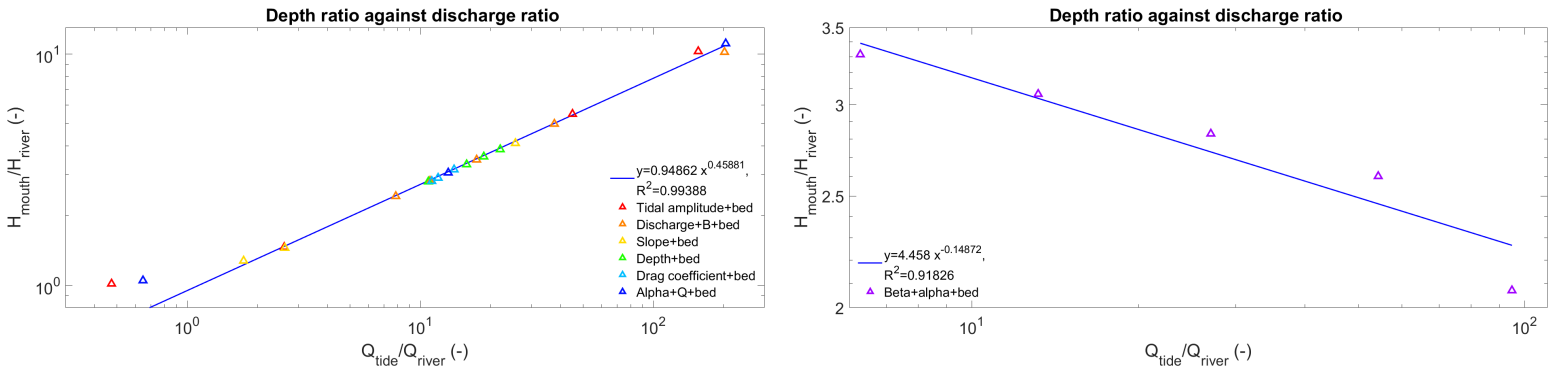

Figure 33: Depth ratio H_{mouth}/H_{river} against the discharge ratio Q_{tide}/Q_{river} at the mouth for the runs with a movable bed. a) shows the relation in all movable bed runs where the model parameter β is unchanged and b) shows how changing the model parameter β changes this relation.

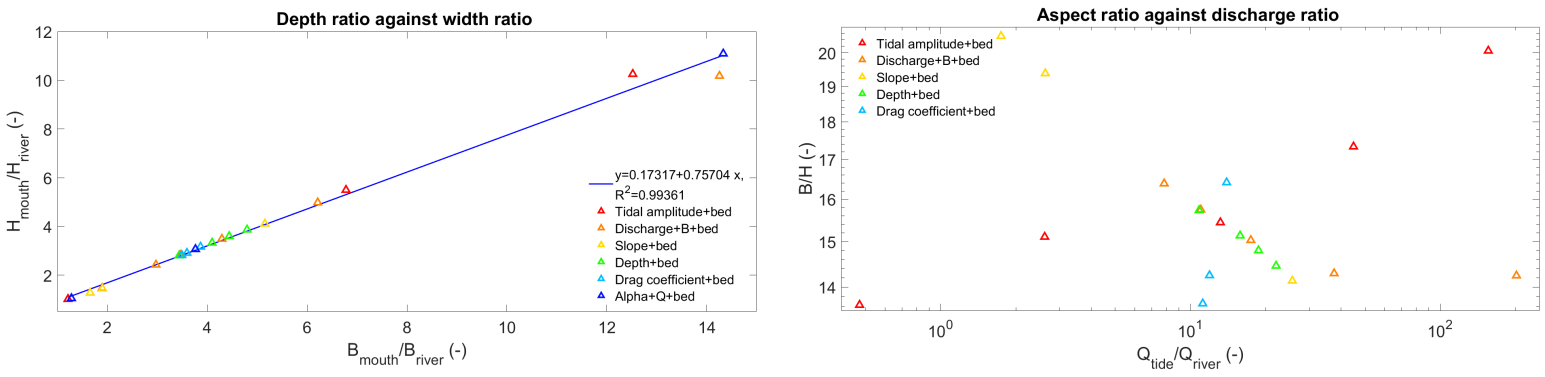

Figure 34: Depth ratio H_{mouth}/H_{river} against the width ratio B_{mouth}/B_{river} at the mouth (a) and the aspect ratio B/H against the discharge ratio Q_{tide}/Q_{river} at the mouth (b) for the runs with a movable bed.

No clear relation could be found between the tide dominance and the estuary length (see figure 35a). However, the data shows that overall, the estuary length becomes longer if the estuary is more tide-dominated, except for the run "Discharge+B+H" (indicated by the orange open circles). In the run "Discharge+B+H", the discharge ratio Q_{tide}/Q_{river} increases when the river discharge is decreased, and additionally, the upstream river width and channel depth is decreased. The discharge ratio and the width ratio are related, and so if the width ratio decreases, the discharge ratio decreases. As explained in section 5.1.2, decreasing the river discharge or the channel depth lead to different responses of the estuary length and the width ratio. In the run "Discharge+B+H", the width ratio depends more on the changing river discharge, and the estuary length depends more on the changing channel depth. This eventually leads to decreasing estuary lengths with increasing width ratio and so additionally increasing discharge ratio.

The e-folding length scale does not show any relation with the tide dominance (35b). The runs where the tidal amplitude or river discharge is changed (runs: Tidal amplitude, Tidal amplitude+bed, Discharge+B, Discharge+B+H and Discharge+B+bed) generally have a shorter e-folding length scale, so the estuary is more convergent if the estuary is more tide-dominated. However, the runs where the slope, depth or drag coefficient is changed (runs: Slope, Slope+bed, Depth, Depth+bed, Drag coefficient, Drag coefficient+bed) show an almost opposite trend; the estuary becomes generally less convergent when it is more tide-dominated. This will be further discussed in section 6.2.

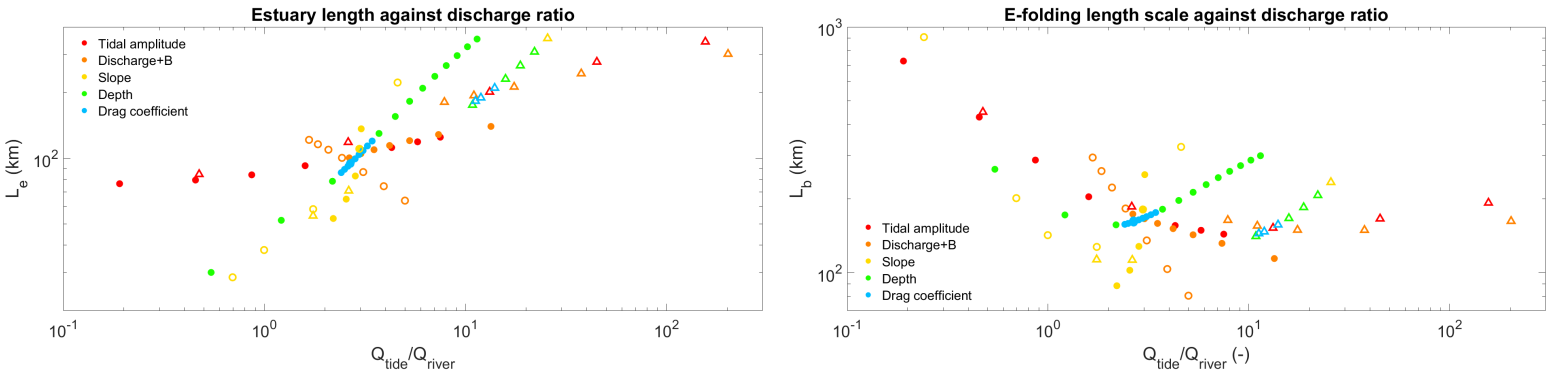

Figure 35: Estuary length L_e and e-folding length scale L_b plotted against the discharge ratio Q_{tide}/Q_{river} at the mouth for the runs with the same model paramter α and β. The closed circles indicate the runs with an adjustable width and stable bed, as indicated in the legend. The open circles indicate the runs with an adjustable width and stable bed, where additionally the channel depth is changed. The triangles indicate the equivalent runs, but with an adjustable width and an adjustable bed. For the complete legend see figure 31.

5.4 Hydraulic geometry relations

As the model determines the channel width using a hydraulic geometry relation, the hydraulic geometry relations that the model's output actually follows were studied. This was done for the runs where the model parameters α and β were not altered, as changing these parameters leads to the model using a different hydraulic geometry relation. As can be seen in figure 36a, the model produces the exact same hydraulic geometry relation between the width B and the total peak discharge $Q_{tide} + Q_{river}$ as is used. This verifies that the model indeed determines the width in the prescribed way. Furthermore, the output of the runs with an adjustable bed shows a hydraulic geometry relation between the depth H and the total peak discharge $Q_{tide} + Q_{river}$, where $H = 0.6(Q_{tide} + Q_{river})^{0.4}$. Only the data of the run "Drag coefficient+bed" does not follow this relation.

Besides the hydraulic geometry relations that relate channel properties to discharge, the hydraulic geometry relation between the cross-sectional area A and the tidal prism P was studied. In figure 37a it can be seen that the runs with a stable bed, where the channel depth and the model parameters α and β are unchanged, follow the relation: $A = 0.027P^{0.62}$. This relation has a smaller exponent than expected. The depth is the same in these runs, namely 6 m, and stays constant through time. Apparently, the width does not adapt such that the cross-sectional and the tidal prism follow an almost linear relation, as presumed (see section 2.3). The runs where the channel depth or the model parameters α or β is changed, do not follow this relation (see figure 37b). When one of these parameters is changed, the cross-sectional area tidal prism relation is altered. The runs where the channel depth is changed additional to another parameter (runs: "Discharge+B+H". "Slope+H", "Drag coefficient+H", "Alpha+Q+H", "Beta+Q+H") follow a bit different cross-sectional tidal prism relation as the channel depth is changed in every runs. Note that this difference is due to a difference in channel depth that is prescribed and not developed by the model itself.

The model develops a better cross-sectional area tidal prism relation in the runs with a movable bed (see figure 38). In these runs, both the width and depth can adapt, so the cross-sectional area in the estuary is not prescribed, and the cross-sectional area tidal prism relation is a combination of the width and depth adapting to the hydrodynamics. An almost linear relation can be fitted through this data, where

$$A = 2.05 \times 10^{-4} P^{0.94}. \tag{5.1}$$

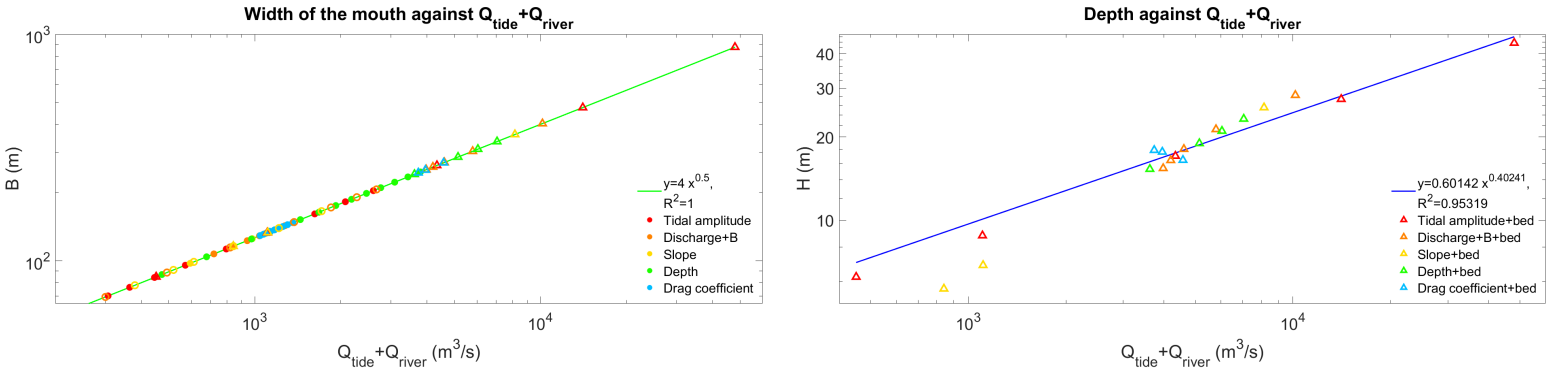

(a) (b)

Figure 36: The channel width B (a) and the channel depth H (b) against the peak discharge $Q_{tide} + Q_{river}$ at the mouth for the runs where the model parameters α and β are unchanged. The closed circles indicate the runs with an adjustable width and stable bed, as indicated in the legend. The open circles indicate the runs with an adjustable width and stable bed, where additionally the channel depth is changed. The triangles indicate the equivalent runs, but with an adjustable width and an adjustable bed. For the complete legend see figure 31.

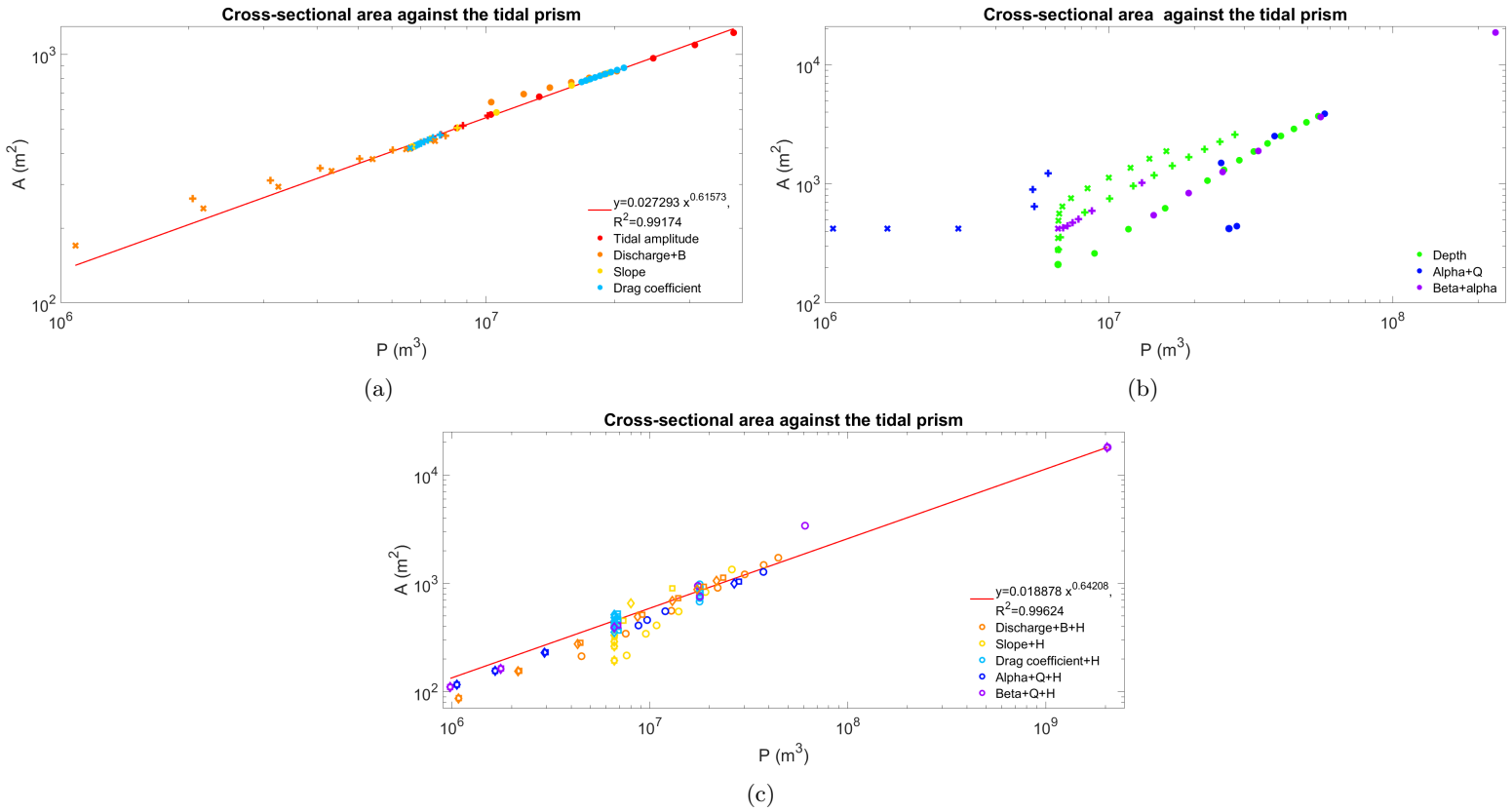

Figure 37: The cross-sectional area A against the tidal prism P for the runs with a stable bed. a) for the runs where the model parameters α and β and the channel depth are unchanged and equal to the default settings. b) for the runs where α, β or the channel depth are changed. c) for the runs where the depth is additionally changed according to the Chézy equation. The different markers indicate the cross-sectional area and tidal prism at different locations along the channel. The closed circles indicate the values at the mouth ($x = 400$ km), the plus signs indicate the values 100 km from the mouth ($x = 300$ km) and the crosses indicate the values 200 km from the mouth ($x = 200$ km).

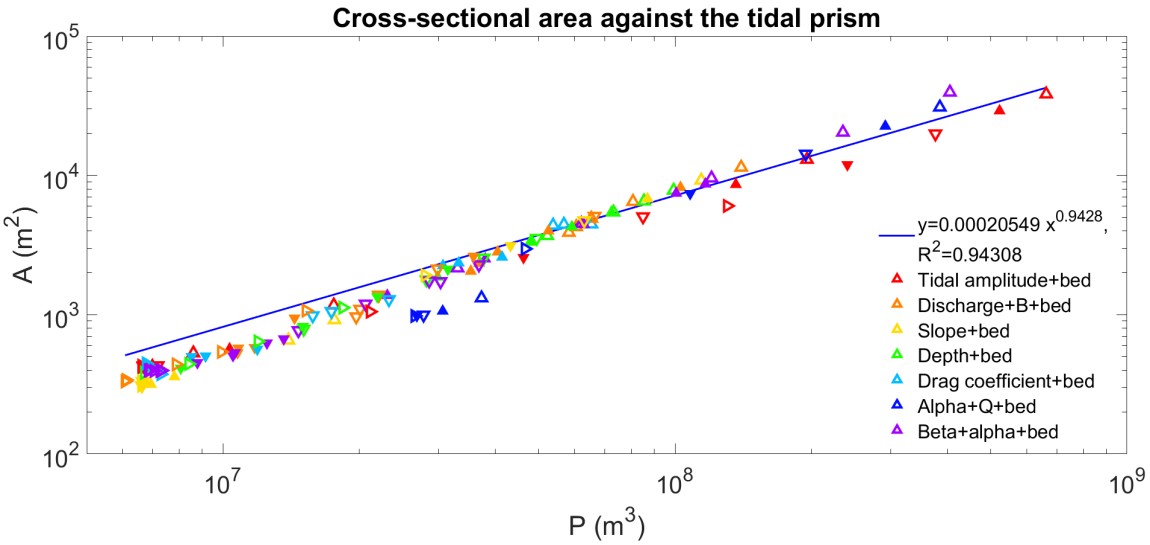

Figure 38: The cross-sectional area A against the tidal prism P for the runs with an adjustable bed. The different markers indicate the cross-sectional area and tidal prism at different locations along the channel. The open triangles pointing up indicate the values at the mouth ($x = 400$ km), the closed triangles pointing up indicate the values 50 km from the mouth ($x = 350$ km), the open triangles pointing down indicate the values 100 km from the mouth ($x = 300$ km), the closed triangles pointing down indicate the values 150 km from the mouth ($x = 250$ km), the open triangles pointing right indicate the values 200 km from the mouth ($x = 200$ km).

6 Discussion

In this section, the results will be discussed. This will be done by looking back at the previously discussed theory about and studies to tide-dominated estuaries and their equilibria (see section 2). The results will moreover be compared to observed estuary characteristics (see table 1 and other characteristics discussed in section 2). The fact that the model developed an equilibrium will be discussed. Then the equilibrium channel width, estuary length and e-folding length scale will be discussed and compared to predictors of previous studies. Thereafter the equilibrium bed level profiles, the hydraulic geometry relation used for the width adjustment and the cross-sectional tidal prism relation will be discussed. Last, there will be some recommendations for future studies.

6.1 Equilibrium

The model that was used in this study developed a steady-state with respect to the channel width and bed level. This was not necessarily expected. When the channel width increases, the tidal prism can likewise increase. This could, in turn, result in larger tidal peak discharges, and this would again increase the width further (as hypothesised by Braat et al. (2017), see section 2.2). However, evidently, an equilibrium between the width and the tidal prism is eventually reached, and the width stabilises. This means that the presence of cohesive sediments or vegetation (not included in this model) is probably not necessarily needed to reach an equilibrium in channel width, as was first thought by Braat et al. (2017). However, that an equilibrium is reached in the model does not directly mean that an equilibrium will be reached in the "real world", as explained in section 2.2. To further note is that most natural estuaries are not in equilibrium and will probably never reach an equilibrium as they are continuously adapting to changing boundary conditions (Braat et al., 2017). The presence of cohesive sediments or vegetation will in any way influence the estuary width and could force another equilibrium on the system. Furthermore, in this model, it is assumed that the underlying geology does not limit the estuary. If the estuary lies in a valley where the underlying geology limits the channel width, this will, of course, lead to a different estuary (Davies & Woodroffe, 2010).

The results show that the timescale for width adjustment does not influence the eventually reached equilibrium in the model, even when the timescale is close to the timescale for bed adjustment (around 20000 year) or even bigger. As the timescale for width adjustment is prescribed, no conclusions can be drawn on typical time scales for width change. Including the width change in the sediment balance and using another Exner equation (equation 4.18 instead of equation 4.9) likewise does not affect the equilibrium, but only the time it takes to reach the steady-state. Moreover, the results show that the initial shape of the width profile does not affect the equilibrium. This is surprising since starting with a convergent channel with a larger initial width at the mouth leads to a larger initial total discharge peak. However, apparently, this will not lead to another equilibrium and both the width and the total discharge peak decrease. This is even more surprising since starting with another initial channel depth, so another initial bed level, but with the same river discharge and other parameters, does lead to another equilibrium width and bed level profile. If the channel has a larger initial depth, the tidal wave can propagate further into the channel, and so a longer estuary is developed. This longer estuary leads to a larger total discharge peak, and so the width and depth at the mouth increase more. Leuven et al. (2021), who modelled the morphodynamic equilibrium in bed level in a model with fixed widths, found that with very similar hydrodynamics, significantly different bed profiles were found. Maybe multiple different equilibria may develop with the same forcing, but with a dependence of the bed level and width profile on each other. Another reason for the dependence of the equilibrium on the initial depth in our model could be the way the friction coefficient C_f is determined. Equation 4.8 shows that the friction coefficient is based on the channel depth, so starting with another initial depth corresponds to starting with another friction coefficient.

6.2 Channel width

The model developed quite small width ratios B_{mouth}/B_{river} with the model parameter α set to 4 and the model parameter β set to 0.5. These width ratios were larger when the bed could adjust but still not in the expected range. Width ratios observed in nature often range from 5 to 40, and even larger width ratios can be observed (Nienhuis et al., 2018). Increasing the model parameters α or β did result in more realistic width ratios. The effect of α and β will be further discussed in section 6.6.

The overall trend in the effect of changing the parameters or boundary conditions on the width ratio B_{mouth}/B_{river} did behave as expected. As was also shown by Todeschini et al. (2005) and Lanzoni and D'Alpaos (2015), larger tidal

amplitudes result in larger width ratios. Moreover, the results show that all parameters settings that lead to a greater tide dominance, so a larger discharge ratio Q_{tide}/Q_{river}, result in larger width ratios. The control of this discharge ratio on the width ratio explains why increasing or decreasing the tidal amplitude or river discharge had one of the greatest effects on the width ratio.

The model results of the runs with a movable bed were tested against the width ratio predictor of Nienhuis et al. (2018) (see equation 2.6 and figure 39). Overall are, the modelled width ratios smaller than the predicted width ratios. However, when the modelled width ratio is larger (> 5) the predicted width ratio is smaller. The predictor especially underpredicts the effect of a larger tidal amplitude or a smaller river discharge. The trend in the predicted width ratio with changing river discharge and changing drag coefficient is different than our results show see figure 22. The predicted width ratio becomes smaller with decreasing river discharge or decreasing drag coefficient, while our results clearly show an increase in width ratio with decreasing river discharge or drag coefficient. Furthermore, the figure shows that increasing the model parameter α or β a bit could better fit the predicted to the modelled width ratio. If the model parameters would be increased too much, the modelled width ratios become would become much larger than the predicted width ratios. A β between the 0.5 and 0.65 would probably lead to the best fit.

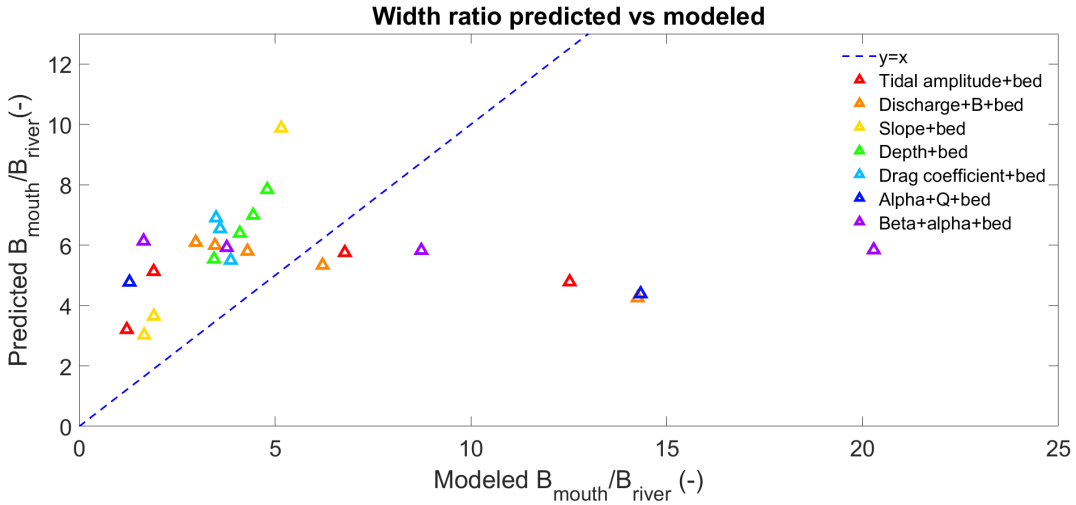

Figure 39: The predicted width ratio plotted against the modeled width ratio for the predictor of Nienhuis et al. (2018) (see equation 2.6). The colors indicate the different sets of runs as labeled in the legend. Note: there is one data point that is not shown in this plot. This data point belongs to the run "Beta+alpha+bed" and lies on (48, 6).

6.3 Estuary length

Generally, the estuary lengths increased with increasing tide dominance (except for the runs "Discharge+B+H" as explained in section 5.3), but the relation was not that clear. Furthermore, the estuary lengths are within the expected range but longer than the average estuary length (see 1). In the runs with a movable bed, estuary lengths that were even longer developed with respect to the runs with a stable bed. This is probably due to the large depths of the channels. In all the runs with a movable bed, the depth profile shows an increase in depth towards the mouth. This increase results in less dampening of the tidal wave so that the wave can propagate further into the channel, and the estuary length increases. Besides, the initial slope of the channel has a significant effect on the estuary length. For the default settings, a slope of 3×10^{-5} was chosen, which is quite a slight slope. The average slope of tide-dominated deltas from the data from Nienhuis et al. (2018) was 5.7×10^{-5}. This slope is almost twice as big as the default setting of the model. When a slope of 5.7×10^{-5} would be used in combination with the other default settings in a run where the bed is adjustable, this would probably result in an estuary length of approximately 120 km instead of 200 km (see 23b).

Another reason for the long estuary lengths could depend on how the estuary length is determined. The upstream boundary of the estuary is the tidal limit, as explained in section 4.2.3. Other options for determining the estuary

length are based on the salinity or facies boundary, as explained in section 2.1, and result in shorter estuaries (see figure 1).

Nienhuis et al. (2018) based the estuary length on the upstream river depth $H_{upstream}$ divided by the delta channel slope $S_{upstream}$ (see section 2.1):

$$L_e = \frac{H_{upstream}}{S_{upstream}}. \tag{6.1}$$

The average estuary length for tide-dominated deltas from their data was 170 km. Determining the estuary length in this way with our data results in somewhat shorter estuary lengths than in the way it was determined for this study (see figure 40, closed triangles). A few other studies tried to derive a relation for estuary length analytically, as briefly discussed in section 2.1. One is the predictor of van Rijn (2011), who derived that the estuary length of an ideal estuary with constant tidal range should depend on the depth at the mouth H_{mouth}, the tidal amplitude $a_{z,mouth}$, the drag coefficient C_d and the phase ϕ:

$$L_e = \frac{12\pi\, H_{mouth}^2}{16\, C_d\, a_{z,mouth}\, \cos(\phi)}. \tag{6.2}$$

Another one is the predictor of Prandle (2004), that is also depended on the depth at the mouth H_{mouth}, the tidal amplitude a_z and the drag coefficient C_d and additionally on the tidal angular velocity $\omega = \frac{2\pi}{T}$:

$$L_e = \frac{4}{5}\frac{(2\,g)^{1/4}}{\sqrt{1.33\, C_d\, \omega}}\frac{H_{mouth}^{5/4}}{a_{z,mouth}^{1/2}}. \tag{6.3}$$

Both these predictors do not show a good fit with the determined modelled estuary length (see figure 40, circles and plus signs, respectively). This could be because the modelled estuaries are not ideal. However, both predictors relate inversely to the tidal amplitude, though we expect the estuary length to become longer with increasing amplitude. Based on the predictor of Nienhuis et al. (2018) and the fact that the determined estuary length is based on the tidal limit, a new predictor was developed:

$$L_e = \frac{a_{z,mouth} + H_{mouth}}{S_{estuary}}, \tag{6.4}$$

which does show a good fit with the determined modeled estuary length (see figure 40, open triangles). This dependence on the tidal amplitude, depth at the mouth and estuary slope could be expected as the results show that these indeed mainly control how far the tide can propagate up the estuary.

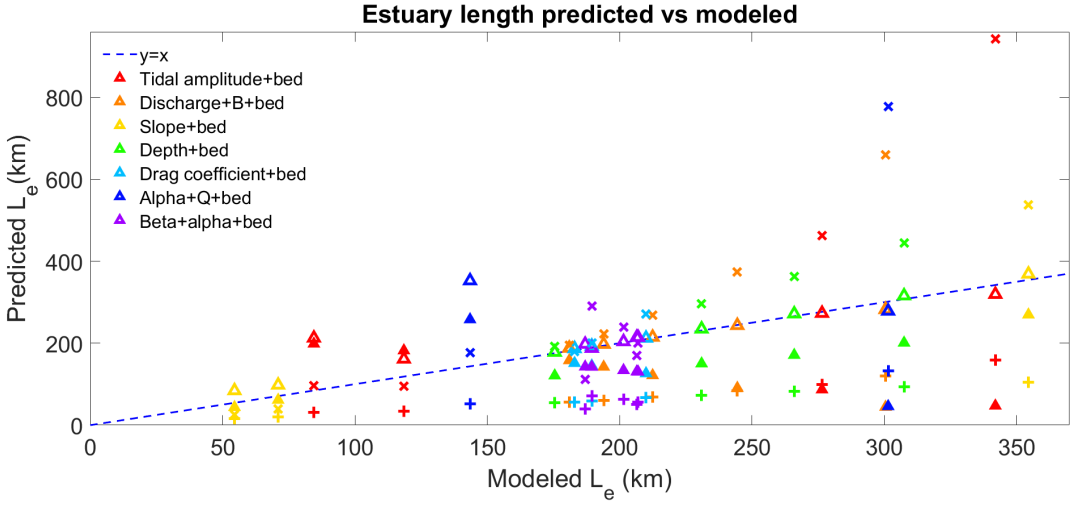

Figure 40: The predicted estuary length plotted against the modeled estuary length for 4 different predictors. The crosses indicates the predictor of van Rijn (2011) (equation 6.2), the plus sign indicates the predictor of Prandle (2004) (equation 6.3), the closed triangle indicates the predictor of Nienhuis et al. (2018) (equation 6.1) and the open triangle indicates our own predictor (6.4). The colors indicate the different sets of runs as labeled in the legend.

6.4 E-folding length scale

The e-folding length scales were longer than expected, as typical estuary e-folding length scales are of an order 10 to 50 km (van Rijn, 2011) (see section 2.1). However, estuaries with larger e-folding length scales up to 230 km are observed in nature (Todeschini et al., 2008). Interesting is that the effect of changing the tidal amplitude, the initial slope or the model parameter α on the e-folding length scale show two different trends in the runs with an adjustable bed (see figure 24). When these parameters are small and are then increased, the e-folding length scale becomes quite rapidly shorter, but if the parameters become even larger, the e-folding length scale increases again. It looks as if the e-folding length scale is limited and can not be shorter only if the model parameter β is increased. This leads us to believe that only increasing the coefficient β with respect to the default settings could lead to the model developing realistic e-folding length scales.

Furthermore, the width profiles of the runs with an adjustable bed do not all show a typical exponential profile. A linear fit would probably be okay in some cases, too. Figure 41 confirms this presumption. If the width profile would indeed be exponential, i.e. $B_{mouth} = B_{river}\mathrm{e}^{L_e/L_b}$, then $B_{mouth}/B_{river} = \mathrm{e}^{L_e/L_b}$. The figure shows that not all data lies on this line. Especially, the data of the runs where the bed is adjustable, and the tidal amplitude or the model parameter α is large, or the river discharge is minimal, deviate from the line. In addition to the data of the runs with a huge model parameter $\beta > 0.85$. Although, this data from the runs with a large β do not deviate because the width profile increases more linear like (see figure 13g, 21g).

Todeschini et al. (2005) used an erosion model to simulate channel widening. Their model did not always produce a perfect convex width profile but concave profiles as well, especially when no river discharge was forced at the upstream boundary. Our result confirms this: they show a less convex shape with minimal river discharge. The runs with a larger tidal amplitude but the same river discharge deviate from this convex shape too. This shows the importance of the balance between the river discharge and the tidal amplitude for the characteristic convex shape. The research of Lanzoni and D'Alpaos (2015) who used a 2-dimensional hydrodynamic and morphodynamic model to study short tidal channels, agrees with this hypothesis as well, as the width profiles likewise showed an almost better linear relation, and in their model, no upstream river discharged was forced upon the tidal channels. Furthermore, Todeschini et al. (2005) hypothesised that the width profile is more convergent if the estuary slope is small. This was confirmed by their results of a run with a fixed horizontal bed, that indeed resulted in a more convergent estuary. The width profiles of our results of the runs with a fixed but sloping bed also show a better exponential fit than their equivalent runs with a movable bed.

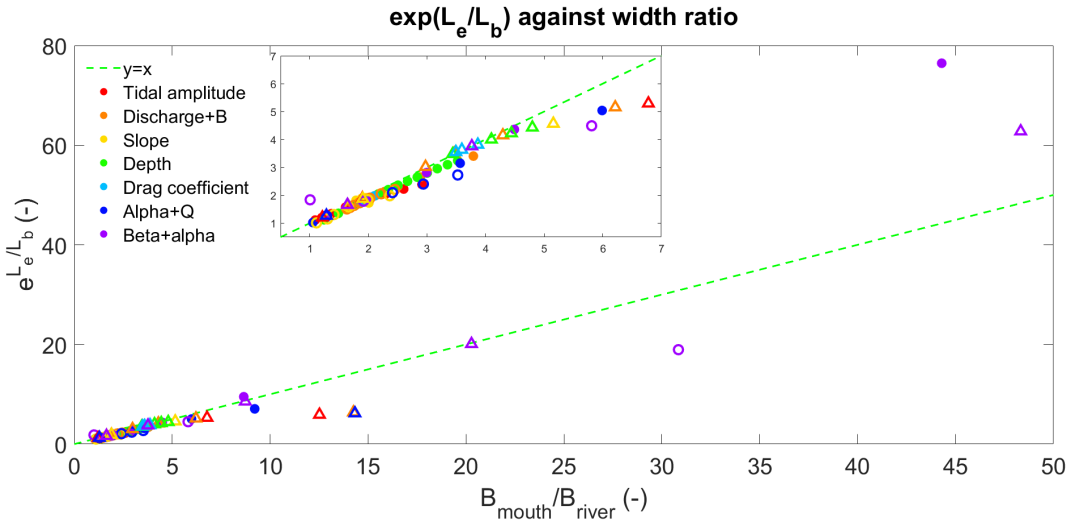

Figure 41: e^{L_e/L_b} plotted against the width ratio B_{mouth}/B_{river}.The circles indicate the runs with an adjustable width and stable bed and the triangles indicate the equivalent runs, but with an adjustable width and an adjustable bed ("Name changing parameter"+bed). The red line indicates the line where $e^{L_e/L_b} = B_{mouth}/B_{river}$.

Interestingly, our results show first more convergent convex width profiles when the river discharge is decreased instead of the concave shape when the river discharge is even more decreased. Leuven, van Maanen, et al. (2018) showed that the e-folding length scale of estuaries are correlated to the upstream channel width, where shorter e-folding length scales were observed, so more convergent channels, with smaller upstream channel width. In the runs in this thesis, the upstream channel width is additionally decreased when the river discharge is decreased. For these runs, we indeed see that until a certain limit, a smaller river discharge, so a smaller river width, results in shorter e-folding length scale. If the river discharge falls below this limit, the estuary shape changes from convex to concave, as explained. This again confirms that the shape and degree of convergence are determined by the balance between the tide and the river discharge. A certain river discharge is needed to result in a convex shape. An even larger river discharge then leads to a more convergent shape, but the convergence rate again decreases if the river discharge is even more prominent. How much river discharge leads to the most convergent convex estuary shape depends on the tidal amplitude and other channel characteristics. This explains why there is no exact relation between the tide dominance and the e-folding length scale. The channel needs to be tide-dominated to have a convergent convex shape, and at first, a more tide-dominated channel is more convergent, but if the channel is even more tide-dominated, the channel has a less convergent convex shape.

Again the e-folding length scale from our results was tested against the predictors that were discussed in section 2.1, the predictor of Savenije (2005) (see equation 2.3) and of Chappell and Woodroffe (1994) (see equation 2.4) (see figure 42). To note is that these predictors were made for ideal estuaries with a constant water level amplitude, velocity amplitude and channel depth. None of our runs developed an ideal estuary. The predictor of Chappell and Woodroffe (1994) largely under predicts the e-folding lengths scales. This predictor related the e-folding length scale to the time-averaged product of the depth H and the flow velocity U, $\overline{HU}$. In the derivation it was assumed that two times the tidal prism P equals the product of this $\overline{HU}$, the channel width B and the tidal period T. However, this leads to a great under prediction of the tidal prism. As from our model results the tidal prism can be determined the predictor can be rewritten to directly use the tidal prism. The corrected predictor is:

$$L_b = \frac{P}{2\,a_z\,B}, \tag{6.5}$$

where P is the tidal prism (m^3), a_z is the water level amplitude (m) and B is the channel width (m). This corrected predictor for the e-folding length scale lies closer to the modelled e-folding length scale, but there is still not a good match. The predictor of Savenije (2005) shows a better match with our results, but the predicted e-folding lengths are still generally shorter than the modelled e-folding length scales. As the data of the model runs "Slope+bed", "Depth+bed" and "Drag coefficient+bed" are parallel to the $y = x$ line, we do think that the predictor of Savenije (2005) shows the same kind of trend between the e-folding length scale and the slope, depth or drag coefficient than our results. However, the figure shows that the predictor does not capture the same trend between the e-folding length scale and the river discharge or tidal amplitude. Interestingly, when the model parameter β is increased, so the modelled e-folding length scales become shorter, the modelled e-folding length scale better matches with the predicted e-folding length scales (best match when $\beta = 0.65$).

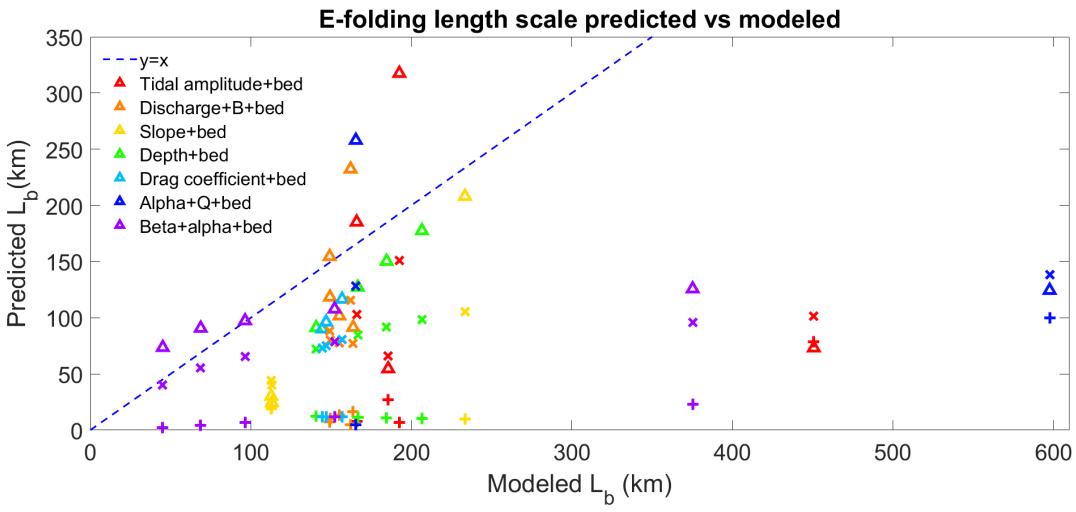

Figure 42: The predicted e-folding length scale plotted against the modeled e-folding length scale for 3 different predictors. The open triangles indicate the predictor of Savenije (2005) (eq 2.3). The plus signs indicate the predictor of Chappell and Woodroffe (1994) (eq 2.4). The crosses indicate the corrected predictor or Chappell and Woodroffe (1994) (eq 6.5). The colors indicate the different sets of runs as labelled in the legend.

6.5 Bed level profiles

The model produces concave down bed level profiles with channel depths at the mouth that are pretty deep. However, these channel depths do lie within the expected range of 1 m to 45 m (see section 2.1). In the model, the depth ratio H_{mouth}/H_{river} scaled with the discharge ratio Q_{tide}/Q_{river}, while estuaries in nature often have an almost constant depth throughout the estuary (Todeschini et al., 2008) or have an increasing depth toward the mouth and at the mouth a sudden decrease in depth (Canestrelli et al., 2014; Hibma et al., 2003; Leuven et al., 2021). Leuven et al. (2021) studied this scour like bed profile in estuaries by using a one-dimensional hydro- and morphodynamic model (with fixed channel widths). A predictor was found based on the ratio between the tidal and river discharge, and e-folding length scale, that predicts if the bed profile will have this sudden decrease at the mouth:

$$\frac{Q_{tide}/Q_{river}}{L_b/(B_{mouth}-B_{river})} > 0.3. \tag{6.6}$$

If this condition is met, the bed profile will show a scour like profile, whereas if this condition is not met, the bed profile will show a constantly increasing depth. The estuaries modelled in this thesis do not meet this requirement, so it is indeed expected that the bed profiles show a constantly increasing depth towards the mouth. This is mainly due to the low convergence. Moreover, Leuven et al. (2021) tested the predictor against the results of the studies of Bolla Pittaluga et al. (2015) and Canestrelli et al. (2014). The results of Bolla Pittaluga et al. (2015) showed bed levels that corresponded more to the bed levels of this thesis, and indeed their estuaries did not follow the condition. The results of Canestrelli et al. (2014) do show a scour like profile and do meet the requirement.

That the convergence of the width profile has a large control on the shape of the estuary bed profile is moreover shown by Toffolon and Lanzoni (2010), Lanzoni and Seminara (2002), Lanzoni and D'Alpaos (2015) and Seminara et al. (2010), who all found that a shorter e-folding length scale, so a more convergent estuary, has a more concave up bed level profile. While channels with longer e-folding length scales develop concave down bed level profiles, as is the case in this thesis. The results showed a relatively good power-law relation between the depth ratio H_{mouth}/H_{river} and the tide dominance ratio Q_{tide}/Q_{river}, and the width ratio B_{mouth}/B_{river}. With keeping in mind the results of the study of Leuven et al. (2021), we hypothesise that if the tide dominance ratio or width ratio will increase even further, the data will deviate from these power-law relations as the depth at the mouth will stabilise or even decrease again.

Furthermore, Leuven et al. (2021) found that the depth at the mouth in case of a concave down profile increases

with increasing tidal amplitude and decreasing river discharge, which the results of this thesis confirm. The role of the river discharge was emphasised by Guo et al. (2015) who specifically studied the role of the river discharge on the bed profile of estuaries. They argued that increasing river discharges supply more sediment, which results in a shallower estuary with smaller slopes, while decreasing river discharges lead to larger depths and steeper slopes. Even smaller discharges would limit the ebb flow and lead to less erosive capacity, and the depths would decrease again. However, the latter can not be deduced from our results. This could be because the river discharge is not decreased that much in our runs. Bolla Pittaluga et al. (2015), Todeschini et al. (2008) and Lanzoni and D'Alpaos (2015) moreover researched the effect of the tide, and all confirmed that the depth at the mouth and estuary slope increases with increasing tidal amplitude.

In the runs where the model parameter β was increased (run called: Beta+alpha+bed), the bed profile showed a decrease in depth at the upstream boundary of the estuary. This decrease in depth was also modelled by Canestrelli et al. (2014) and Todeschini et al. (2008), where likewise this decrease became more pronounced with shorter e-folding length scales. Tambroni et al. (2005) moreover showed that this "beach" developed in experimental settings. Canestrelli et al. (2014) hypothesised that this deposition is a result of the break in the trend of the width profile from convergent to straight.

6.6 Hydraulic geometry relation coefficients

The chosen hydraulic geometry relation coefficients α and β for the width adjustment (see equation 4.16) have a large influence on the results of the model. As a first approximation, a β of 0.5 and an α of 4 were chosen for the default settings. However, as previously mentioned, do these settings lead to smaller width ratios B_{mouth}/B_{river}, larger channel depths at the mouth H_{mouth}, and longer e-folding length scales L_b than expected. As explained in section 2.3, there has been much discussion around hydraulic geometry relations. Our choice for the value for β and α was mostly based on rivers generally corresponding to these values. Most hydraulic geometry relations for tidal channels relate to the cross-sectional area instead of width, so determining a β from these relations is quite complex as the width-to-depth ratio is not necessarily constant. (If the width-to-depth ratio B/H is constant than $B = \sqrt{A}$ and $\beta = 0.5\beta_A$.) The underestimation of the model parameter β and perhaps α could explain the small width ratios, large channel depths, and long e-folding length scales.

In section 2.3 the exponents determined by Myrick and Leopold (1963) and Langbein (1963) were also discussed. They arrived at a exponent b for the relation between width and discharge of 0.71 and 0.72 respectively. This is confirmed by Rinaldo et al. (1999) as well, who used the data of various tidal channels to related the total peak discharge $Q_{tide} + Q_{river}$ to the channel width by $Q_{tide} + Q_{river} \propto B^{1.38}$. Rewriting this equation gives $B \propto (Q_{tide} + Q_{river})^{0.72}$. Furthermore, does Leuven, De Haas, et al. (2018) show that $B = 0.05P^{0.59}$ corresponds to data of 35 estuaries. Rewriting this equation with using equation 2.16, gives $B \propto (Q_{tide} + Q_{river})^{0.70}$. This in combination with our results make us believe that using a β around 0.70 in the model would better simulate the width profile of an estuary.

Even less studies have been done to the coefficient α in estuaries or a of equation 2.9 in rivers. There is a possibility that α is not universal and describes some channel properties indirectly and will vary between estuaries with different channel properties. For example, Simons and Albertson (1960) showed that for rivers a depended on soil properties of the bank where a is 3.1 for coarse material and 6.3 for sand (Savenije, 2005). Also, Gleason (2015) pointed out that some researchers included other bank strength variables in this coefficient a so the hydraulic geometry relations better match nature.

6.7 Cross-sectional area tidal prism relation

Interesting is that even though the model develops channel widths that are smaller than expected and channel depths that are deeper than expected, the cross-sectional area follows a realistic relation with the tidal prism along the estuary in case of the runs with a movable bed that is in independent of any boundary conditions, channel characteristics and model parameters (see equation 5.1). The tidal prism at the mouth varies between the 8×10^6 and 7×10^8, which is in the range observed in estuaries of 10^6 to 10^{11} (see section 2.1, Leuven, De Haas, et al. (2018); Nienhuis et al. (2018)). As discussed, the exponent β_{AP} of the cross-sectional tidal prism relation often lies between the 0.85 and 1.1 and the coefficient α_{AP} can vary between 6.6×10^{-5} and 1.2×10^{-3}. The model developed a relation with an exponent

$\beta_{AP} = 0.94$ and a coefficient $\alpha_{AP} = 2.05 \times 10^{-4}$, so these are all in the expected range. That the cross-sectional area does follow a good relation with the tidal prism could be why large channel depths are developed. The channel width remains quite small and is limited by the empirical hydraulic geometry relation that is used. The channel depth then adapts and becomes quite large to still meet the cross-sectional area tidal prism relation. If the model parameter α and β would be optimized to develop more realistic wider channel width profiles, the developed channel depths will probably be smaller and so too be more realistic. This is because cross-sectional area tidal prism relation is not dependent on the model parameters α or β.

6.8 Future research

A hydraulic geometry relation determined the width in this model because the effect of the hydrodynamics and sediment transport on the width of an estuary is not yet entirely clear. However, the hydraulic geometry relations for estuaries are moreover not intensively studied. This leads to a significant knowledge gap in the theory about estuary width. This knowledge gap becomes even more apparent in this thesis, where one of the most significant results is the effect of the chosen coefficients β and α on the width and bed level profile. When looking at the long term evolution of estuaries, it is essential to study the bed level and the width profile. This is why this knowledge gap must be closed. Hydraulic geometry relations can be beneficial in predicting the width profiles, so it is meaningful to study these more in relation to estuaries. Testing the model with different coefficients α and β to data of estuaries would be a significant first step. It is essential that future studies also include the coefficient α in their research since this coefficient was less intensively investigated in the past. As discussed, the coefficient α could depend on other channel characteristics, like soil properties. Integrating these characteristics into the hydraulic geometry relation could lead to a more universal hydraulic geometry relation.

Another option for future research is to use an erosion law in combination with a sedimentation law to simulate bank adjustment of an estuary. Models that only include an erosion law do produce realistic widths and e-folding length scales but do not reach an equilibrium, as the width constantly widens (Braat et al., 2017; Lanzoni & D'Alpaos, 2015; Van der Wegen & Roelvink, 2008). Adding a sedimentation law is a good solution to oppose this constant widening. Xu et al. (2019) modelled erosion and sedimentation processes in a coupled 2D model, and it would be interesting to apply this method in a 1D model. However, this would complicate the model further as modelling erosion and sedimentation processes are still quite complex (Kleinhans et al., 2011). Researchers have made good steps in studying these processes for upstream rivers. Parker et al. (2011) reconsidered the eroding and depositing bank processes and Dunne and Jerolmack (2020) studied which factors determine river width.

Suppose the model would be adjusted by changing the hydraulic geometry coefficients or using erosion and sedimentation laws. In that case, this model could predict the effect of changing boundary conditions on estuaries and tidal channels, for example, sea-level rise or a decrease in sediment supply. Sea level rise induces deepening of the channel, decreases friction and increases the tidal dominance over the fluvial dominance (Leuven et al., 2021). The model results show that this will lead to longer and broader estuaries. Leuven et al. (2021) explained that if the banks are fixed, sea-level rise will lead to large scour, which in turn can lead to bank instability. Reducing the sediment supply can have the same effect and lead to bank instability (Hackney et al., 2020). This could probably be mitigated by the estuary laterally expanding (Leuven et al., 2021). If this indeed can be mitigated by letting the estuary expand can be studied with this model if it would be optimized.

7 Conclusion

In this thesis, the morphodynamic equilibrium of the width and the bed level profile of an estuary in response to adjustable channel widths are studied. This was done by using an one-dimensional hydrodynamic and morphodynamic model that included variable channel widths. The width in this model was determined by a hydraulic geometry relation that related the width to the peak in total discharge. This total peak discharge is the sum of the river discharge and the peak in tidal discharge, so the hydraulic geometry relation includes the tidal and fluvial influence. In the first runs, the bed was kept stable to single out the effect of channel properties and boundary conditions on the equilibrium width profile. Then runs were done where the bed was moreover variable, and the response of the bed and width to each other could be studied.

The modelled estuaries evolved towards a stable width and bed level profile, so a morphodynamic equilibrium in width and bed level profile was reached. This means an equilibrium exists between the channel width and total peak discharge, so also between the channel width and the tidal prism. This equilibrium was not dependent on the chosen time scale for width adjustment or on the initial width shape of the channel. The eventually reached equilibrium did furthermore not change if the width change was taken into account in the sediment balance by adding a term to the Exner equation. However, the equilibrium was dependent on the initial channel depth, so another equilibrium was reached if the initial bed shape was changed.

The model results showed a large dependence on the choice of the model parameters β and α used in the hydraulic geometry relation for the width adjustment. Especially the width ratio and e-folding length scale were greatly influenced by β and α in all runs. Additionally, the channel depth and estuary slopes were greatly affected by β and α in the runs where the bed was not fixed. The model parameter β has the most effect on the width ratio and e-folding length scale, and the model parameter α has the most effect on the depth and slope. The default setting of $\beta = 0.5$ and $\alpha = 4$ were probably an underestimation. A value of β around 0.7 is suggested for future studies and studying the option to include other channel properties in the model parameter α. The model did show a realistic cross-sectional tidal prism relation in the runs with an adjustable width and bed that did not depend on the model parameter β or α or any other channel characteristics or boundary conditions.

The equilibrium generally showed larger ratios between the width at the mouth and the width upstream B_{mouth}/B_{river} and longer estuary lengths as a result of increased tidal amplitude or initial channel depth or decreasing river discharge, initial bed slope or drag coefficient. E-folding length scales generally decreased with increasing tidal amplitude, initial bed slope or drag coefficient and increased with increasing river discharge and initial channel depth. These trends were also seen in the runs with a movable bed. Including the bed level adjustment led to overall larger width ratios and longer estuary lengths but had less effect on the e-folding length scales. The most important factors influencing the width ratio were the tidal amplitude, the river discharge and the initial channel depth, next to the model parameters β and α. There is a robust power-law relation between the width ratio and the tide dominance ratio Q_{tide}/Q_{river}, so all factors influencing the tide dominance ratio influence the width ratio. The slope and depth mainly determine the estuary length. This was moreover made clear by the modelled estuary length following a good fit with the ratio between the sum of the tidal amplitude and depth at the mouth and the estuary slope $(a_{z,mouth} + H_{mouth})/S_{estuary}$. The most important factor affecting the e-folding length scale is the tidal amplitude and river discharge, next to the model parameters α and β. Interesting is that the e-folding length scales show that to develop the most convergent convex estuary shape, the tidal amplitude and river discharge should not be too small and not be too large, but that there is a certain optimum that probably depends on other channel characteristics like channel depth, slope and drag coefficient.

The bed level profile generally showed concave down profiles, with a change in bed slope between upstream and the estuary. Quite large channel depths were developed at the mouth. This could be due to the model parameters α and β or the small initial slopes, as larger initial slopes led to smaller depths. Overall, channel depths at the mouth increase with increasing tidal amplitude, initial depth or drag coefficient or increasing river discharge. The channel depths upstream varied less and more erosion (so larger depths) due to increasing tidal amplitude or initial slope or decreasing river discharge, initial depth or drag coefficient. Steeper estuary and upstream slopes were developed with larger tidal amplitudes, initial slopes or drag coefficients and smaller river discharges and initial channel depths. That no other bed profiles developed, like a profile with constant depth or a profile with a decrease in depth at the mouth,

is probably due to estuaries having a long e-folding length scale. The results match with the proposed condition by Leuven et al. (2021) for bed level profiles with a scour, as the condition is not met in the model, and the model does not develop bed profiles with a scour.

Overall, this thesis showed that it is crucial that the knowledge gap in the theory of hydraulic geometry relations for estuaries and the theory of what determines estuary width needs to be closed if we want to gain insight into the long term evolution of estuaries. If this insight is gained, it can be used in numerical models like the one used in this thesis. These numerical models can be of great importance in predicting effects on estuary width and bed level of human interference, like rapid sea-level rise or decreasing sediment supply.

A Notation

Symbol	Property	Unit
a_u	tidal velocity amplitude	m/s
a_z	tidal water level amplitude	m
A	cross-sectional area	m^2
B	channel width	m
B_e	equilibrium channel width	m
B_{mouth}	channel width at mouth	m
B_{river}	channel width of upstream river	m
C	chézy coefficient	$m^{1/2}/s$
C_d	drag coefficient	-
C_f	friction coefficient	-
D_{50}	median grain size	m
g	gravitational acceleration	m/s^2
H	water depth	m
$H_{upstream}$	water depth at upstream boundary	m
H_{mouth}	water depth at mouth	m
I	discharge ratio	-
k_e	lateral erosion rate	m/s
k_t	tidal efficiency coefficient	1/m
k_s	roughness heigth	m
L	channel length of whole modeled channel	m
L_b	e-folding length scale	m
L_e	estuary length	m
p_s	sediment porosity	-
P	tidal prism	m^3
q_s	total sediment transport per unit width	m^2/s
$q_{s,bank}$	total sediment transport affecting the channel banks per unit width	m^2/s
q_b^*	dimensionless total sediment load per unit width	-
Q	total discharge	m^3/s
$\overline{Q}$	tidally averaged total discharge	m^3/s
Q_b	bankfull discharge	m^3/s
Q_l	tidal discharge constituent	m^3/s
Q_{peak}	total peak discharge	m^3/s
Q_{river}	river discharge	m^3/s
Q_s	total sediment transport	m^3/s
Q_t	tidal discharge	m^3/s
$Q_{t,max}$	maximum tidal discharge amplitude	m^3/s
Q_{tide}	tidal discharge peak	m^3/s
R	specific gravity of sediment	-
S	slope	m/m
t	time	s
t_{morfac}	morphological time	s
t_{run}	run time	s

Symbol	Property	Unit
T	tidal period	s
T_w	width adjustment timescale	s
U	flow velocity	m/s
v_k	Von Karman constant	-
W_p	wetted perimeter	m
x	spatial axis	m
z	water level	m
η	bed level	m
ϕ	phase of constituent	rad
ρ	density of water	kg/m^3
ρ_s	density of sediment	kg/m^3
ω	angular velocity	1/s
θ	Shields number	-
θ_{cr}	critical Shields number	-
τ_b	bed shear stress	N/m^2
τ_b^*	critical bed shear stress	N/m^2
a	coefficient for empirical relation river width	-
b	exponent for empirical relation river width	-
c	coefficient for empirical relation river depth	-
f	exponent for empirical relation river depth	-
k	coefficient for empirical relation flow velocity	-
m	exponent for empirical relation flow velocity	-
α	coefficient empirical relation estuary width	-
α_{AP}	coefficient for tidal prism relation	-
α_A	coefficient for empirical relation estuary cross-sectional area	-
β	exponent empirical relation estuary width	-
β_A	exponent for empirical relation estuary cross-sectional area	-
β_{AP}	exponent for tidal prism relation	-

B List of figures

List of Figures

C List of tables

List of Tables

References

Ahmed, T., Egashira, S., Harada, D., Yorozuya, A., Kwak, Y., Shrestha, B., ... Koike, T. (2018). On bank erosion in estuary of sittaung river in myanmar. In *Proceedings of the 9th international conference on scour and erosion* (pp. 161–166).

Bolla Pittaluga, M., Tambroni, N., Canestrelli, A., Slingerland, R., Lanzoni, S., & Seminara, G. (2015). Where river and tide meet: The morphodynamic equilibrium of alluvial estuaries. *Journal of Geophysical Research: Earth Surface*, *120*(1), 75–94.

Braat, L., van Kessel, T., Leuven, J. R., & Kleinhans, M. G. (2017). Effects of mud supply on large-scale estuary morphology and development over centuries to millennia. *Earth Surface Dynamics*, *5*(4), 617–652.

Brückner, M. Z., Schwarz, C., van Dijk, W. M., van Oorschot, M., Douma, H., & Kleinhans, M. G. (2019). Salt marsh establishment and eco-engineering effects in dynamic estuaries determined by species growth and mortality. *Journal of Geophysical Research: Earth Surface*, *124*(12), 2962–2986.

Canestrelli, A., Lanzoni, S., & Fagherazzi, S. (2014). One-dimensional numerical modeling of the long-term morphodynamic evolution of a tidally-dominated estuary: The lower fly river (papua new guinea). *Sedimentary Geology*, *301*, 107–119.

Chappell, J., & Woodroffe, C. (1994). Macrotidal estuaries. *Coastal evolution: Late Quaternary shoreline morphodynamics*, 187–218.

Cunge, J. (1980). Practical aspects of computational river hydraulics. *Pitman Publishing Ltd. London,(17 CUN), 1980, 420*.

D'Alpaos, A., Lanzoni, S., Marani, M., & Rinaldo, A. (2010). On the tidal prism–channel area relations. *Journal of Geophysical Research: Earth Surface*, *115*(F1).

Dalrymple, R. W., & Choi, K. (2007). Morphologic and facies trends through the fluvial–marine transition in tide-dominated depositional systems: a schematic framework for environmental and sequence-stratigraphic interpretation. *Earth-Science Reviews*, *81*(3-4), 135–174.

Dalrymple, R. W., Zaitlin, B. A., & Boyd, R. (1992). Estuarine facies models; conceptual basis and stratigraphic implications. *Journal of Sedimentary Research*, *62*(6), 1130–1146.

Darby, S. E., & Thorne, C. R. (1996). Numerical simulation of widening and bed deformation of straight sand-bed rivers. i: Model development. *Journal of Hydraulic Engineering*, *122*(4), 184–193.

Davies, G., & Woodroffe, C. D. (2010). Tidal estuary width convergence: Theory and form in north australian estuaries. *Earth Surface Processes and Landforms: The Journal of the British Geomorphological Research Group*, *35*(7), 737–749.

Dronkers, J. (2017). Convergence of estuarine channels. *Continental Shelf Research*, *144*, 120–133.

Dronkers, J. (2021). *Morphology of estuaries.* Retrieved 2021-12-18, from `http://www.coastalwiki.org/wiki/Morphology_of_estuaries/`

Dunne, K. B., & Jerolmack, D. J. (2020). What sets river width? *Science advances*, *6*(41), eabc1505.

Dyer, K. R. (1973). *Estuaries: a physical introduction.* John Wiley.

Elliott, M., & McLusky, D. S. (2002). The need for definitions in understanding estuaries. *Estuarine, coastal and shelf science*, *55*(6), 815–827.

Engelund, F., & Hansen, E. (1967). A monograph on sediment transport in alluvial streams. *Technical University of Denmark 0stervoldgade 10, Copenhagen K.*.

Eslami, S., Hoekstra, P., Trung, N. N., Kantoush, S. A., Van Binh, D., Quang, T. T., & van der Vegt, M. (2019). Tidal amplification and salt intrusion in the mekong delta driven by anthropogenic sediment starvation. *Scientific reports*, *9*(1), 1–10.

Fairbridge, R. (1980). The estuary: its definition and geodynamic cycle. In E. Olousson & I. Cato (Eds.), *Chemistry and biochemistry of estuaries* (p. 1-35). New York: Wiley.

Fischer, H. B. (1976). Mixing and dispersion in estuaries. *Annual review of fluid mechanics*, *8*(1), 107–133.

Friedrichs, C. T., & Aubrey, D. G. (1988). Non-linear tidal distortion in shallow well-mixed estuaries: a synthesis. *Estuarine, Coastal and Shelf Science*, *27*(5), 521–545.

Friedrichs, C. T., & Aubrey, D. G. (1994). Tidal propagation in strongly convergent channels. *Journal of Geophysical Research: Oceans*, *99*(C2), 3321–3336.

Galloway, W. E. (1975). Process framework for describing the morphologic and stratigraphic evolution of deltaic depositional systems. In M. L. Broussard (Ed.), *Deltas-models for exploration* (p. 87-98). Houston Geological Society.

Gisen, J. I. A., & Savenije, H. H. (2015). Estimating bankfull discharge and depth in ungauged estuaries. *Water Resources Research*, *51*(4), 2298–2316.

Gleason, C. J. (2015). Hydraulic geometry of natural rivers: A review and future directions. *Progress in Physical Geography*, *39*(3), 337–360.

Gugliotta, M., & Saito, Y. (2019). Matching trends in channel width, sinuosity, and depth along the fluvial to marine transition zone of tide-dominated river deltas: the need for a revision of depositional and hydraulic models. *Earth-Science Reviews*, *191*, 93–113.

Guo, L., van der Wegen, M., Roelvink, D. J., Wang, Z. B., & He, Q. (2015). Long-term, process-based morphodynamic modeling of a fluvio-deltaic system, part i: The role of river discharge. *Continental Shelf Research*, *109*, 95–111.

Hackney, C. R., Darby, S. E., Parsons, D. R., Leyland, J., Best, J. L., Aalto, R., ... Houseago, R. C. (2020). River bank instability from unsustainable sand mining in the lower mekong river. *Nature Sustainability*, *3*(3), 217–225.

Hey, R. D., & Thorne, C. R. (1986). Stable channels with mobile gravel beds. *Journal of Hydraulic engineering*, *112*(8), 671–689.

Hibma, A., Schuttelaars, H. M., & Wang, Z. B. (2003). Comparison of longitudinal equilibrium profiles of estuaries in idealized and process-based models. *Ocean Dynamics*, *53*(3), 252–269.

Hume, T. M., & Herdendorf, C. E. (1988). A geomorphic classification of estuaries and its application to coastal resource management—a new zealand example. *Ocean and Shoreline Management*, *11*(3), 249–274.

Iwantoro, A. P., van der Vegt, M., & Kleinhans, M. G. (2021). Effects of sediment grain size and channel slope on the stability of river bifurcations. *Earth Surface Processes and Landforms*.

Jarrett, J. (1976). *Tidal prism: inlet area relationships (vol.3)*. US Army Engineer Waterways Experiment Station.

Jia, Y., Yi, Y., Li, Z., Wang, Z., & Zheng, X. (2017). Integrating hydraulic equivalent sections into a hydraulic geometry study. *Journal of Hydrology*, *552*, 407–420.

Kleinhans, M. G., Cohen, K. M., Hoekstra, J., & IJmker, J. M. (2011). Evolution of a bifurcation in a meandering river with adjustable channel widths, rhine delta apex, the netherlands. *Earth Surface Processes and Landforms*, *36*(15), 2011–2027.

Kleinhans, M. G., Van Scheltinga, R. T., Van Der Vegt, M., & Markies, H. (2015). Turning the tide: Growth and dynamics of a tidal basin and inlet in experiments. *Journal of Geophysical Research: Earth Surface*, *120*(1), 95–119.

Langbein, W. B. (1963). The hydraulic geometry of a shallow estuary. *Hydrological Sciences Journal*, *8*(3), 84–94.

Lanzoni, S., & D'Alpaos, A. (2015). On funneling of tidal channels. *Journal of Geophysical Research: Earth Surface*, *120*(3), 433–452.

Lanzoni, S., & Seminara, G. (2002). Long-term evolution and morphodynamic equilibrium of tidal channels. *Journal of Geophysical Research: Oceans*, *107*(C1), 1–1.

Leopold, L. B., & Maddock, T. (1953). *The hydraulic geometry of stream channels and some physiographic implications* (Vol. 252). US Government Printing Office.

Leuven, J. R., De Haas, T., Braat, L., & Kleinhans, M. (2018). Topographic forcing of tidal sandbar patterns for irregular estuary planforms. *Earth Surface Processes and Landforms*, *43*(1), 172–186.

Leuven, J. R., van Keulen, D., Nienhuis, J., Canestrelli, A., & Hoitink, A. (2021). Large-scale scour in response to tidal dominance in estuaries. *Journal of Geophysical Research: Earth Surface*, *126*(5).

Leuven, J. R., van Maanen, B., Lexmond, B. R., van der Hoek, B. V., Spruijt, M. J., & Kleinhans, M. G. (2018). Dimensions of fluvial-tidal meanders: Are they disproportionally large? *Geology*, *46*(10), 923–926.

Leuven, J. R., Verhoeve, S. L., Van Dijk, W. M., Selaković, S., & Kleinhans, M. G. (2018). Empirical assessment tool for bathymetry, flow velocity and salinity in estuaries based on tidal amplitude and remotely-sensed imagery. *Remote Sensing*, *10*(12), 1915.

Luketina, D. (1998). Simple tidal prism models revisited. *Estuarine, Coastal and Shelf Science*, *46*(1), 77–84.

Marchi, E. (1990). Sulla stabilitá delle bocche lagunari a marea. *Rendiconti Lincei*, *1*(2), 137–150.

Miori, S., Repetto, R., & Tubino, M. (2006). A one-dimensional model of bifurcations in gravel bed channels with erodible banks. *Water Resources Research*, *42*(11).

Myrick, R. M., & Leopold, L. B. (1963). *Hydraulic geometry of a small tidal estuary.* US Government Printing Office.

Nienhuis, J. H., Ashton, A. D., Edmonds, D. A., Hoitink, A., Kettner, A. J., Rowland, J. C., & Törnqvist, T. (2020). Global-scale human impact on delta morphology has led to net land area gain. *Nature*, *577*(7791), 514–518.

Nienhuis, J. H., Hoitink, A., & Törnqvist, T. E. (2018). Future change to tide-influenced deltas. *Geophysical Research Letters*, *45*(8), 3499–3507.

O'Brien, M. P. (1931). Estuary tidal prisms related to entrance areas. *Civil Engineering*, *1*, 738–739.

Park, C. C. (1977). World-wide variations in hydraulic geometry exponents of stream channels: an analysis and some observations. *Journal of Hydrology*, *33*(1-2), 133–146.

Parker, G., Shimizu, Y., Wilkerson, G., Eke, E. C., Abad, J. D., Lauer, J., ... Voller, V. (2011). A new framework for modeling the migration of meandering rivers. *Earth Surface Processes and Landforms*, *36*(1), 70–86.

Potter, I. C., Chuwen, B. M., Hoeksema, S. D., & Elliott, M. (2010). The concept of an estuary: a definition that incorporates systems which can become closed to the ocean and hypersaline. *Estuarine, Coastal and Shelf Science*, *87*(3), 497–500.

Prandle, D. (2004). How tides and river flows determine estuarine bathymetries. *Progress in Oceanography*, *61*(1), 1–26.

Pritchard, D. W. (1967). What is an estuary: physical viewpoint. In G. H. Lauff (Ed.), *Estuaries* (p. 3-5). American Association for the Advancement of Science.

Rhodes, D. D. (1977). The bfm diagram; graphical representation and interpretation of at-a-station hydraulic geometry. *American journal of science*, *277*(1), 73–96.

Rhodes, D. D. (1987). The bfm diagram for downstream hydraulic geometry. *Geografiska Annaler: Series A, Physical Geography*, *69*(1), 147–161.

Rijn, L. C. v. (1984). Sediment transport, part ii: suspended load transport. *Journal of hydraulic engineering*, *110*(11), 1613–1641.

Rinaldo, A., Fagherazzi, S., Lanzoni, S., Marani, M., & Dietrich, W. E. (1999). Tidal networks: 3. landscape-forming discharges and studies in empirical geomorphic relationships. *Water Resources Research*, *35*(12), 3919–3929.

Sassi, M., Hoitink, A., de Brye, B., & Deleersnijder, E. (2012). Downstream hydraulic geometry of a tidally influenced river delta. *Journal of Geophysical Research: Earth Surface*, *117*(F4).

Savenije, H. H. (2005). *Salinity and tides in alluvial estuaries*. Gulf Professional Publishing.

Savenije, H. H., & Veling, E. J. (2005). Relation between tidal damping and wave celerity in estuaries. *Journal of Geophysical Research: Oceans*, *110*(C4).

Scanes, P., Ferguson, A., & Potts, J. (2017). Estuary form and function: implications for palaeoecological studies. In *Applications of paleoenvironmental techniques in estuarine studies* (pp. 9–44). Springer.

Schuttelaars, H., & De Swart, H. (2000). Multiple morphodynamic equilibria in tidal embayments. *Journal of Geophysical Research: Oceans*, *105*(C10), 24105–24118.

Seminara, G., Lanzoni, S., Tambroni, N., & Toffolon, M. (2010). How long are tidal channels? *Journal of fluid mechanics*, *643*, 479–494.

Seminara, G., Pittaluga, M. B., & Tambroni, N. (2012). Morphodynamic equilibrium of tidal channels. *Environmental Fluid Mechanics-Memorial Volume in Honour of Prof. Gerhard Jirka (ed. W. Rodi & M. Uhlmann)*, 153–174.

Shepard, F. P. (1954). Nomenclature based on sand-silt-clay ratios. *Journal of sedimentary Research*, *24*(3), 151–158.

Simons, D. B., & Albertson, M. L. (1960). Uniform water conveyance channels in alluvial material. *Journal of the Hydraulics division*, *86*(5), 33–71.

Syvitski, J. P. (2008). Deltas at risk. *Sustainability science*, *3*(1), 23–32.

Tambroni, N., Bolla Pittaluga, M., & Seminara, G. (2005). Laboratory observations of the morphodynamic evolution of tidal channels and tidal inlets. *Journal of Geophysical Research: Earth Surface*, *110*(F4).

Todeschini, I., Toffolon, M., & Tubino, M. (2005). Long term evolution of self-formed estuarine channels. *River, Coastal and Estuarine Morphodynamics: RCEM*, 161–170.

Todeschini, I., Toffolon, M., & Tubino, M. (2008). Long-term morphological evolution of funnel-shape tide-dominated estuaries. *Journal of Geophysical Research: Oceans*, *113*(C5).

Toffolon, M., & Lanzoni, S. (2010). Morphological equilibrium of short channels dissecting the tidal flats of coastal lagoons. *Journal of Geophysical Research: Earth Surface*, *115*(F4).

Townend, I. (2012). The estimation of estuary dimensions using a simplified form model and the exogenous controls. *Earth Surface Processes and Landforms*, *37*(15), 1573–1583.

van der Wegen, M., Dastgheib, A., & Roelvink, J. (2010). Morphodynamic modeling of tidal channel evolution in comparison to empirical pa relationship. *Coastal Engineering*, *57*(9), 827–837.

Van der Wegen, M., & Roelvink, J. (2008). Long-term morphodynamic evolution of a tidal embayment using a two-dimensional, process-based model. *Journal of Geophysical Research: Oceans*, *113*(C3).

Van Rijn, L. C. (1984). Sediment transport, part i: bed load transport. *Journal of hydraulic engineering*, *110*(10), 1431–1456.

van Rijn, L. C. (2011). Analytical and numerical analysis of tides and salinities in estuaries; part i: tidal wave propagation in convergent estuaries. *Ocean dynamics*, *61*(11), 1719–1741.

Williams, P. B., Orr, M. K., & Garrity, N. J. (2002). Hydraulic geometry: a geomorphic design tool for tidal marsh channel evolution in wetland restoration projects. *Restoration Ecology*, *10*(3), 577–590.

Xu, F., Coco, G., Tao, J., Zhou, Z., Zhang, C., Lanzoni, S., & D'Alpaos, A. (2019). On the morphodynamic equilibrium of a short tidal channel. *Journal of Geophysical Research: Earth Surface*, *124*(2), 639–665.

Xu, F., Coco, G., Townend, I., Guo, L., He, Q., Zhao, K., & Zhou, Z. (2021). Rationalizing the differences among hydraulic relationships using a process-based model. *Water Resources Research*, *57*(8), e2020WR029430.

Zhang, W., Feng, H., Zheng, J., Hoitink, A., Van Der Vegt, M., Zhu, Y., & Cai, H. (2013). Numerical simulation and analysis of saltwater intrusion lengths in the pearl river delta, china. *Journal of Coastal Research*, *29*(2), 372–382.

Zhao, J., Guo, L., He, Q., Wang, Z. B., van Maren, D., & Wang, X. (2018). An analysis on half century morphological changes in the changjiang estuary: Spatial variability under natural processes and human intervention. *Journal of Marine Systems*, *181*, 25–36.

Zhou, Z., Coco, G., Townend, I., Olabarrieta, M., Van Der Wegen, M., Gong, Z., ... Gelfenbaum, G. (2017). Is "morphodynamic equilibrium" an oxymoron? *Earth-Science Reviews*, *165*, 257–267.